

**GEOLOGICAL HAZARDS AND ENGINEERING GEOLOGY MAPS
OF DILA NB 37-6**

EXPLANATORY NOTES

Habtamu Eshetu *(Chief Compiler)*

Vladislav Rapprich *(Editor)*

The Main Project Partners



The Czech Development Agency (CzDA)

cooperates with the Ministry of Foreign Affairs on the establishment of an institutional framework of Czech development cooperation and actively participates in the creation and financing of development cooperation programs between the Czech Republic and partner countries.

www.czda.cz



The Geological Survey of Ethiopia (GSE)

is accountable to the Ministry of Mines and Energy, collects and assesses geology, geological engineering and hydrogeology data for publication. The project beneficiary.

www.gse.gov.et



The Czech Geological Survey

collects data and information on geology and processes it for political, economical and environmental management. The main contractor.

www.geology.cz



AQUATEST a.s.

is a Czech consulting and engineering company in water management and environmental protection. The main subcontractor.

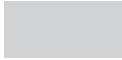
www.aquatest.cz

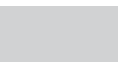


Acknowledgment *Acknowledgment*

Fieldwork and primary compilation of the map and explanatory notes was done by a team from the Geological Survey of Ethiopia (GSE) consisting of staff from the Geo Hazard Investigation Directorate, Groundwater Resources Assessment Directorate and Czech experts from AQUATEST a.s. and the Czech Geological Survey in the framework of the Czech Development Cooperation Program. We would like to thank the SNNPR Regional Water Bureau, the Dila, Sidamo and Sodo-Woleita Zone Administrations, Water, Mines and Energy offices for their hospitality, guidance and relevant data delivery. The team is grateful to the management of the Geological Survey of Ethiopia, particularly to Director General (GSE) Mr. Masresha G/Selassie and Mr. Lata Alemayehu, Head of the Geo Hazard Investigation Directorate as well as Mr. Muhuddin Abdela, Head of the Groundwater Resources Assessment Directorate for their support.

Finally, we would like to acknowledge the untiring support of the local people who assisted the team by all means possible and facilitated the data collection and those who helped us in various different ways.





Contents

<i>Acknowledgment</i>	3
<i>Extended Summary</i>	13
<i>Introduction</i>	15
1. Basic Characteristics of the Area	17
1.1 Location and Accessibility	17
1.2 Population, Settlements and Health Status.....	18
1.3 Land Use and Land Cover	22
2. Selected Physical and Geographical Settings	25
2.1 Geomorphology	25
2.2 Soil and Vegetation Cover.....	28
2.3 Climatic Characteristics	29
2.3.1 Climatic Zones and Measurements.....	29
2.3.2 Wind speed and direction	32
2.3.3 Precipitation.....	33
2.4 Hydrology of the Area.....	38
2.4.1 Surface Water Network Development	38
2.4.2 River Flow Regime	39
2.4.3 Lakes.....	48
3. Geological Settings	51
3.1 Previous studies	51
3.2 Stratigraphy	51
3.3 Lithology.....	52
3.4 Tectonics	59
3.4.1 Primary structures	59
3.4.2 Ductile structures	59
3.4.3 Brittle structures	63
3.5 Geochronology	66
3.6 Geological Evolution.....	67
4. Rock properties and economic perspectives	69
4.1 Engineering geology.....	69
4.1.1 Engineering classification of rocks.....	69
4.1.2 Engineering classification of soils.....	75
4.2 Economic geology	78
4.2.1 Construction materials	78
4.2.2 Absorption materials	82
4.2.3 Ceramics materials.....	83
4.3 Geothermal energy	83
4.4 Geotourism potential.....	84
5. Geological hazards	85
5.1 Endogenous geological hazards	85
5.1.1 Seismic hazards	85
5.1.2 Ground cracks (fissures).....	87
5.1.3 Volcanic hazards.....	88
5.2 Exogenous geological hazards	94

5.2.1 Erosion hazards	94
5.2.2 Inundations and accumulation of sedimentary material	96
5.2.3 Slope deformation hazards	102
5.3 Hydrological and hydrogeological hazards	111
5.3.1 Fluoride.....	111
5.3.2 Unexpected discharge of thermal water	113
<i>References</i>	115
Annex 1 Geochemical analyses data	119
Annex 2 Wet lands.....	125
Annex 3 Rock property data.....	127
Annex 4 Existing Quarries.....	133
Annex 5 Proposed Quarries.....	137

List of Figures

Fig. 1.1	Location map.....	17
Fig. 1.2	Administrative zones and main roads.....	18
Fig. 1.3	Recovering of devastated landscape to the north of Lake Abaya.....	23
Fig. 1.4	Land cover.....	24
Fig. 1.5	Grass plains and open shrublands in the Nech Sar National Park.....	24
Fig. 2.1	Generalized geomorphological units.....	25
Fig. 2.2	Generalized geomorphological classes.....	26
Fig. 2.3	Floor of the MER in its narrow segment near Arba Minch.....	27
Fig. 2.4	Rift scarp to the north of Arba Minch.....	27
Fig. 2.5	Genale Gorge.....	28
Fig. 2.6	Climatic zones.....	30
Fig. 2.7	Wind-rose diagrams for Arba Minch station.....	32
Fig. 2.8	Wind-rose diagrams for Hawasa station.....	33
Fig. 2.9	Precipitation pattern in Arba Minch, Dila, Wolaita Sodo and Hager Selam meteo-stations.....	34
Fig. 2.10	The principal river basins of the area.....	38
Fig. 2.11	Flow diagram of the Bilate River at the Bilate Tena river gauge.....	41
Fig. 2.12	Annual variability of the mean annual flow of the Bilate River at the Bilate Tena river gauge.....	42
Fig. 2.13	Flow diagram of the Hamasa (syn. Amesa) River at the Humbo river gauge.....	43
Fig. 2.14	Annual variability of the mean annual flow of the Hamasa (syn. Amesa) River at the Humbo river gauge.....	43
Fig. 2.15	Flow diagram of the Kulfo River at the Arba Minch river gauge.....	44
Fig. 2.16	Annual variability of the mean annual flow of the Kulfo River at the Arba Minch river gauge.....	44
Fig. 2.17	Flow diagram of the Demie River at the river gauge.....	45
Fig. 2.18	Annual variability of the mean annual flow of the Demie River at the river gauge.....	45
Fig. 2.19	Flow diagram of the Gidabo River at the Aposto river gauge.....	46
Fig. 2.20	Annual variability of the mean annual flow of the Gidabo River at the Aposto river gauge.....	46
Fig. 2.21	Flow diagram of the Upper Genale River at the Girja river gauge.....	47
Fig. 2.22	Annual variability of the mean annual flow of the Upper Genale River at the Girja river gauge.....	47
Fig. 2.23	Lake Chamo, seen from Tosa Sucha (God ' s Bridge).....	50
Fig. 3.1	Outcrop of altered greenschists and amphibolites.....	53
Fig. 3.2	Microphotograph of amphibolite (sample KV 122). Plane-polarized light.....	53
Fig. 3.3	Outcrop of mica-shist with amphibolite dykes exposed in a road cut near Kibre Mengist.....	54
Fig. 3.4	Outcrop of metagranite.....	54
Fig. 3.5	Columnary jointed lower basalt.....	55
Fig. 3.6	Fiamme in rhyolitic ignimbrite of the Dino Formation.....	56
Fig. 3.7	Aligned scoria cones within the Hamasa River (Humbo) Volcanic Field.....	57
Fig. 3.8	Active quarry exploiting trachytic intrusion from a central rhyolitic volcano (Mt. Damota near Wolaita Sodo).....	57
Fig. 3.9	Gravels of an alluvial fan filling the river channel on the shore of Lake Abaya to the north of Arba Minch.....	58
Fig. 3.10	Travertine mound on an active hot spring (Bolocho).....	58

Fig. 3.11	Orientation diagrams of ductile and primary structures	59
Fig. 3.12	Flat-lying depositional fabrics in volcanic sequence (Arbe Gona).....	60
Fig. 3.13	Bedding in pyroclastic deposits of a basaltic scoria cone near Arba Minch	60
Fig. 3.14	Stretching lineation and parallel elongation of a mafic microgranular enclave in biotite orthogneiss (Mejo).....	61
Fig 3.15	Asymmetric folds of leucogranite dike (Meleka).....	61
Fig. 3.16	Asymmetrically stretched quartz–feldspar melt indicating oblique thrusting (NW-side-up) kinematics (Chebe).....	62
Fig. 3.17	Superposition of ~S to SW dipping axial cleavage (Meleka)	62
Fig. 3.18	Regional NNE – SSW trending fault with a normal component of movement (Chencha).....	63
Fig. 3.19	Subvertical slickensides associated with WNW – ESE trending faults (Dila).....	64
Fig. 3.20	Orientation diagrams of faults and associated slickensides.....	64
Fig. 3.21	Regional N – S trending extensional joints.....	65
Fig. 3.22	Orientation diagram of the extensional joints in different units (poles).....	66
Fig. 3.23	Location of K-Ar geochronological results on the Dila sheet	66
Fig. 3.24	Phreatomagmatic pyroclastic deposits overlain by basaltic scoria – quarried scoria cone near Arba Minch.....	68
Fig. 4.1	Nazret Group basalt exposed in the Keangnam quarry near Bore town on the eastern plateau	71
Fig. 4.2	Jointed ignimbrite exposed by an active quarry	72
Fig. 4.3	Thick-columnary jointed rhyolitic ignimbrite to the north of Dila.....	72
Fig. 4.4	Coherent rhyolite exposed in the cut of the road from Birbir to Arba Minch	72
Fig. 4.5	Wide spacing of joints in metagranite.....	72
Fig. 4.6	Weathered foliated high-grade metamorphic rocks exposed in a road cut.....	73
Fig. 4.7	Close up of banded clays resulting from weathering of foliated metamorphic rocks.....	73
Fig. 4.8	Coarse-grained pumiceous deposits near Yirga Alem town.....	74
Fig. 4.9	Thick deposits of bedded pumice on the slope of Duguna Fango Volcano.....	74
Fig. 4.10	Scheme of soil granulometry variability within the Dila map sheet area	76
Fig. 4.11	Scheme of distribution of paleorelief plains with thick accumulations of residual soils	77
Fig. 4.12	Thick residual soil outcropped along the road from Aleta Wendo to Hagere Selam	77
Fig. 4.13	Scheme of existing and proposed quarry sites in the area of the Dila sheet	79
Fig. 4.14	Keangnam basalt quarry site near Bore town.....	79
Fig. 4.15	Quarry for first-rate road and pavement material near Solemo town	80
Fig. 4.16	Scoria quarry to the north of Lake Abaya	80
Fig. 4.17	Quarry in rhyolitic ignimbrite to the north of Dila	81
Fig. 4.18	Quarry in massive granite for dimension stone near Meleka town	81
Fig. 4.19	Soil borrow quarry for the Gidabo dam core material, 20 km to the west of Dila Town.....	82
Fig. 4.20	Kaolin quarry near Bwanbua Woha	83
Fig. 4.21	Bobicho thermal spring.....	83
Fig. 4.22	Northwest Abaya fault-zone hot-springs.....	84
Fig. 4.23	Herd of zebra in the Nech Sar National Park.....	84
Fig. 4.24	Crocodile at Lake Chamo	84
Fig. 5.1	Duguna Fango Volcano.....	88
Fig. 5.2	Pyroclastic deposits of Duguna Fango Volcano exposed in a road cut on the eastern slope of the volcano.....	89
Fig. 5.3	White tuff embedded within brown soil to the east of Dimtu.....	89
Fig. 5.4	Obsidians altered by fumaroles (Bilbo fumaroles) on the southern foothill of Duguna Fango Volcano	89
Fig. 5.5	Chericha Volcano seen over the Bilate River from the Bolocho hot springs	90
Fig. 5.6	Korke Seluwa Volcano and its recent obsidian lava	91
Fig. 5.7	Equiline diagram of $^{230}\text{Th}/^{232}\text{Th}$ and $^{238}\text{U}/^{232}\text{Th}$ isotopic ratios.....	92
Fig. 5.8	Scoria cones of the Hamasa Volcanic Field on the faulted tectonic landscape	93
Fig. 5.9	Kale Korke scoria cone on Nech Sar plain	93
Fig. 5.10	Ganjule Island – scoria cone on Lake Chamo	93
Fig. 5.11	Pyroclastic deposits of a scoria cone exposed by a quarry on the shore of Lake Chamo	94
Fig. 5.12	TAS diagram (Le Bas et al. 1986) with chemical analyses of volcanic rocks erupted in the North Chamo Volcanic Field.....	94
Fig. 5.13	Surface run-off during stormy rains in badlands situated to the northwest of Dila town.....	95
Fig. 5.14	Residual silty soils and pumice prone to erosion, to the east of Dimtu, Bilate river catchment	95
Fig. 5.15	Rill erosion in highly weathered tuffs, to the west of Belela	95
Fig. 5.16	Badlands along a deep canyon of the Tiliku Mancha River, to the north-east of Lake Abaya	95

Fig. 5.17	System of deep gullies, to the south of Belela.....	96
Fig. 5.18	Landslide of gully slope triggered by lateral erosion, to the south of Belela.....	96
Fig. 5.19	Lateral erosion of banks of the Bilate River, Dimtu village.....	97
Fig. 5.20	Inundated farm located in surface crevasse splay, Bilate River Delta, July 2013. Image from Google Earth View	97
Fig. 5.21	Crevasse splay formed during floods in 2013, Bilate River. Image from Google Earth View.....	98
Fig. 5.22	Sandy accumulation of crevasse splay after floods in 2013, Bilate river flood basin.....	98
Fig. 5.23	Lateral sandy bar accumulated during floods in 2013. Bilate River	98
Fig. 5.24	Wetland with temporal lake in tectonic graben situated in the lowermost part of the Gibado River catchment. Image from Google Earth View	99
Fig. 5.25	Temporally active overflow channel in the flood basin of the Kulfa River between Arba Minch and Nechi Sar National Park	99
Fig. 5.26	Active part of alluvial fan situated on the western shore of Lake Abaya near Dante village.....	100
Fig. 5.27	In-channel bars of the Kulfa River on the northern margin of Arba Minch	100
Fig. 5.28	Abandoned river channel, filled with gravel, to the north of Arba Minch	100
Fig. 5.29	Abandoned channel in an alluvial fan near Lante.....	100
Fig. 5.30	Avulsion points in the Kulfa River, northern margin of Arba Minch	100
Fig. 5.31	Lateral erosion along braided channels, alluvial fan near Lante.....	101
Fig. 5.32	Bridge construction over the Sodo-Arba Minch road, high lateral erosion risk, to the north of Arba Minch.....	101
Fig. 5.33	Floods in the Amaro River causing inaccessibility to Arba Minch, November 2012 (photo V. Žáček)....	101
Fig. 5.34	Monthly lake water levels of Lake Abaya at the Arba Minch gauging station (Seleshi 2001).....	102
Fig. 5.35	The hillshade of the south-eastern quadrant of the Dila map sheet with highlighted slope edges as the result of retrograde erosion and slope movement.....	103
Fig. 5.36	Shallow debris slide on the toe of a rock rotational slide (Fig. 3) on an escarpment terrace.....	104
Fig. 5.37	Slope deformation of Rock rotational slide on escarpment terrace, occur below the road leading from Gambelo river valley to Mejo town	104
Fig. 5.38	Boulders and debris fall to debris slide in the Gambelo – Mejo road cut.....	105
Fig. 5.39	Position of a deep-seated slope deformation in the Gonjobe river valley (Google Earth).....	105
Fig. 5.40	Detail of the topographic map Mejo 0638-D2	106
Fig. 5.41	The main scarp is affected by selective rock and linear erosion (Bing maps).....	107
Fig. 5.42	View on deposits of blocky ignimbrites representing of slide accumulation	107
Fig. 5.43	Horst and graben features in the upper part of the deformation	108
Fig. 5.44	Detail of the shear zone	109
Fig. 5.45	Basal segment of the shear zone in this case follows a weak horizon of paleosoils.....	109
Fig. 5.46	Masses of the rock body have shifted the stream channel	109
Fig. 5.47	Open cracks mapped in November 2013.....	109
Fig. 5.48	The source area of debris flow is shaped by landslides	109
Fig. 5.49	Alluvial gravels representing resedimented debris-flow deposits along the Baso River.....	109
Fig. 5.50	View of the Baso River channel from Dorze Giyorgis church.....	110
Fig. 5.51	Scheme of the area affected by high fluorine concentrations in the Dila map sheet area	111
Fig. 5.52	High content of fluoride is caused by its leaching from silicic pyroclastic deposits.....	112
Fig. 5.53	Overflow of the hot water from well at Dimtu	113
Fig. 5.54	Documentation of slope deformations at the edge of erosional gully near Bedele.....	114



List of Tables

Tab. 1.1	Team members	16
Tab. 1.2	Population in the study area	19
Tab. 2.1	Ethiopian climate classification	30
Tab. 2.2	Mean and extreme monthly temperature [°C] of Hawasa	31
Tab. 2.3	Wind speed in Dila and Woleita Sodo	32
Tab. 2.4	Characterization of the precipitation pattern in Ethiopia	34
Tab. 2.5	Mean monthly precipitation in selected stations (source Halcrow, 2008).....	34
Tab. 2.6	Summary of precipitation data (in mm)	35
Tab. 2.7	Runoff data.....	40
Tab. 2.8	Lake level stations	49
Tab. 2.9	Basic characteristics of lakes.....	49
Tab. 3.1	Lithostratigraphy of the mapped area	51
Tab. 3.2	K-Ar data obtained on volcanic rocks from different volcanic fields (2013)	66
Tab. 4.1	ISRM terms for weathering descriptionRocks with very high rock mass strength (VHRMS).....	70
Tab. 5.1	Earthquakes of magnitude $M > 4.3$ between 1983 and 2013 in the map sheet area (USGS catalog).....	86
Tab. 5.2	Measured U and Th isotopic ratios.....	91

 ***Under Separate Cover (attached CD)***

Maps:

Engineering geology map of Dila NB 37-6 – full size and A3 size

Geological hazards map of Dila NB 37-6 – full size and A3 size

Extended Summary

The Dila map sheet (NB 37-6) at the scale of 1:250,000 is located in Southeastern Ethiopia covering an area of 17,236 km². The area is a part of the Oromia and Southern Nations, Nationality and People (SNNPR) regional states, its population exceeds 5.5 million and it is moderately cultivated.

Elevation in the study area copies its main geomorphological parts represented by the Rift Valley, Eastern Highlands, Western Highlands and the gorges of Genale and Omo. Elevation varies between 1,200 and 1,700 m a.s.l. on the rift valley floor, whereas along the escarpment the elevation rises to about 2,600 m a.s.l., and the edge of the plateau is flanked by high volcanic complexes with elevation from 2,970 to 3,270 m a.s.l. The area is part of the Omo-Gibe, Wabe Shebele, Genale and Rift Valley Lakes basins. The rainy season is bimodal from April to May and from September to October; the annual mean rainfall was adopted as being 1,200 mm/year for the Dila area. There is also a bimodal wind direction distribution during the year in the area of the Dila sheet. From November to March the winds blow from the northeast and east. April and October are transitional months with highly variable wind directions and from May to September the winds blow from the south and southwest. There are two principal permanent rivers (Bilate and Genale) and a large lake (Abaya).

The area investigated is influenced by endogenous as well as exogenous hazardous geological phenomena and processes. The endogenous geological hazards comprise seismic and volcanic activity. The seismic activity is associated with the Main Ethiopian Rift manifested by a network of normal faults. Unfortunately, there is a lack of data on the precise location of earthquakes reaching a magnitude of up to 6. For this reason, seismically active faults cannot be identified within the observed tectonic network. Earthquakes would cause damage to buildings constructed in areas with thick accumulations of sediments or loose non-welded pyroclastic deposits. Large volumes of soft rock amplify seismic effects. The volcanic activity is represented by composite ("central") rhyolitic volcanoes and a field of monogenetic basaltic volcanoes. The Chericha Volcano was not reached and therefore its eruptive history remains unclear. The Korke Seluwa Volcano produced voluminous lavas of crystal-rich obsidian associated with minor pumice fall. The Hamasa volcanic field comprises numerous scoria cones and appears to still be an active zone. Individual eruptions affect a limited area but these cones are scattered and widespread. A smaller volcanic field in the northern part of Lake Chamo last erupted approximately 0.5 Ma and is now extinct. The main problem in assessing the volcanic hazard remains the critical lack of historical or geochronological data on Holocene eruptions.

Tectonic activity creates dynamic morphology with steep scarps prone to debris flows and landslides. Zones with frequent rock-fall features follow the scarps of the Main Ethiopian Rift.

One of the most serious environmental problems of Ethiopia remains erosion and degradation of soil. Areas with intense soil erosion were mapped and features triggering and enabling the erosion identified. Light sandy soils developed upon Late Pleistocene rhyolitic ignimbrites are extremely prone to erosion. Streams and creeks with high flow rates are frequently responsible for gully erosion, namely during the rainy season. In addition, alluvial fans of larger streams and rivers are characterized by rapid sedimentation in particular during the rainy season. Lowlands and depressions frequently formed on tectonically subsided blocks lacking drainage may be affected by inundation. Such areas can be found to the east of Lake Abaya.

High aggradation of sedimentary material in alluvial fans on the foothills of tectonic scarps leads to river avulsion and represents a serious hazard to towns and villages on the western banks of Lake Abaya.

Introduction

Introduction

Background

Nature manifests its destructive power in many ways in Southern Ethiopia. There are not many regions in the world where such a wide spectrum of natural hazards is present. The Main Ethiopian Rift - a zone of active spreading associated with intense seismic and volcanic activity, crosscuts Ethiopia. The fault scarps are prone to slope deformations and loose pyroclastic deposits are easily eroded. Ethiopia is also endangered by sheet erosion and several areas within the rift lacking drainage, namely recently developing tectonic grabens, are prone to inundation. The topography together with the increasing population aggravates the environmental problems. It is therefore important to compile a map of natural hazards to be able to propose and implement appropriate measures to protect inhabitants and infrastructure. In this context a geohazard investigation was performed in the area of the Dila sheet, which comprises most of the types of geological hazards, in 2012 – 2014 by the Geological Survey of Ethiopia with the assistance of experts from the Czech Geological Survey. The work was conducted in the framework of bilateral cooperation between the Czech and Ethiopian governments, where the participation of the Czech experts was financed by the Czech Development Agency in the framework of the Czech Republic Development Assistance Program and the participation of the Ethiopian professionals was financed by the Ethiopian government. This report deals with the assessment of the characteristics of engineering geology and geological hazards acquired during the desk and field work and discussion between stakeholders and the joint Czech-Ethiopian team of professionals, supported by the analytical work of experts from other European countries.

Objective and Scope

Geological hazards endanger most of Ethiopia's population. To enable ongoing development of the country better knowledge of geological hazards and the limits they represent for land-use and construction is crucially needed. The main objectives of the study for geohazard mapping were to identify individual types of geological hazards and to map the extents of zones influenced by these hazardous processes. The work covers the interpretation of aerial photos and satellite images, meteorological and geological data analysis, collection of representative rock and soil samples for geological, structural and geochronological analyses, and evaluation of geohazard distribution within the area. The geohazard investigation of the Dila map sheet is part of the project entitled "Capacity building in Environmental Geology – Mapping of Geo-risks including Hydrogeological Condition in Dila and Hosaina areas, Ethiopia" that was conducted between 2012 and 2014 to reduce undesirable effects of geological processes on society and the environment.

In order to achieve the main objectives a number of tasks were undertaken at different levels having unique specific objectives that led to the final compilation of the geohazard map and completion of the explanatory notes. These specific objectives are as follows:

- To identify young faults with the potential of ongoing seismic activity and thick accumulations of sediments potentially amplifying seismic effects
- To identify links between the tectonic setting and evolution of fluvial systems including gully erosion and rapid accumulation endangered areas
- To identify potentially hazardous volcanoes, areas endangered by these volcanoes, their eruptive styles, eruption frequencies and the time since their last eruption
- To define zones prone to slope deformation
- To define areas endangered by sheet erosion and identify the principal features triggering the degradation of soil
- To identify the source of fluorine in the groundwater

The desktop study and field work were carried out by mixed groups of Ethiopian and Czech geologists. The geochronological analyses were carried out in Hungary and Great Britain. Final assessment and publication of the map were carried out by a joint Czech-Ethiopian team of professionals. The names of participating experts are shown in Tab. 1.1.

Tab. 1.1 Team members

Name	Institution	Participation field
Vladislav Rapprich	Czech Geological Survey	Volcanology, project leader, main editor
Leta Alemayehu	Geological Survey of Ethiopia	Project coordinator, Engineering geology
Petr Kycl	Czech Geological Survey	Engineering geology, landslides
Habamu Eshetu	Geological Survey of Ethiopia	Engineering geology, compiler of the engineering geology part
Tomáš Hroch	Czech Geological Survey	Geomorphology, erosion and sedimentation
Kryštof Verner	Czech Geological Survey	Structural geology
Jan Malík	Czech Geological Survey	Engineering geology
Jiří Málek	Institute of Rock Structure and Mechanics, Czech Academy of Sciences v.v.i.	Seismology
Veronika Kopačková	Czech Geological Survey	Remote sensing
Jan Mišurec	Czech Geological Survey	Remote sensing
Petra Hejtmánková	Czech Geological Survey	GIS
Jiří Šíma	AQUATEST a.s.	Hydrogeology
Craig Hampson	AQUATEST a.s.	English editing
Yewubinesh Bekele	Geological Survey of Ethiopia	Engineering geology
Tsighana Tesema	Geological Survey of Ethiopia	Geomorphology
Ermias Filfilu	Geological Survey of Ethiopia	Engineering geology
Firdawok Legesa	Geological Survey of Ethiopia	Geophysics
Habamu Bewket	Geological Survey of Ethiopia	Structural geology
Ezra Tadesse	Geological Survey of Ethiopia	Geophysics
Tutan Negash	Geological Survey of Ethiopia	Engineering geology
Alula Demewez	Geological Survey of Ethiopia	Engineering geology
Ermias Filfilu	Geological Survey of Ethiopia	Engineering geology
Zoltán Pécskay	Hungarian Academy of Sciences	K-Ar geochronology
Heye Freymuth	University of Bristol, GB	U-Th series disequilibria

1. Basic Characteristics of the Area

1.1 Location and Accessibility

The study area is located in Southern Ethiopia, in the part of the Main Ethiopian Rift and adjacent eastern and western Ethiopian Plateau. Geographically, the study area is bounded from north to south by latitudes 6°00' N and 7°00' N, and from west to east by longitudes 37°30' E and 39°00' E. The area covers approximately more than 17,236 km² of the topographic map sheet of Dila (NB 37-6) at a scale of 1:250,000. The location of the map is illustrated in Fig. 1.1. The sheet is bounded by the Hosaina sheet to the north, the Dodola sheet to the east, Agere Mariam sheet to the south and by the Dime sheet to the west.



Fig. 1.1 Location map

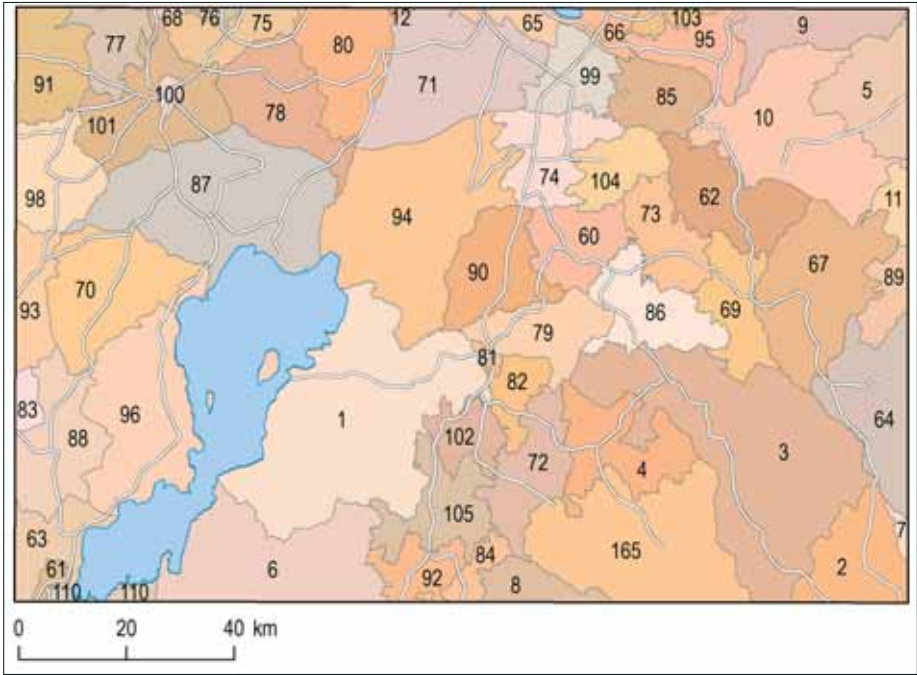


Fig. 1.2 Administrative zones and main roads:

1) Abaya; 2) Adola; 3) Bore; 4) Dima; 5) Dodola; 6) Gelana; 7) Girja; 8) Hambela Wamena; 9) Kofele; 10) Kokosa; 11) Nensebo; 12) Siraro; 60) Aleta Wondo; 61) Arba Minch Town; 62) Arbegona; 63) Arba Minch Zuriya; 64) Aroresa; 65) Hawasa Zuriya; 66) Hawasa Town; 67) Bensa; 68) Bolossa Sore; 69) Bona Zuriya; 70) Boreda; 71) Boricha; 72) Bule; 73) Bursa; 74) Dale; 75) Damot Gale; 76) Damot Pulasa; 77) Damot Sore; 78) Damot Woyide; 79) Dara; 80) Deguna Fango; 81) Dila Town; 82) Dila Zuriya; 83) Dita; 84) Gedeb; 85) Gorche; 86) Hula; 87) Humbo; 88) Chenchä; 89) Chire; 90) Chuko; 91) Kindo Koyisha; 92) Kochore; 93) Kucha; 94) Loko Abaya; 95) Malga; 96) Mirab Abaya; 98) Ofa; 99) Shebedino; 100) Sodo Town; 101) Sodo Zuriya; 102) Wenago; 103) Wendo Genet; 104) Wensho; 105) Yirgachefe; 110) Nech Sar National Park; 165) Uraga.

The area can be accessed by the road connecting the capital city of Addis Ababa with Butajira – Hosaina – Sodo – Arba Minch and Mojo – Ziway – Shashemene – Hawasa – Dila and the main Nazret – Asela – Shashemene asphalt roads. The all-weather gravel roads within the study area are in good condition and the area is accessible for mapping work. Most of the central-eastern part (both the rift floor and the escarpment) can be accessed via the all-weather gravel road that branches off from the main Hawasa – Dila – Agere Mariam road and connects the towns of Daye, Hager Salam in the eastern and Dimtu and Bedesa in the central part of the sheet. The western part of the sheet can be accessed via the main Hosaina – Sodo – Arba Minch asphalt road and its branch roads to Bele, Gesuba and Chenchä.

The main accessible roads are shown in Fig. 1.2.

1.2 Population, Settlements and Health Status

The Dila map sheet is located within the Oromia and SNNP regional states. Most of the dwellers are Oromo people. Permanent settlement is concentrated along two old traditional roads, where

the biggest towns Leku, Yirga Alem, Wondo, Hagere Salam and Dila are located in the western and Sodo, Humbo and Arba Minch in the eastern part of the sheet.

The southeastern part of the study area is inhabited by Oromo people. Population settlement is mostly limited to the towns and villages. The northern and western parts of the study area are inhabited by different ethnic groups of the southern peoples (Woleita, Sidama etc.). The Amhara people are also found in the study area, mostly limited to the main towns.

There are 8 Zones and 59 Weredas within the mapped area (see Fig. 1.2); however, some of them are not located entirely within the boundary of the map sheet. To calculate the total number of people living in the mapped area the number of people living in the Weredas was assessed from the total Wereda population and by the percentage of the area within the map sheets. Tab. 1.2 shows the population in the different Weredas within the mapped area.

Based on the data provided by the Central Statistics Authority, the total population is assumed to be 5,550,108; however, this figure could in reality be several thousands higher. The urban population comprises about 35 % (Dila and Sodo towns with 81 and 76 thousand inhabitant are the biggest urban settlements of the sheet – Hawasa and Arba Minch are the biggest towns of the southern region, but they are only partly extending on the sheet area) and the remaining 65 % of the population lives in rural areas.

Tab. 1.2 Population in the study area

Region	Zone	Wereda	Wereda area in the mapped area		Total population	Assessed population in the mapped area
			[km ²]	[%]		
Oromia	Borena	Abaya	1,189.5	100.0	104,374	104,374
Oromia	Borena	Gelana	626.5	45.8	70,291	32,165
Oromia	Guji	Adola	307.8	25.3	136,672	34,556
Oromia	Guji	Bore	1,236.0	96.3	210,078	202,248
Oromia	Guji	Dima	322.8	100.0	64,214	64,214
Oromia	Guji	Girja	19.3	2.1	50,153	1,032
Oromia	Guji	Hambela Wamena	128.5	22.6	110,931	25,028
Oromia	Guji	Uraga	746.0	80.8	177,170	143,162
Oromia	West Arsi	Dodola	284.3	17.2	194,817	33,457
Oromia	West Arsi	Kofele	223.4	33.8	179,508	60,682
Oromia	West Arsi	Kokosa	629.4	99.2	144,505	143,310
Oromia	West Arsi	Nensebo	66.9	4.2	114,524	4,800
Oromia	West Arsi	Siraro	5.2	0.9	145,404	1,272
SNNP	Awassa Town	Awassa Town	75.4	48.0	259,803	124,688
SNNP	Gamo Gofa	Arba Minch T.	32.1	97.3	74,843	72,858

Tab. 1.2 Population in the study area (part 2)

Region	Zone	Wereda	Wereda area in the mapped area		Total population	Assessed population in the mapped area
			[km ²]	[%]		
SNNP	Gamo Gofa	Arba Minch Z.	192.5	19.9	165,680	32,964
SNNP	Gamo Gofa	Boreda	464.1	100.0	67,947	67,947
SNNP	Gamo Gofa	Dita	51.1	18.0	83,953	15,136
SNNP	Gamo Gofa	Chencha	337.4	90.3	111,680	100,876
SNNP	Gamo Gofa	Kucha	176.5	12.7	149,835	19,000
SNNP	Gamo Gofa	Mirab Abaya	617.4	100.0	74,901	74,901
SNNP	Gamo Gofa	Nech Sar NP	47.4	17.3	0	0
SNNP	Gedeo	Bule	274.0	100.0	105,921	105,921
SNNP	Gedeo	Dila Town	18.0	100.0	81,644	81,644
SNNP	Gedeo	Dila Zuria	122.3	100.0	97,327	97,327
SNNP	Gedeo	Gedeb	80.9	25.3	146,732	37,117
SNNP	Gedeo	Kochore	147.1	68.3	131,418	89,809
SNNP	Gedeo	Wenago	142.7	100.0	117,630	117,630
SNNP	Gedeo	Yirgachefe	268.5	100.0	199,077	199,077
SNNP	Sidama	Aleta Wondo	230.5	100.0	188,932	188,932
SNNP	Sidama	Arbegona	336.5	100.0	144,300	144,300
SNNP	Sidama	Aroresa	373.5	54.8	170,143	93,221
SNNP	Sidama	Awasa Zuryia	66.2	21.7	139,891	30,336
SNNP	Sidama	Bensa	547.5	100.0	251,070	251,070
SNNP	Sidama	Bona Zuriya	229.9	100.0	128,462	128,462
SNNP	Sidama	Boricha	588.4	99.4	236,341	234,916
SNNP	Sidama	Bursa	222.0	100.0	100,642	100,642
SNNP	Sidama	Dale	276.9	100.0	215,693	215,693
SNNP	Sidama	Dara	250.0	100.0	157,866	157,866
SNNP	Sidama	Gorche	212.3	100.0	139,780	139,780
SNNP	Sidama	Hula	287.3	100.0	130,433	130,433
SNNP	Sidama	Chire	108.2	29.6	114,413	33,823

Tab. 1.2 Population in the study area (Part 3)

Region	Zone	Wereda	Wereda area in the mapped area		Total population	Assessed population in the mapped area
			[km ²]	[%]		
SNNP	Sidama	Chuko	308.1	100.0	171,667	171,667
SNNP	Sidama	Loko Abaya	874.7	100.0	99,216	99,216
SNNP	Sidama	Malga	201.3	97.4	114,030	111,065
SNNP	Sidama	Shebedino	197.1	100.0	189,835	189,835
SNNP	Sidama	Wendo Genet	49.8	22.0	153,283	33,698
SNNP	Sidama	Wensho	179.5	100.0	120,655	120,655
SNNP	Wolayita	Bolossa Sore	8.8	2.9	196,607	5,731
SNNP	Wolayita	Damot Gale	168.7	66.0	154,610	102,081
SNNP	Wolayita	Damot Pulasa	20.5	12.4	108,083	13,404
SNNP	Wolayita	Damot Sore	163.3	90.3	106,180	95,871
SNNP	Wolayita	Damot Woyide	352.0	100.0	96,299	96,299
SNNP	Wolayita	Deguna Fanigo	318.7	79.4	96,472	76,580
SNNP	Wolayita	Humbo	854.8	100.0	125,286	125,286
SNNP	Wolayita	Kindo Koyisha	261.5	49.7	109,176	54,256
SNNP	Wolayita	Ofa	285.5	74.1	104,276	77,244
SNNP	Wolayita	Sodo Town	25.6	100.0	76,780	76,780
SNNP	Wolayita	Sodo Zuriya	404.3	100.0	163,771	163,771
TOTAL						5,550,108

Source: Population by Zone, Central Statistics Authority Statistical Abstract (2012)

The majority of the rural population of the region practices crop production which is in some areas highly developed, and commercial plantations are common. The agriculture in the SNNPR is small scale subsistence farming, producing products mostly for family consumption. The contribution of industry as well services has increased over the last decade indicating the structural transformation of the economy from agriculture towards industry and services. Oromia made the largest industrial contribution to Ethiopia's economy, with an estimated 60 % of foreign exchange earnings. The largest proportion of Ethiopia's export commodities originates in Oromia, including the following products: coffee, oilseeds, leather products, fruits and vegetables, flowers, gold, etc.

Considering the trends in population growth in Oromia (2.6 %) and SNNPR (2.8 %), access to water will become worse by 2015 in urban areas and 2025 in rural areas, respectively. People in the area of map sheet could face water scarcity i.e. less than 1,000 m³/year, and/or even water stress i.e. availability of less than 500 m³/year (Tsfay Tafese, 2001). The life expectancy at birth is 49 years for males and 51 years for females (WHO, 2006).

Access to safe drinking water is limited and some statistics suggest that only 15 % of rural inhabitants have access to safe drinking water. The WHO (2006) statistics show that 31 % of the rural population has sustainable access to improved drinking water sources (96 % of the urban population). This low number is alarming because 70 % of contagious diseases are caused by contaminated water. This is a serious problem for Ethiopia in the effort to establish a strong agricultural community that will be able to safeguard the supply of food for the whole country. The main source of water supply is groundwater accessed through dug wells, from alluvial and other sedimentary and loose pyroclastic deposits and from fractured or weathered volcanic and basement rocks through deep wells. Embankment dams are also sources of water for domestic animals and livestock. Surface water like the Bilate River and water of lakes is used for domestic, livestock and irrigation purposes in nearby settlements. The supply of safe water is not equal in all of the Weredas of the region.

1.3 Land Use and Land Cover

Poor land use practices, improper management systems and lack of appropriate soil conservation measures have played a major role in causing land degradation problems in the country. Because of the rugged terrain, the rates of soil erosion and land degradation in Ethiopia are high. Setegn (2010) mentions the soil depth of more than 34 % of the Ethiopian territory is already less than 35 cm, indicating that Ethiopia loses a large volume of fertile soil every year and the degradation of land through soil erosion is increasing at a high rate. The highlands and some parts of the Rift Valley floor are now so seriously eroded that they will no longer be economically productive in the foreseeable future.

The land and water resources are in danger due to the rapid growth of the population, deforestation and overgrazing, soil erosion, sediment deposition, storage capacity reduction, drainage and water logging, flooding, and pollutant transport. In recent years there has been an increased concern over climate change caused by increasing concentrations of CO₂ and other trace gases in the atmosphere. A major effect of climate change is alterations in the hydrologic cycles and changes in water availability. Increased evaporation combined with changes in precipitation characteristics has the potential to affect runoff, frequency and intensity of floods and droughts, soil moisture, and water supplies for irrigation and generation of hydroelectric power.

Human interference in the physical environment is great due to the high population growth rate and migration of people resulted in people searching for additional farmlands by clearing the existing small patches of vegetation cover. Sheet and gully types of soil erosion are mainly observed. Cultivation and deforestation have considerably changed the natural vegetation cover over much of the area, aggravating the rates of weathering and erosion; farming is also practiced on slopes, which can add to the erosion rate. Large areas have been totally devastated by sheet erosion of soil. Some areas to the north of Lake Abaya (Fig. 1.3) are protected to enable the soil to recover.

Land cover includes cultivated land (large scale farms and family farms with different intensity of cultivation), vegetation (shrub lands and natural forest, grassland riparian vegetation, swamp), manmade features (urban or built-up areas), rocky outcrops, bare sand/soil, and water bodies. Land cover is shown in Fig. 1.4. The land use is characterized according to FAO-UNESCO (2000) by the arrangements, activities and inputs people undertake in a certain land cover type to produce change or maintain it.

Land use information is derived from land cover maps and provides land use classes. It shows that only a part of the Dila area is not cultivated. The floor of the Rift Valley is used for irrigation to plant different types of vegetation and fruit. This land use classified as "Intensive Annual Crop Production" describes areas where annual crops (cereals, pulses, oilseeds and vegetables) are cultivated. "Intensive Perennial and Annual Crop Production" describes areas of mixed agriculture

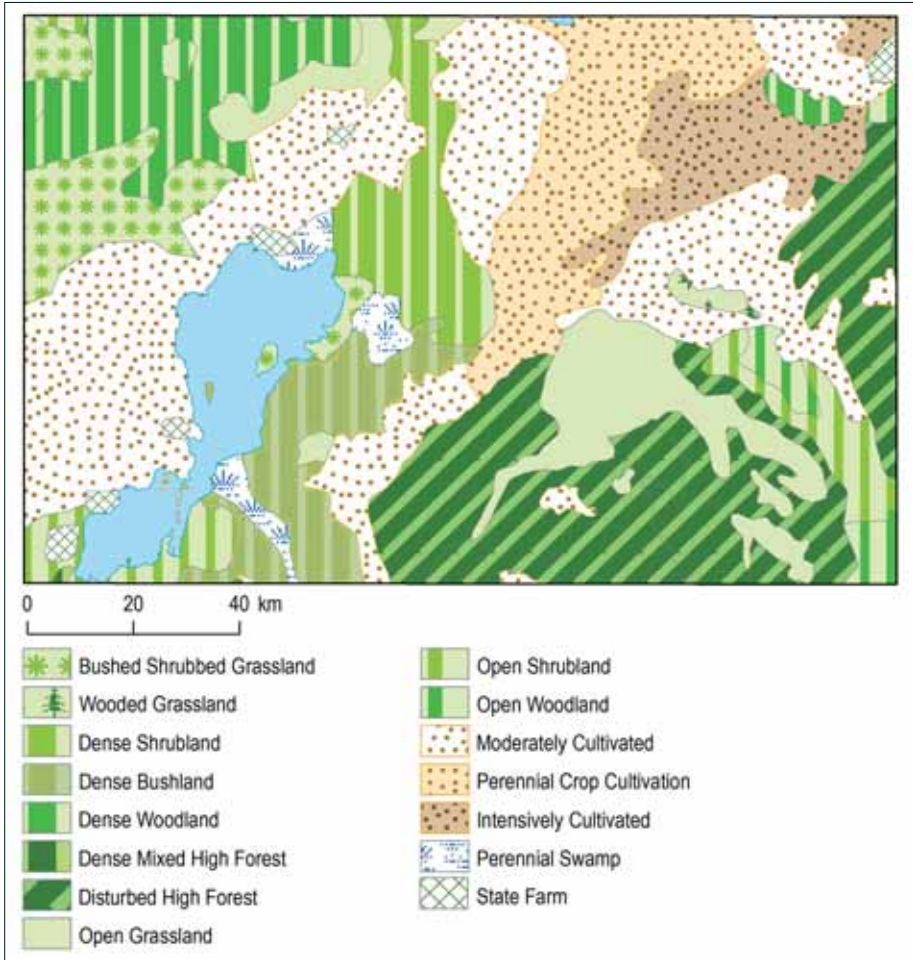


Fig. 1.3 Recovering of devastated landscape to the north of Lake Abaya

where both perennial (enset, coffee, chat, fruit trees, bananas, etc) and annual crops are the main sources of income. "Pastoral-Grazing and Browsing with some fuel wood production" is extensive throughout the area and ranges from afro-alpine vegetation in Sidama in the east to woodland, shrub land, wooded grassland and even bare land with some vegetation in the center of the area.

Vegetation

Vegetation cover helps to minimize water loss and soil degradation. The type of vegetation and its distribution in the area varies mainly based on temperature, altitude, soil type and humidity and/or precipitation. The population density is also an important factor for vegetation cover. Most of the Dila map sheet is covered with agricultural land. The vegetation types are varied from place to place. Eucalyptus trees, Junipers, Hagenia abyssinica, Podocarpus grcilior (zigba), and Vernonia amygdalina (bisana) are common on the highland plateaus. The low land area especially

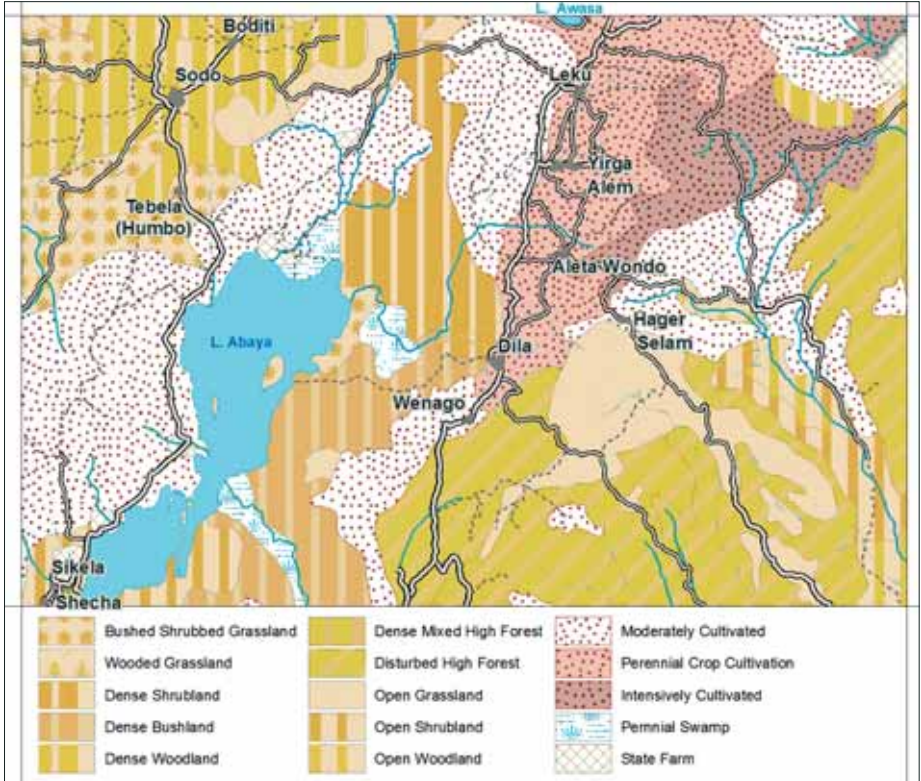


Fig. 1.4 Land cover

the rift floor is dominated by acacia 'girar', thorn bushes, small shrubs and many undifferentiated evergreen plants. Natural vegetation can be classified into forest (Wondo Genet area), woodland and savanna regions.



Fig. 1.5 Grass plains and open shrublands in the Nech Sar National Park

2. Selected Physical and Geographical Settings

The entire study area is located in the Rift Valley, adjacent rift escarpment and parts of eastern and western Ethiopian Plateau dissected by river valleys.

2.1 Geomorphology

The geomorphology of the area is highly variable and it is generally the result of repeated volcanic and tectonic events with the associated erosion of volcanic rocks and deposition processes. The principal feature of the Rift Valley is that it is a graben, a block fault geological structure in which the floor of the valley has become vertically displaced with respect to the valley sides. The tectonic activity and lithological variation in the area also partly or wholly control the drainage density

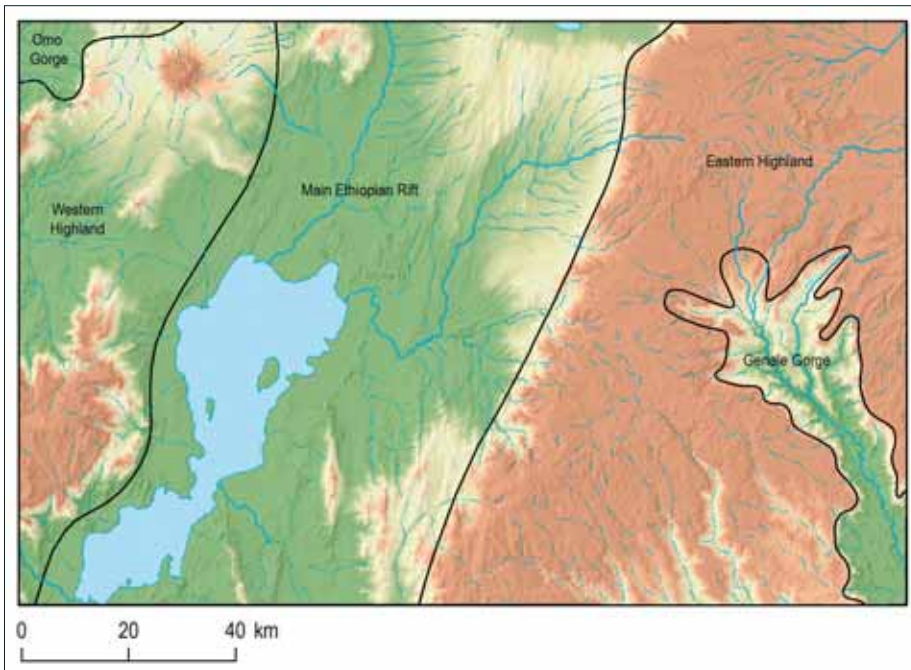


Fig. 2.1 Generalized geomorphological units

and drainage pattern. Most of the river channels follow the young lineaments and discharge their water into lakes at the bottom of the rift. The most distinct geomorphological units are shown in Fig. 2.1. The units are characterized by distinct processes and evolution displayed in a scheme of geomorphological classes (Fig. 2.2).

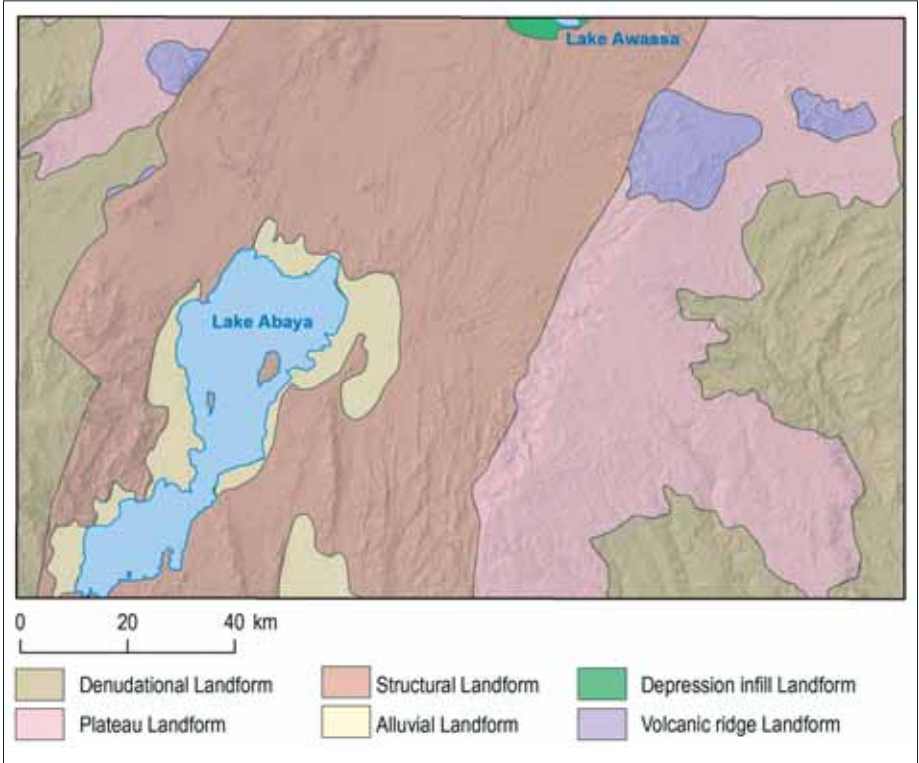


Fig. 2.2 Generalized geomorphological classes

Elevation in the study area copies its main geomorphological parts and is between 1,200 and 1,700 m a.s.l. on the Rift Valley floor, raising along the escarpment to an elevation of about 2,600 m a.s.l. The edge of the plateau is flanked by high volcanic complexes with an elevation from 2,970 to 3,270 m a.s.l. A detailed description of the main geomorphological categories is as follows:

MER floor (Lake Abaya 1,184.19 m a.s.l. – Lake Awasa 1,690 m a.s.l.) covering about 7,865 km² (46 %) is located in the central part of the map (Fig. 2.3). Sedimentary formations form a flat plain and are eroded only along river/wadi banks and dominant volcanic structures are located throughout the whole rift floor. The area between the lakes of Abaya and Hawasa is almost flat in the valley bed with several mounds of hills in the west and volcanic bodies. The hills are mostly in the shape of a cone or semi-conical crests that leave evidence of past volcanic activity.

Rift Escarpment (1,200–2,600 m a.s.l.) covering 2,016 km² (12 %) rises on both edges of the rift, connecting its bottom with the eastern and western highlands. The escarpment is delineated by many fault bounded blocks (Fig. 2.4). The margins of the rift are characterized by a few widely



Fig. 2.3 Floor of the MER in its narrow segment near Arba Minch



Fig. 2.4 Rift scarp to the north of Arba Minch

spaced faults with very large vertical displacements to the rift floor. The eastern margin is well developed and is defined by a more or less continuous system of faults, whereas the western border is marked by only a few major faults in the Arba Minch area. The tectonic escarpment itself is formed by a narrow strip of blocks, but for hydrogeological assessment this narrow strip was enlarged up to the main water divide bounding the Rift Valley Lakes basin.

Eastern and western highlands – plateau (2,600–3,550 m a.s.l.) covering 7,389 km² (42 %) in the eastern and western part of the map sheet. The landform in this region is a result of major regional tectonics and associated volcanism. In addition, residual landforms also dominate this region due to the weathering of volcanic products. The highest peak area (nameless mountain 3,338 m a.s.l.) is located on the edge of the eastern plateau in the area of Mt. Holo and the second highest peak (nameless mountain 3,273 m a.s.l.) is located on the edge of the western plateau in the Chencha area.

Omo and Genale Gorges

The Omo and Genale (Fig. 2.5) river gorges are found in the north western and eastern corners of the study area forming a deep valley cut in the western and eastern highlands (representing about 3 and 7 % of the highlands area).



Fig. 2.5 Genale Gorge

2.2 Soil and Vegetation Cover

Soil and vegetation cover reflects the basic climatic condition of the area as well as the regional and site specific hydrological, meteorological, geological, geomorphological and erosion characteristics. Part of the central area was cultivated but the types of cultivation led to devastation of the soil, its erosion by left tributaries of the Bilate River and right tributaries of the Gidabo River, and movement of soil into Lake Abaya.

Soil

Soils store rainwater in their pores before it infiltrates to greater depths and recharges the aquifer system. Water stored in upper layers evaporates directly. Soil water that is stored in deeper layers is absorbed by vegetation roots then transpires to leaves where it is evaporated. The amount of evapotranspiration from soils is controlled by soil attributes such as texture, structure and moisture content, therefore the ability of soils to store and transport water is different for every soil type. Deeper soil has a larger moisture reserve than thinner soil, which can supply more water to be evaporated. The development of soils depends primarily on geological and climatic conditions. Soils are formed from different types of rocks and occurrence is restricted to these parent rocks and along the transporting agents. The hydrology of soils is dependent on the texture of the rocks and the degree of weathering. Soils derived from coarse-grained rocks inherit a coarse texture, whereas those derived from fine-grained rocks are characterized by a fine texture. They are variable in spatial distribution even in the same climate zone. The soil classes used for soil water balance and groundwater recharge evaluation are based on the hydrological properties of the FAO classification of soil (FAO-UNESCO 2000). According to the soil map provided by the Ministry of Agriculture, the study area is covered by eight major types of soil Cambisols, Luvisols, Vertisols, Fluvisols, Nitisols, Lithosols, Andosols, Acrisols.

Vegetation

The vegetation cover of an area helps to minimize water loss or degradation through surface runoff or flooding by intercepting rainfall and increasing infiltration of water to the soil and groundwater. The type of vegetation and its distribution in the area varies mainly based on

temperature, altitude, soil type and humidity and/or precipitation. The population density is also an important factor for vegetation cover. Most of the Dila map sheet is covered with agricultural land. The vegetation types of the area are varied from place to place. Eucalyptus trees, Junipers, *Hagenia abyssinica*, *Podocarpus gracilior* (zigba), and *Vernonia amygdalina* (bisana) are common on the highland plateaus. The lowland areas especially the rift floor are dominated by acacia 'girar', thorn bushes, small shrubs and many undifferentiated ever green plants. Natural vegetation can be classified into regions of forest (Sidamo area), woodland and savanna. Cultivation and deforestation have considerably changed the natural vegetation cover over much of the area, aggravating the rates of weathering and erosion.

2.3 Climatic Characteristics

The area is climatically highly variable and is mainly characterized by the subtropical Weina Dega on the rift floor and temperate to humid Dega climatic zones on the escarpment and adjacent highlands. The highest point of the map is characterized by sub-alpine Wurch and the bottoms of the Omo and Genale river gorges and areas adjacent to the Abaya Lake are characterized by arid Kolla climatic zones. The rainy season within the area passes from March to May and from July to October. The mean annual rainfall is about 1,100 mm. The mean annual temperature is about 20°C. The weather of the Dila map sheet is mainly controlled by the seasonal migration of the inter-tropical convergence zone (ITCZ), which is conditioned by the convergence of trade winds of the northern and southern hemispheres and the associated atmospheric circulation.

2.3.1 Climatic Zones and Measurements

The climatic conditions of Ethiopia are mostly dominated by altitude. According to Daniel Gamatchu (1977) there are wide varieties in climatic zones. Climatic zones defined by Javier Gozálbz and Dulce Cebrián (2006) and Tesfaye Chernet (1993) are shown in Tab. 2.1.

Tab. 2.1 Ethiopian climate classification (Part 1)

Name / Altitude / Mean annual temperature	Precipitation below 900 mm	Precipitation between 900 and 1,400 mm	Precipitation above 1,400 mm
High Wurch (Kur) above 3,700 m below 5 °C			Afro-alpine meadows of grazing land and steppes, no farming <i>Helichrysum, Lobelia</i>
Wurch (Kur) 3,200–3,700 m 5–10 °C		Sub-afroalpine barley <i>Erica, Hypericum</i>	Sub-afroalpine barley <i>Erica, Hypericum</i>
Dega 2,300–3,200 m 10–15 °C		Afro-mountain (temperate) forest – woodland barley, wheat, pulses <i>Juniperus, Hagenia, Podocarpus</i>	Afro-mountain (temperate) bamboo forest barley, wheat, nug, pulses <i>Juniperus, Hagenia, Podocarpus, bamboo</i>
Weina Dega 1,500–2,300 m 15–20 °C	Savannah (sub-tropical) wheat, teff, some corn acacia savannah	Shrub-savannah (sub-tropical) corn, sorghum, teff, enset, nug, wheat, barley <i>Acacia, Cordia, Ficus</i>	Wooded savannah (sub-tropical) corn, teff, nug, enset, barley <i>Acacia, Cordia, Ficus, bamboo</i>

Tab. 2.1. Ethiopian climate classification (Part 2)

Name / Altitude / Mean annual temperature	Precipitation below 900 mm	Precipitation between 900 and 1,400 mm	Precipitation above 1,400 mm
Kolla 500–1,500 m above 30 °C	Tropical sorghum and teff acacia bushes	Tropical sorghum, teff, nug, penuts <i>Acacia, Cordia, Ficus</i>	Wet tropical mango, sugar cane, corn, coffee, oranges <i>Cyathea, Albizia</i>
Bereha below 500 m above 40 °C	Semi-desert and desert crops only with irrigation thorny acacias, <i>Commiphora</i>		

Remark: after Javier Gozálbex and Dulce Cebrián (2006), Tesfaye Chernet (1993)

Climatic zones of the project area defined based on elevation and precipitation are shown in Fig. 2.6.

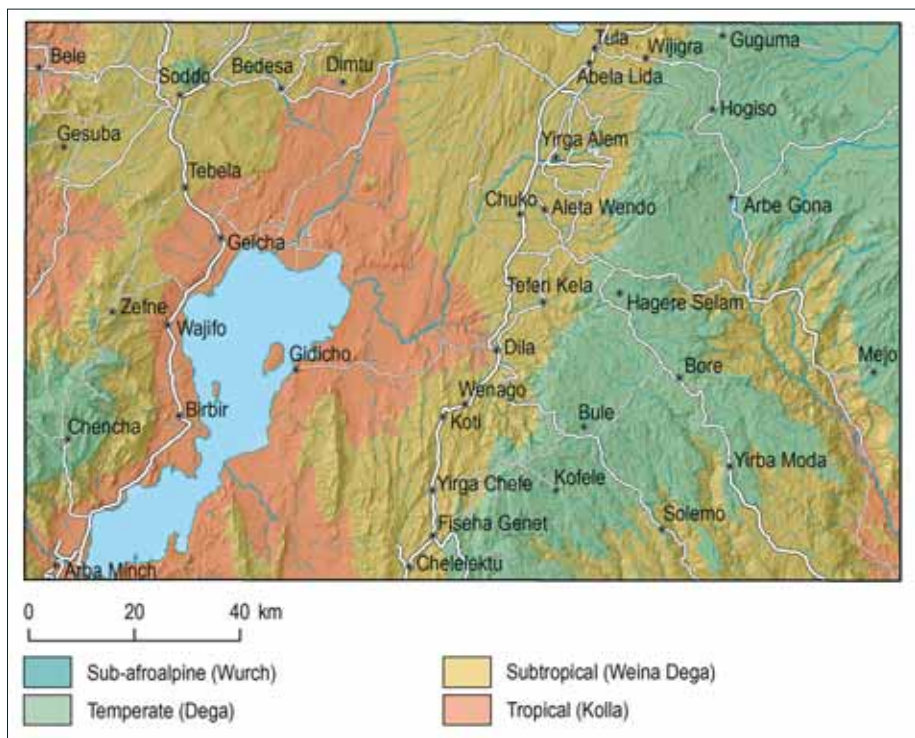


Fig. 2.6 Climatic zones

The outstanding modern quantitative climatic classification of Koeppen (1989) defines the climatic types according to the values of temperature and precipitation regardless of the

geographic location of the region. Criteria for classification of principal climatic types in a modified Koeppen system are based on mean annual and mean monthly precipitation and temperature values. The actual application of the Koeppen system to climatological statistics shows that the Ethiopian climate is grouped into three main categories, each divided into three or more types making a total of 11 principal climatic types. The Rift Valley bottom belongs to the Bsh – hot semi-arid climate and Aw – tropical climate with distinct dry winters, whereas the plateau area belongs to the Cwb – warm temperate rainy climate with dry winters.

There are a large number of meteorological stations operated by the Meteorological Institute and WMO within the mapped area and several others are located in the near surroundings.

The mean annual ambient air temperature of Dila is 20.8 °C and 19.3 °C in Wolata Sodo (Tab 2.2). Minimum, maximum and mean temperatures were calculated from the original data supplied by NMSA. The hottest months are in February and August and the coldest in December and January in Dila and in Wolaita Sodo they are February and July, respectively.

Tab. 2.2 Mean and extreme monthly temperature [°C] of Dila and Woleita Sodo

	Dila			Wolaita Sodo		
	Mean	Mean Max	Mean Min	Mean	Mean max	Mean min
Jan	20.1	30	10.2	20.2	27	13.3
Feb	20.9	31.3	10.4	21.2	28	14.4
Mar	21.8	31	12.6	21.0	27.6	14.3
Apr	21.15	28.5	13.8	20.0	26	13.9
May	20.4	27.4	13.4	19.4	25	13.7
Jun	20.0	26.5	13.4	18.2	23.1	13.3
Jul	22.1	30	14.1	17.2	21.7	12.6
Aug	22.7	31.3	14.1	17.5	22.1	12.8
Sep	22.2	31	13.4	18.4	23.9	12.9
Oct	20.9	28.5	13.3	19.1	25.1	13
Nov	19.4	27.4	11.4	20.1	26.6	13.5
Dec	18.4	26.5	10.2	20.1	26.9	13.3
Average	20.8			19.3		

The analysis of temperature trends was made by NMSA (1996) for the annual minimum temperatures, which were expressed in terms of temperature differences from the mean and averaged for 40 stations. There has been a warming trend in the annual minimum temperature over the past 55 years. It increases by about 0.37 °C every ten years. The analysis of annual rainfall shows that precipitation remained more or less constant when averaged over the whole country.

Tab. 2.3 Wind speed in Dila and Woleita Sodo

	Wind speed	
	Dila	Woleita
Jan	0.5	2.4
Feb	0.7	2.3
Mar	0.7	2.0
Apr	0.6	1.7
May	0.5	1.5
Jun	0.5	1.4
Jul	0.4	1.7
Aug	0.4	1.8
Sep	0.4	1.4
Oct	0.4	1.7
Nov	0.4	2.6
Dec	0.5	2.6
Average	0.5	1.9

2.3.2 Wind speed and direction

An important factor controlling the deposition of pyroclastic material is wind. In Dila and Woleita Sodo the wind speed is high from January to July and the lowest wind speed is recorded in October. The mean annual wind speed is given in Tab. 2.3. According to the measured data, the prevailing wind directions differ significantly in the north-eastern and south-western part of the map sheet (Fig. 2.7 and 2.8). We adopt the data from Hawasa station for the northeast. The southwest is characterized by data measured at a station in Arba Minch. On the other hand, two seasons of different wind direction can be identified in Arba Minch (Fig. 2.7). From November until March, the winds mainly blow from northeast and east. April and October are transitional months with highly variable wind directions and from May until September up to 60 % of winds blow from the south. In June, the wind direction switches to the southwest until August, whereas during September both directions as well as wind from the south and southeast appear. The strongest winds (over 8.5 m/s) occur in Arba Minch from May until September, blowing from the south. In Hawasa the winds blow dominantly from the west from October until April and from the west, southwest and south from May until September (Fig. 2.8).

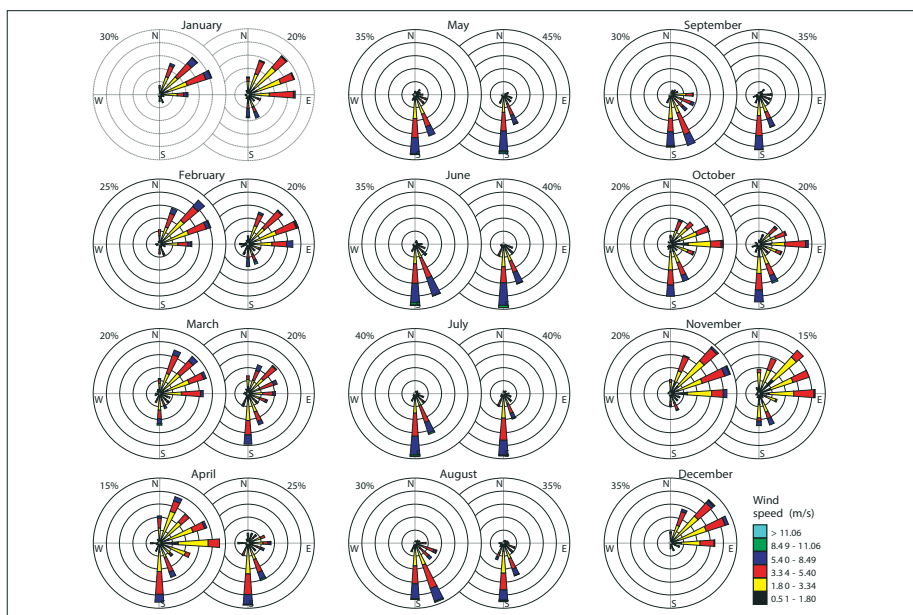


Fig. 2.7 Wind-rose diagrams for Arba Minch station, data for each month represent wind distribution at 12:00 hours (left) and 15:00 hours (right) (based on 1987–2000 data by the Ethiopian National Meteorological Agency). Concentric circles represent percentages in the distribution of wind direction (the highest value given next to the diagram for each month and time). For December, only 12:00 data are available.

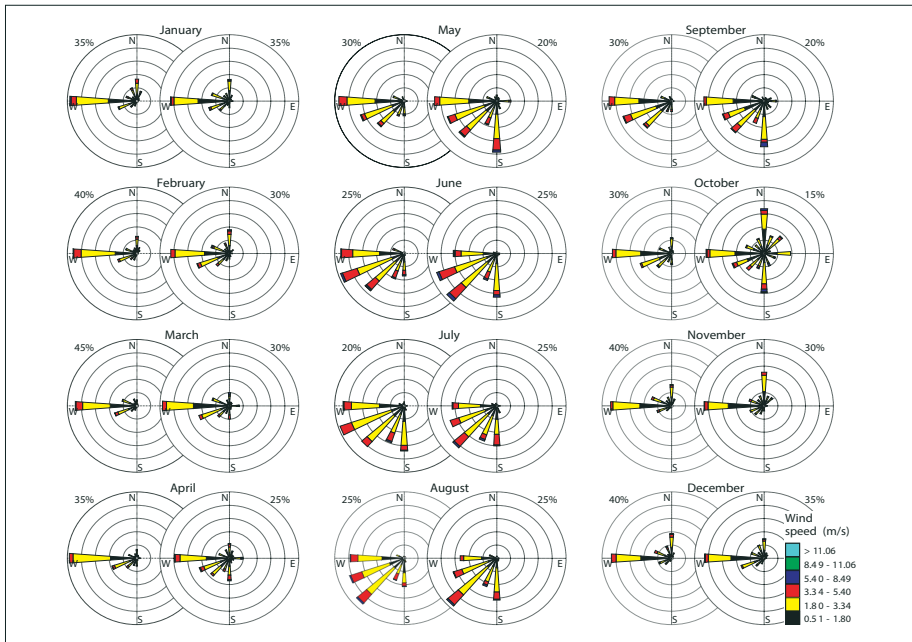


Fig. 2.8 Wind-rose diagrams for Hawasa station, data for each month represent wind distribution at 12:00 hours (left) and 15:00 hours (right) (based on 1987–2003 data by the Ethiopian National Meteorological Agency). Concentric circles represent percentages in the distribution of wind direction (the highest value given next to the diagram for each month and time).

2.3.3 Precipitation

The Ethiopian territory is divided into four zones marked as A, B, C, and D, each of them with different precipitation patterns. The seasonal classification and precipitation regimes of Ethiopia (after NMSA, 1996) are characterized in Tab. 2.4.

Tab. 2.4 Characterization of the precipitation pattern in Ethiopia

Zone	Precipitation pattern
A	This region mainly covers the central and central eastern part of the country. It is characterized by three distinct seasons, and by bimodal precipitation patterns with small peaks in April and the main rainy season during mid June to mid September with peaks in July.
B	This region covers the western part of the country. It is characterized by a single precipitation peak. Two distinct seasons, one being wet and the other dry, are encountered in this region. The analysis of mean monthly precipitation patterns shows that this zone can be split into southwestern (b1) with the wet season during February/March to October/November, western (b2) with the wet season during April/May to October/November, and northwestern (b3) with the wet season from June to September.

Tab. 2.4 Characterization of the precipitation pattern in Ethiopia

Zone	Precipitation pattern
C	This region mainly covers the southern and southeastern parts of the country. It has two distinct precipitation peaks with a dry season between. The first wet season is from March to May and the second is from September to November.
D	The Red Sea region in the extreme northeastern part of the country receives diffused precipitation with no distinct pattern; however, precipitation occurs mainly during the winter.

Tab.2.5 Mean monthly precipitation in selected stations (source Halcrow, 2008)

Station	Jan	Feb	Mar	Apr	May	Jun	Jul	Aug	Sep	Oct	Nov	Dec
Arba Minch	26.4	31.0	46.6	147.8	135.5	58.7	48.2	57.7	81.9	119.8	60.8	31.6
Dila	35.4	45.6	93.0	206.8	211.1	116.2	133.8	111.3	143.7	124.3	70.0	32.6
Hager Selam	60.4	54.3	86.9	164.0	164.8	126.8	123.0	149.0	145.7	156.4	56.1	39.7
Wolaita Sodo	34.7	44.1	83.2	166.7	183.9	139.7	201.1	184.3	109.9	99.1	48.9	33.0

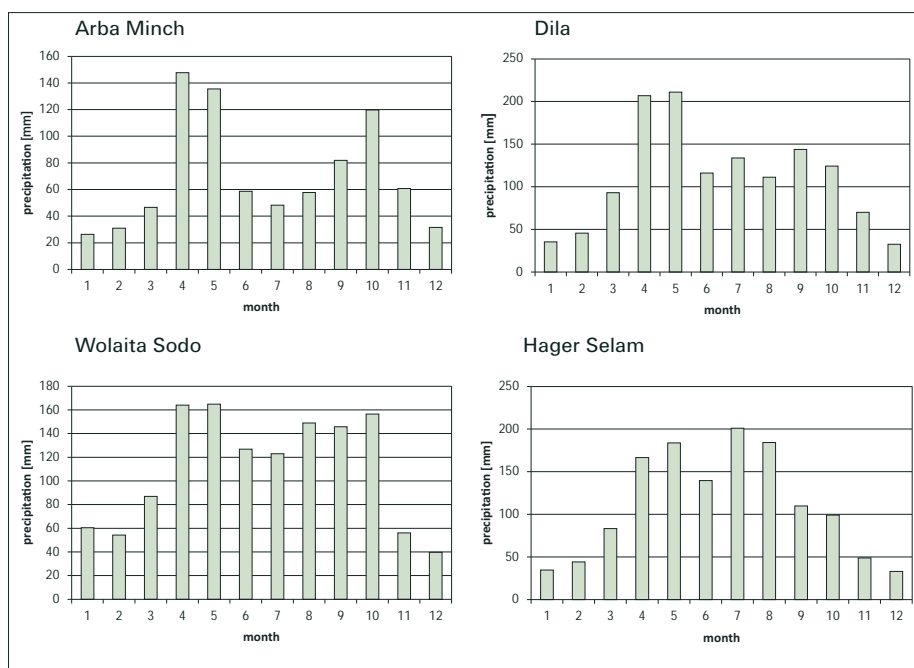


Fig. 2.9 Precipitation pattern in Arba Minch, Dila, Wolaita Sodo and Hager Selam meteo-stations

The mapped area belongs mainly to zone A which is characterized by four distinct seasons and by bimodal precipitation patterns with two peaks, the first occurring in March–May and the second September–November. The importance of rain during April is more in the southwest of the sheet. The western highlands area belongs to zone B which is characterized by a single precipitation peak. There are two distinct seasons, one being wet and the other dry. Precipitation patterns in selected stations are listed in Tab.2.5 and shown in Fig. 2.9.

The results of analyses by JICA (2012) for the average annual rainfall in Tab. 2.6. show that the values range from 492 mm to 2,582 mm, which is a 5-fold difference. This is a relatively large difference, but there is a relatively small difference in the minimum and maximum rainfall amounts at the individual stations. The average difference between the minimum and maximum for the RVLB is 62.4 % and it varies from 24 to 85 %. This shows that drought problems are chronic in the RVLB; however, the basin is not classified as a drought prone area. The study of NMSA (1996) considers an occurrence of meteorological drought when seasonal rainfall over a region is less than 19 % of its mean. In addition, a drought is classified as moderate and severe if seasonal rainfall deficiency is between 21–25 % and more than 25 %, respectively.

Tab. 2.6 Summary of precipitation data (in mm) (Part 1)

Name	Average [mm]	Max [mm]	Year	Min [mm]	Year	Rainfall deficit [%]
Aje	2,582	5,215	1982	1,111	1987	57
Alaba - Kulito	992	1,261	1993	763	1999	23
Alem Tena	826	1,042	2008	589	2002	29
Aleta Wondo	1,577	2,079	2007	1,236	1999	22
Amarokele	972	1,497	1988	672	2008	31
Angacha	1,541	2,408	2001	949	1994	38
Aposto	1,117	1,517	1989	675	1999	40
Arata	789	1,042	2010	575	2002	27
Arba Minch	880	1,283	1997	572	1976	35
Arbegona	866	1,319	1998	479	1991	45
Arsinegele	928	1,487	2004	539	2009	42
Asela	1,103	1,439	2001	780	2002	29
Awasa	969	1,198	2006	704	2009	27
Bedesa	1,109	1,347	2001	712	1999	36
Belela	1,039	1,612	2010	559	2009	46
Beto	1,018	1,525	2006	494	1999	51
Bilatetena	927	1,344	1996	405	1984	56
Bilate	793	1,111	2010	493	1999	38

Tab. 2.6 Summary of precipitation data (in mm) (Part 2)

Name	Average [mm]	Max [mm]	Year	Min [mm]	Year	Rainfall deficit [%]
Bodity	1,238	1,540	1998	952	2010	23
Buie	1,060	1,518	2010	759	1994	28
Bulbula	665	999	1989	355	1971	47
Burji	918	1,267	1972	628	1999	32
Butajira	1,089	1,783	2005	513	2009	53
Chencha	1,353	2,355	1997	757	2004	44
Dadim	659	952	2010	399	1999	39
Degaga	1,086	1,354	1996	821	2004	24
Derara	1,222	2,579	1992	823	1999	33
Dila	1,319	1,755	1958	950	1961	28
Ejersalele	822	1,263	1996	438	2002	47
Erbore	492	934	1997	211	1999	57
Fonko	1,258	1,665	1997	892	1994	29
Gato	895	1,740	1982	481	1975	46
Gedeb	1,478	2,873	1996	914	2004	38
Geresse	2,139	3,991	1996	1,163	2002	46
Gumaide	928	1,614	1989	533	2000	43
Hagere Mariam	905	1,467	1987	509	1995	44
Hosaina	1,194	1,624	1982	846	1981	29
Humbotebel	1,134	1,854	1996	680	1991	40
Jinka	1,278	1,747	1989	812	1985	36
Kamba	1,394	1,683	2010	1,096	1991	21
Kebado	1,416	1,767	1996	1,009	1991	29
Keyafer	1,215	2,323	1997	724	1994	40
Kolme	854	1,255	2006	438	1980	49
Konso	777	1,006	2001	452	2000	42
Koshe	926	1,780	1983	508	2009	45

Tab. 2.6 Summary of precipitation data (in mm) (Part 3)

Name	Average [mm]	Max [mm]	Year	Min [mm]	Year	Rainfall deficit [%]
Kulumsa	829	955	2008	708	2002	15
Kuyera	923	2,644	2008	521	1966	44
Langanoo	777	1,603	2010	465	1991	40
Meki	735	1,145	1983	387	1995	47
Mirababaya	712	1,217	1997	397	1992	44
Ogolcho	708	825	2010	544	2005	23
Shone	1,519	2,463	1997	938	1984	38
Shashemene	835	1,241	1982	402	2009	52
Sire	906	1,123	1998	534	2002	41
Teltele	711	976	1997	478	1976	33
Tora	895	1,246	1993	499	1984	44
Wajifo	2,061	3,886	2006	962	1984	53
Wolaita Sodo	1,297	2,788	1981	312	1986	76
Wondo Genet	1,135	1,477	1997	688	2009	39
Wulberg	1,262	2,196	1979	672	1981	47
Yabelo	606	874	2004	372	1999	39
Yirga Chefe	1,394	2,130	1996	964	1998	31
Ziway	740	960	1989	482	2002	35
Abomsa	1,094	1,408	1967	844	1974	23
Adami Tullu	597	962	1977	368	1932	38
Bokoji farm	1,011	1,439	1977	737	1984	27
Durame	1,062	1,595	1977	657	1984	38
Gidole	1,163	1,729	1961	934	1957	20
Jinka Baco	1,357	1,957	1957	888	1080	35
Kella	1,268	1,734	1977	833	1984	34
Kofelle	1,184	1,463	1982	969	1955	18
Kore	1,161	1,568	1983	856	1984	26

Since the data periods covered differ considerably from station to station, maximum and minimum levels of precipitation naturally appear in different years. However, based on the collected data, the maximum annual precipitation occurs in 1997 (in 9 stations), and in 2010 (in 8 stations), and the minimum annual precipitation occurs in 1999 (in 11 stations) and in 1984 and 2002 (in 8 stations). The maximum and minimum recorded levels of annual precipitation were 5,152 mm (at Aje station) and 211 mm (at Erboke station), showing a 20-fold difference. The difference between the maximum and minimum levels of precipitation from the data of a single station ranges from 247 mm (at Kulumsa station) to 4,104 mm (at Aje station). In terms of the ratio, it is within the range of 1.34 (at Kulumsa) to 8.94 (at Wolaita Sodo station).

2.4 Hydrology of the Area

The Dila area is found mainly within the RVLB, with Wabe Shebelle, Genale-Dawa and Omo-Gibe basins in east and west. The principal river basins of the area are shown in Fig. 2.10.

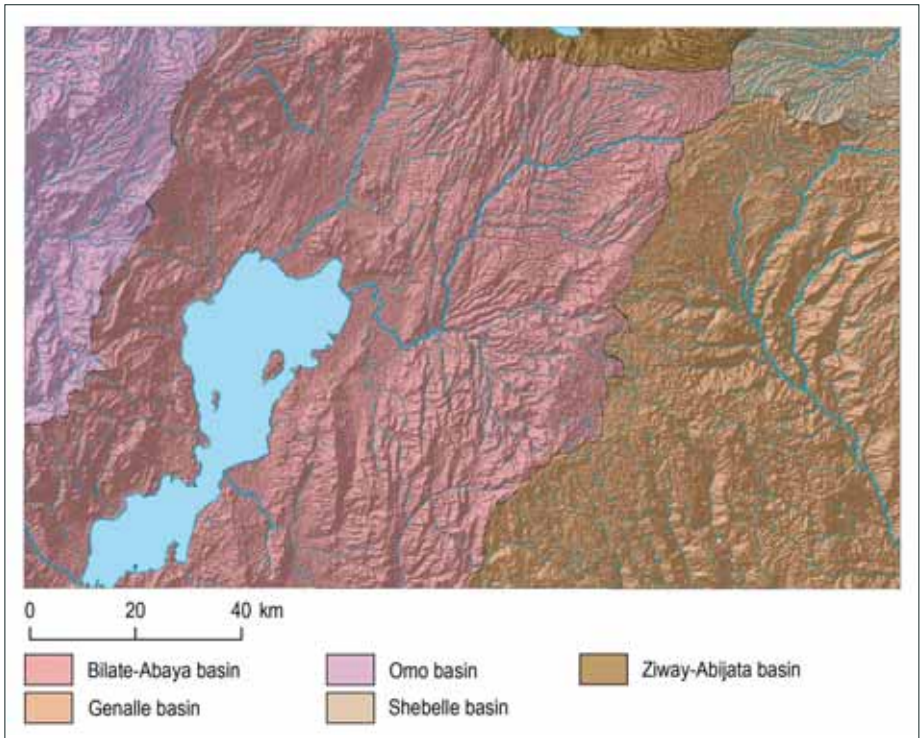


Fig. 2.10 The principal river basins of the area

2.4.1 Surface Water Network Development

The Dila topographic map sheet is divided by the main surface water divide and the largest part in the western and central part of the sheet belongs to the Rift Valley Lakes basin, the northwestern corner belongs to the Omo-Gibe basin northeastern corner belongs to the Wabe Shebelle and southeastern part belongs to the Genale-Dawa basins.



Fig. 2.11 The Bilate River is the main supply to Abaya Lake

The Omo-Gibe basin covers 1,714 km² of the sheet. The basin is drained by small rivers flowing to the western (Milike, Gamo) and northwestern direction (Kulano) from the main water divide. These are small left tributaries of the Omo River.

The Wabe Shebelle basin covers 553 km² of the sheet. The basin is drained by small streams (Arasa, Gelcha, Halila) forming tributaries of the upper reach of the Wabe River. These small rivers flow from the main water divide in a NE direction to form the Wabe Shebelle River.

The Genale -Dawa basin covers 5,576 km² of the sheet. The basin is drained by the Genale River and its small tributaries. The Genale and these small rivers flow from the main water divide in a SE direction.

The Rift Valley Lakes basin (RVLB) covers 10,491 km² of the sheet. The RVLB is a closed basin and surface water is drained by small rivers into its lakes and marshes which form the drainage for collected water. Four of the seven main lakes of the RVLB are terminal in themselves, and those which are not (Ziway, Langano and Abaya) flow into terminal lakes and are thus part of a terminal lake system. Halcrow (2008) supposes groundwater outflows from RVLB but there is no real evidence for this at this time there is little data to support this hypothesis either way. The Abaya – Chamo – Chew Bahir sub-basins are grouped as one because these lake complexes and river systems are spatial and temporally strongly interlinked. Significant inflow on the map sheet is formed by the Bilate River, which has an estimated inflow of 830 Mm³/year to the south into Lake Abaya, other rivers flowing into the lake are Gidabo, Kulfo Gina, Gelana and Amesa.

2.4.2 River Flow Regime

There are a large number of river gauging stations within the RVLB, Wabe Shebelle, Genale-Dawa and Omo-Gibe basins. Some of them are operational but many of the stations have no data.

On the Dila sheet there are 23 registered gauging stations and 3 Abaya lake level monitoring stations (see Fig. 2.22a and Fig. 2.22b), there is also a lake level station at Lake Hawasa. Other river gauging stations are within the neighboring sheets and data from these stations were also calculated for the assessment of surface as well as baseflow values and used for comparison and for correction of data from the Dila area. Records from all stations reflect the fact that the river discharge is directly proportional to the intensity of rainfall within the basin. There is a high discharge fluctuation between the wet and dry seasons of the year. The first high flow period is usually from April to May, the highest flow period is from June to October and the peak flow for majority of rivers is usually recorded in August. The period from December to March is characterized by low flow when most of the smaller rivers are completely without water. Different patterns are also known within the map area and its near surroundings. Runoff data are summarized in Tab. 2.7.

Tab. 2.7 Runoff data (Part 1)

Map ID	River	Station	Mean flow [m ³ /s]	Annual flow [mm]	Annual precip. [mm]	Area [km ²]	Specific runoff [l/s.km ²]	Dominant Aquifer
	Bilate	Nr Alaba	11.06	174.0	1,131	2,009.0	5.50	Volcanic/floor
	Wesha	Wondo Genet	0.63	497.0	1,139	40.0	15.80	Volcanic/esc
	Guder	Nr Hosaina	1.18	247.0	1,270	151.0	7.80	Volcanic/esc
	Butara / Werka	Nr Wondo Genet	0.26	200.0	1,140	41.0	6.30	Volcanic/esc
	Sokie	Nr Ajora Falls	1.96	ND	1,250	ND	ND	Volcanic/plat
	Ajanchon	Nr Areka	1.17	121.0	1,250*	306.0	3.80	Volcanic/plat
	Shopa	Nr Areka	1.45	2,408.0	1,250*	19.0	76.30	Volcanic/plat
	Weibo	Nr Areka	1.75	23.0	1,250*	2,368.4	0.73	Volcanic/plat
	Sana	Nr Tunto	3.53	51.0	1,250*	2,190.0	1.60	Volcanic/plat
1	Amesa	Wajifo	ND	ND	1,537	ND	ND	Volcanic/esc
2	Amesa	Humbo	0.60	996.6	1,537	19.0	30.58	Volcanic/esc
3	Bilate	Tena	20.50	117.2	1,165	5,518.0	3.72	Volcanic/floor
4	Dimtu	Bore	4.70	5,186.0	1,700	28.6	164.30	Volcanic/plat
5	Upper Gelana	Yirga Chefe	0.25	83.0	1,140	95.0	2.63	Volcanic/floor
6	Logita	Bensa	4.50	688.3	1,700	729,4*	6.17	Volcanic/plat
7	Bonora	Daye	8.00	736.5	1,700	342,8*	23.32	Volcanic/plat
8	Gelana	Bona Kike	7.10	595.9	1,700	376,2*	18.88	Volcanic/plat
9	Ererte	Bona Kike	1.30	414.4	1,700	99,3*	13.13	Volcanic/plat
10	Morodo	Bona Kike	0.90	330.3	1,700	85,9*	10.48	Volcanic/plat
11	Konkona	Daye	1.00	606.9	1,700	52,3*	19.13	Volcanic/plat

Tab. 2.7 Runoff data (Part 2)

Map ID	River	Station	Mean flow [m ³ /s]	Annual flow [mm]	Annual precip. [mm]	Area [km ²]	Specific runoff [l/s.km ²]	Dominant Aquifer
12	Gambetu	Aroresa	4.90	572.1	1,700	270,3 ⁺	18.15	Volcanic/plat
13	Upper Genale	Girja	74.10	736.0	1,700	3,177.4 ⁺	23.32	Volcanic/plat
14	Gidabo	Aposto	6.40	312.6	1,244	646.0	9.91	Volcanic/esc
15	Gidabo	Meass		ND	1,244	72.0	ND	Volcanic/esc
16	Kolla	Aleta Wondo	2.90	443.6	1,244	206.3	14.08	Volcanic/esc
17	Sala	Dila College	4.20	1,963.6	1,244	67.5	62.22	Volcanic/esc
18	Bedesa	Dila	1.90	740.2	1,244	81.0	23.46	Volcanic/esc
19	Kulfo	Arba Minch	9.20	797.6	878	364.0	25.27	Volcanic/esc
20	40 Springs	Arba Minch		ND	878	ND	ND	Volcanic/esc
21	Harie		1.84	273.9	878	212.0	8.68	Volcanic/esc
22	Demie	ND	4.00	112.8	1,200	1,119.0	3.57	Volcanic/plat
23	Gorega	Dana	4.20	498.8	1,200	266.0	15.79	Volcanic/plat

⁺Approximation from Halcrow (2008) Isohyetal map; ND = not defined, + area approximated from map

Measured discharge of the Bilate River at the Bilate Tena river gauge in the period from 1970 to 2006 is shown in Fig. 2.11. The figure shows that the flow is relatively regular; however, the total value of annual flow and particularly maximal monthly flow can vary substantially from year

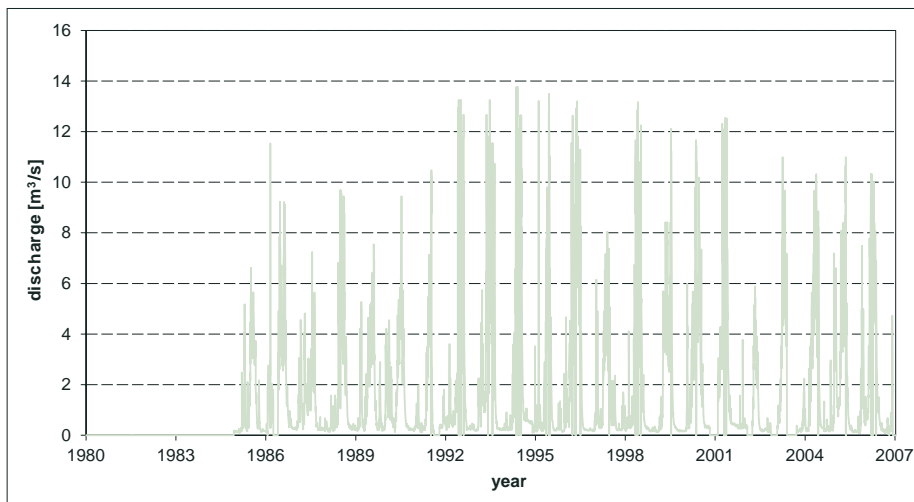


Fig. 2.11 Flow diagram of the Bilate River at the Bilate Tena river gauge

to year. The lowest discharge is usually between December and March and the river did not flow most days in the period from November 1975 to June 1976. The highest daily discharge of 284.5 m³/s (29th of June, 1986) was recorded at the river gauge. The calculated mean annual flow of 20.5 m³/s for the station represents flow generated mainly in the western highlands, escarpment and western part of the rift floor where the Bilate River originates and through which the river is flowing.

Annual variability of the mean annual flow of the Bilate River at the Bilate Tena river gauge is shown in Fig. 2.12.

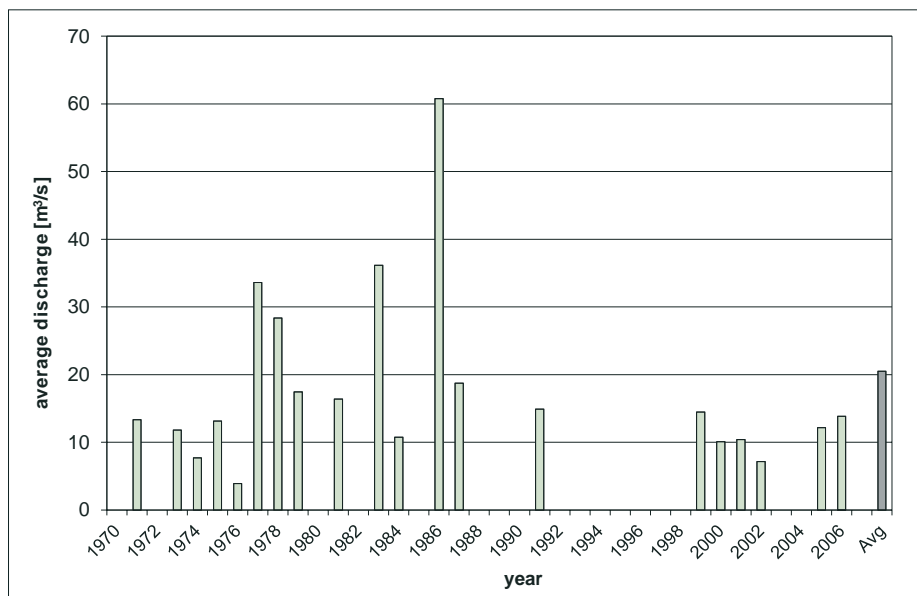


Fig. 2.12 Annual variability of the mean annual flow of the Bilate River at the Bilate Tena river gauge

Measured discharge of the Hamasa (syn. Amesa) River at the Humbo river gauge in the period from 1985 to 2006 is shown in Fig. 2.13. The figure shows that the flow is relatively regular; however, the total value of annual flow and particularly maximal monthly flow can vary substantially from year to year. The lowest daily discharge of 0.02 m³/s is a value measured many times during the period from October to April and the highest daily discharge of 23.6 m³/s (surprisingly on 23rd of November, 1997) was recorded at the river gauge. The calculated mean annual flow of 0.6 m³/s for the Humbo station represents flow generated mainly in the western escarpment where the Hamasa (syn. Amesa) River originates and which receives a relatively high volume of precipitation within the map area.

Annual variability of the mean annual flow of the Hamasa (syn. Amesa) River at the Humbo river gauge is shown in Fig. 2.14.

Measured discharge of the Kulfo River at the Arba Minch river gauge in the period from 1979 to 2008 is shown in Fig. 2.15. The figure shows that the flow is relatively regular; however, the total value of annual flow and particularly maximal monthly flow can vary substantially from year to year. The lowest daily discharge are measured in the period from November to April and the

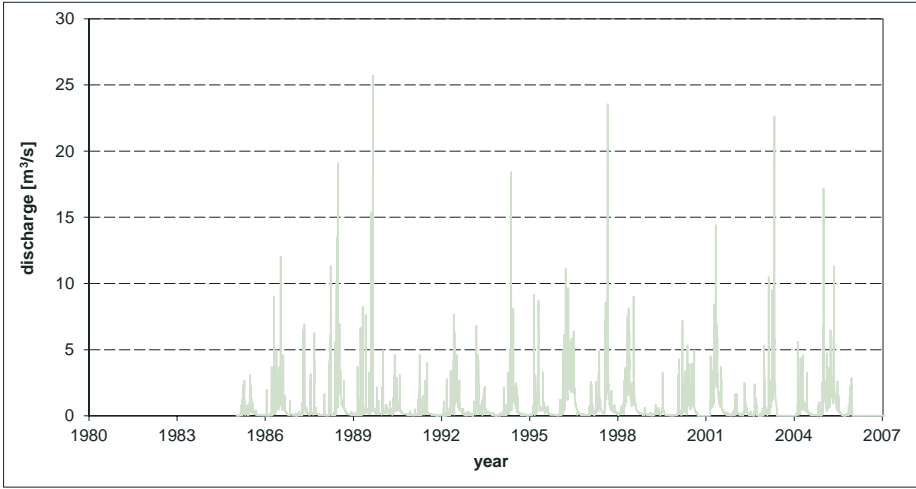


Fig. 2.13 Flow diagram of the Hamasa (syn. Amesa) River at the Humbo river gauge

river did not flow in the period from November to April in the years 1987-1989 and 1991- 1992. The highest daily discharge of 70.3 m³/s (on the 26th of October, 1997) was recorded at the river gauge. The calculated mean annual flow of 9.2 m³/s for the Arba Minch station represents flow generated mainly in the western escarpment where the Kulfo River originates and which receives a relatively high volume of precipitation within the map area.

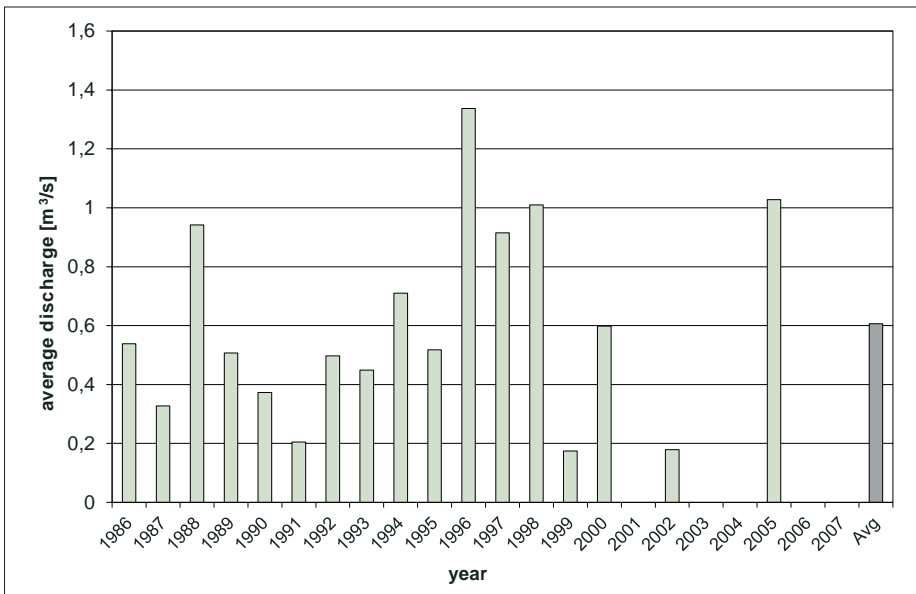


Fig. 2.14 Annual variability of the mean annual flow of the Hamasa (syn. Amesa) River at the Humbo river gauge

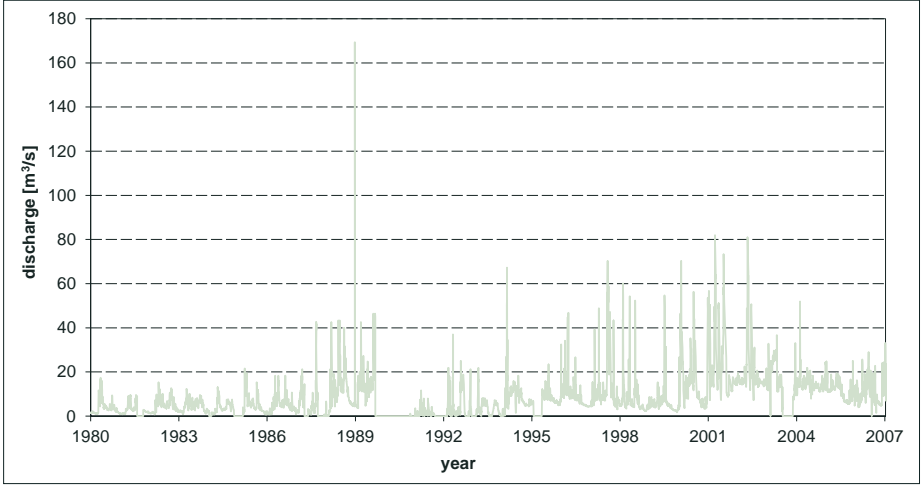


Fig. 2.15 Flow diagram of the Kulfo River at the Arba Minch river gauge

Annual variability of the mean annual flow of the Kulfo River at the Arba Minch river gauge is shown in Fig. 2.16.

Measured discharge of the Demie River (Omo river basin) in the period from 1982 to 2007 is shown in Fig. 2.17. The figure shows that the flow is relatively regular; however, the total value of annual flow and particularly maximal monthly flow can vary substantially from year to year. The

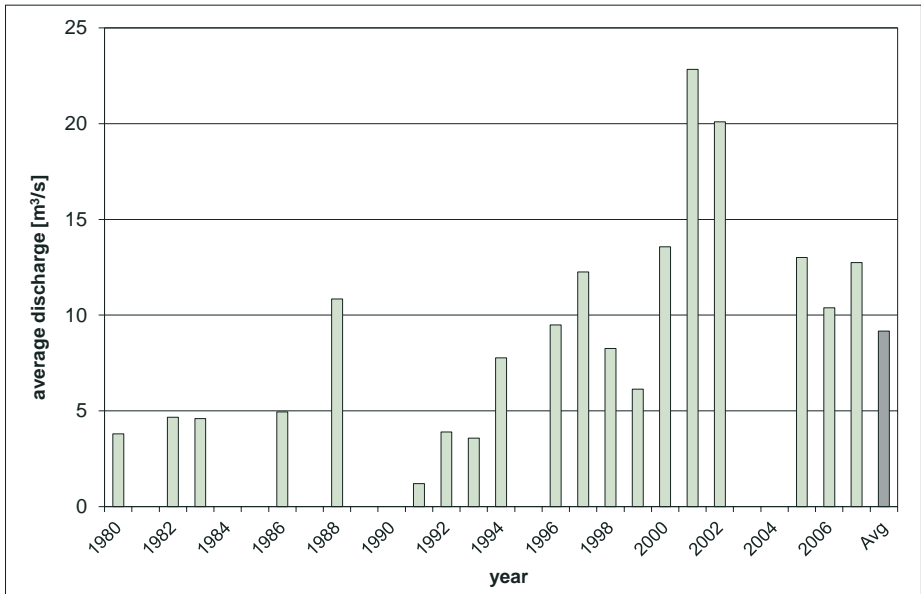


Fig. 2.16 Annual variability of the mean annual flow of the Kulfo River at the Arba Minch river gauge

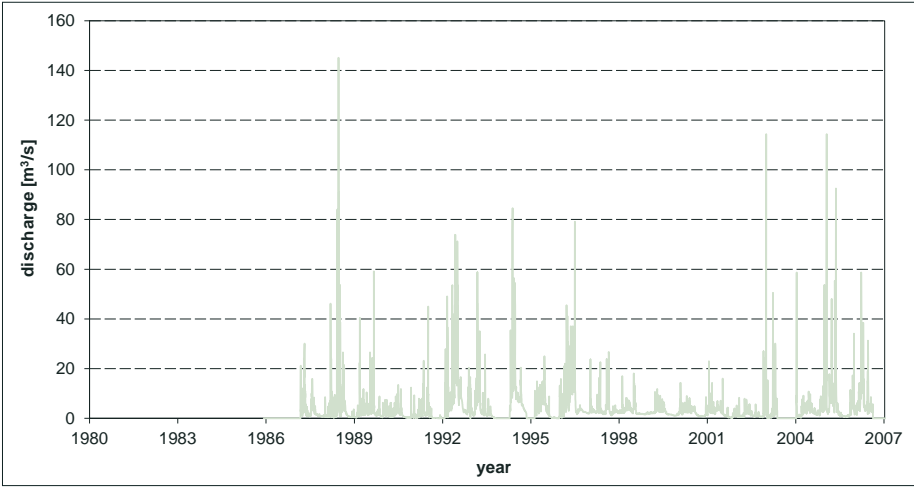


Fig. 2.17 Flow diagram of the Demie River at the river gauge

lowest daily discharge was measured in the period from November to April and the river did not flow in the period from January to March in 1992 and during February 1996. The highest daily discharge of 79.3 m³/s (on the 21st of September, 1996) was recorded at the river gauge. The calculated mean annual flow of 4.0 m³/s for the station represents flow generated mainly in the western highlands where the Demie River originates and which receives a relatively high volume of precipitation within the map area.

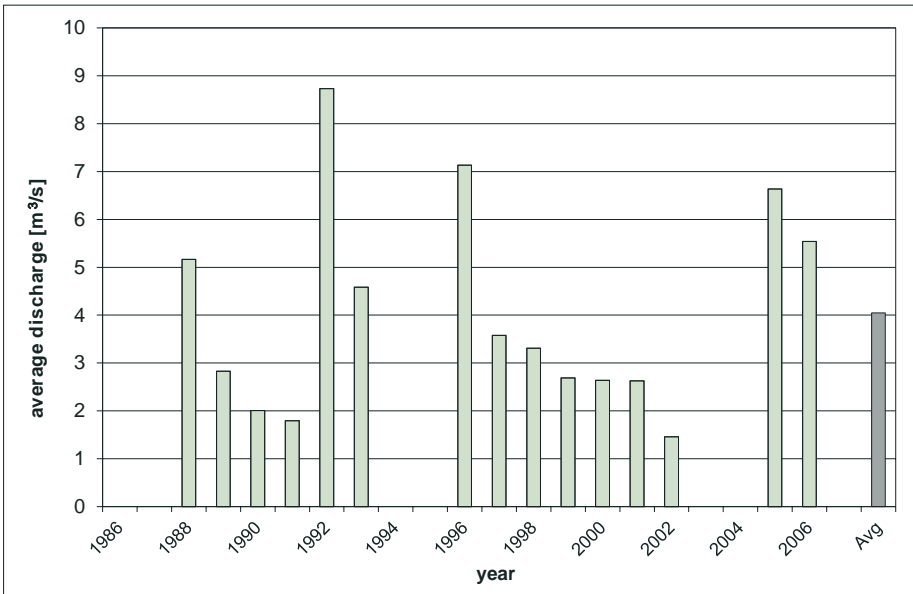


Fig. 2.18 Annual variability of the mean annual flow of the Demie River at the river gauge

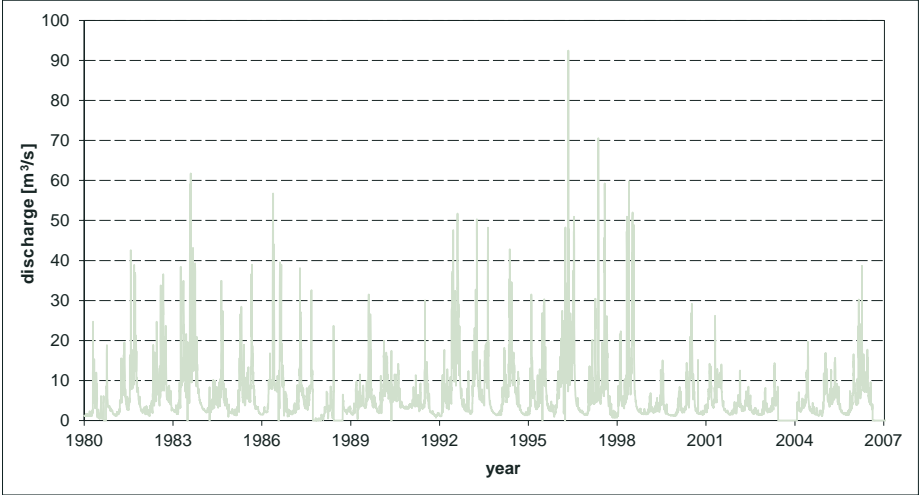


Fig. 2.19 Flow diagram of the Gidabo River at the Aposto river gauge

Annual variability of the mean annual flow of the Demie River at the river gauge is shown in Fig. 2.18.

Measured discharge of the Gidabo River at the Aposto river gauge in the period from 1979 to 2008 is shown in Fig. 2.19. The figure shows that the flow is relatively regular; however, the total value of annual flow and particularly maximal monthly flow can vary substantially from year to

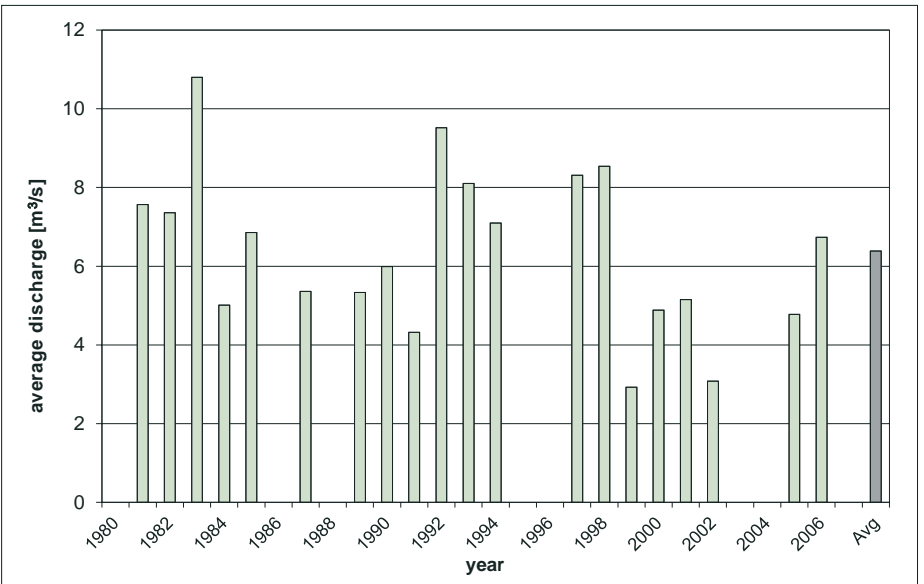


Fig. 2.20 Annual variability of the mean annual flow of the Gidabo River at the Aposto river gauge

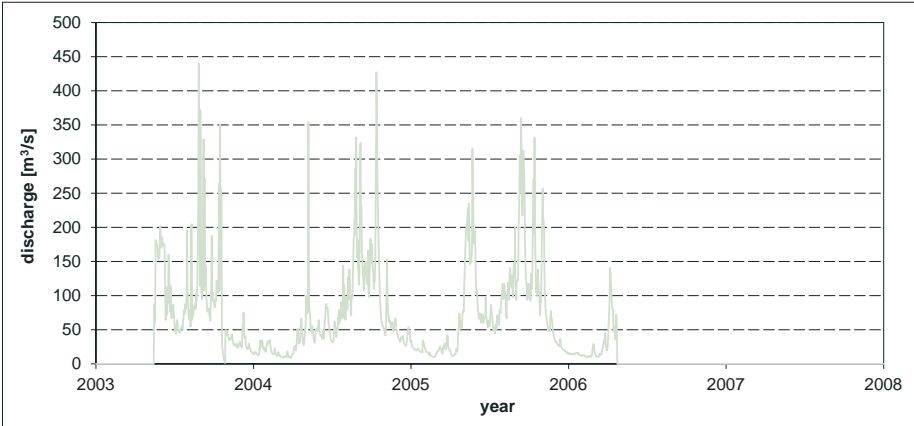


Fig. 2.21 Flow diagram of the Upper Genale River at the Girja river gauge

year. The lowest daily discharge is measured in the period from November to April and the river did not flow in the period from November to January in years 1987-1989. The highest daily discharge of 92 m³/s (on the 30th of July, 1996) was recorded at the river gauge. The calculated mean annual flow of 6.4 m³/s for the Aposto station represents flow generated mainly in the eastern escarpment where the Gidabo River originates and eastern part of the rift floor through which the river is flowing. This area receives a relatively high volume of precipitation within the map area.

Annual variability of the mean annual flow of the Gidabo River at the Aposto river gauge is shown in Fig. 2.20.

Discharge of the Upper Genale River measured at the Girja river gauge for a short period from 2003 to 2005 is shown in Fig. 2.21. The figure shows that the flow is relatively regular in 2004 and 2005. The lowest daily discharge was measured in October to April (1.22 m³/s on the 27th of October, 2003). The highest daily discharge of 439 m³/s (on the 27th of August, 2003) was recorded at the river gauge. The calculated mean annual flow of 74.1 m³/s from the two years of measurement at

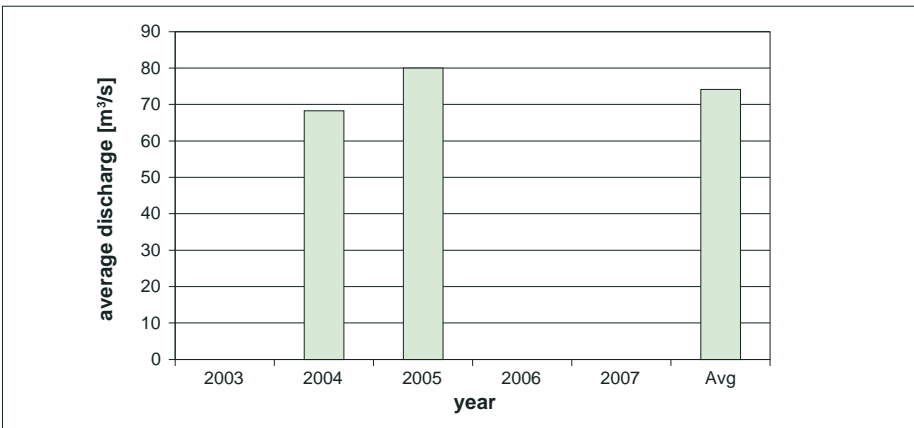


Fig. 2.22 Annual variability of the mean annual flow of the Upper Genale River at the Girja river gauge

the Girja station represents flow generated mainly in the eastern highlands where the Upper Genale River originates and which receives relatively high precipitation within the map area.

Annual variability of the mean annual flow of the Upper Genale River at the Girja river gauge is shown in Fig. 2.22.

The assessment of specific runoff based on data from flow measurements and calculated specific runoff in the gauging stations is shown in Tab. 2.14 and the appropriate area of the pertinent river basin within the Dila sheet considering the altitude and rock composition of the area.

The specific runoff is assessed for the Dila sheet based on data from the river gauges shown in Tab. 2.7, and is as follows:

- 16.0 l/s.km² for the eastern highlands,
- 10.0 l/s.km² for the western highlands,
- 16.0 l/s.km² for the RVLB escarpment areas
- 4.0 l/s.km² for the RVLB, excluding escarpment areas

Soil erosion due to deforestation and farming of marginal lands on steep slopes is a major concern in the area, as well as the resulting potential for lake sedimentation (Halcrow, 2008). A sediment transport equation developed from sampling and measurements is given in a general (indicative) form for the Awassa-Abaya-Chamo basin. The western of the basin comprises the Bilate, Hamasa (syn. Amesa) River and Hare rivers flowing into Lake Abaya. The regional sediment equation is given by:

$$Q_s = 37.637 Q^{1.401} (R^2=0.77)$$

The eastern catchment comprises the Wesho River near Wendo Genet and rivers flowing into Lake Hawassa and the Sala, Gidabo, Gelana and Kola rivers flowing into Lake Abaya. The regional sediment equation is given by:

$$Q_s = 13.237 Q^{1.204} (R^2=0.69)$$

Q_s = Suspended sediment transport rate (tons/day)
 Q = Discharge (m³/s)

2.4.3 Lakes

There are two lakes in the area, namely Abaya and Awasa. Lake Awasa covers only a very small part in the north and it was described in detail in the explanatory notes for the Hosaina sheet (Tilahun and Šima, 2013). Lake Chamo is located to the south of the area but it is connected by the Kulfo River with Lake Abaya. Monthly measurements of lake levels are conducted at stations of which a list is given in Tab. 2.8. A commentary on recorded lake levels by Halcrow (2008) is given as follows:

- A review and updating of the rating equations at station 082005 (Bilate) is required to address non-stationarity of the flow record, enabling verification of the flow record discharging into Lake Abaya.
- The installation of a gauging station on the Gidabo River downstream of its confluence with river Bala, enabling an improved estimate of the discharge into Lake Abaya. This has previously been identified by the MoWR as a priority undertaking.
- According to site suitability and access constraints, a review of the downstream gauging station on the Gelana River (082017) to identify whether the station should be reopened or the installation of a new gauging station near the discharge of the Gelana River into Lake Abaya, enabling an improved estimate of the discharge into Lake Abaya. This has previously been identified by the MoWR as a high priority undertaking.

Tab. 2.8 Lake level stations

Map_ID	Lake name	Site	X UTM	Y UTM	Altitude [m a.s.l.]	Start date	End date
L1	Abaya	Nr Arba Minch (Lante) Station	345053	665614	1,179	Jul 1969	Apr 2006
L2	Abaya	Nr Arba Minch (old)	348402	676662	1,185	Jan 1970	Oct 2005
L3	Abaya	Gidicho Odola island	383878	707540	1,184	Feb 1986	Dec 2001

Basic descriptive data about the lakes are given in Tab. 2.9.

Tab. 2.9 Basic characteristics of lakes

Lake	Elevation [m a.s.l.]	Max. depth [m]	Mean depth [m]	Surface area [km ²]	Storage volume [Mm ³]	Level fluctuation [m]	Salinity [g/l]
Awasa	1,500–1,687	20 (32.2)	10.7	130	1,300	3.49	0.7
Cheleleka	1,686	Filled with silt since 1972					
Abaya	1,171	12	7	1,121	9,818	Lante 3.05 Old 4.19	1.0
Chamo	1,107	14	12	335	4,100	4.05	1.5

Lake Hawasa and Lake Cheleleka to the east are situated in the Hawasa caldera and were united as a single lake as recently as the 19th century (Zenaw, 2003). The existence of terraced pumiceous lacustrine sediments on both sides of the fresh transverse faulting, which limits the present Lake Hawasa basin to the north, suggests that in pluvial times this basin was connected to that of Ziway – Shalla. They were separated by post pluvial block faulting and tilting (Mohr, 1960).

The studies performed by WWDSE (2001) and by Zenaw (2003) concluded that the gradual increasing trend of the water level of Lake Hawasa is mainly caused by the gradual depletion of the physical capacity of Lake Cheleleka. The rise in the level of Lake Hawasa in recent years is perceived to be a major threat to the town of Hawasa, as the increase inundates vast areas around the lakeshore leading to many buildings, properties and infrastructures being ruined and also people living around the lake being displaced.

In general, a rehabilitation program is necessary to minimize erosion and flooding in the catchments. The catchments of Hawasa and Abaya lakes need soil and water conservation measures such as reforestation, construction of check dams across gullies, and terracing etc. This is an affective and lasting solution to mitigate the lake level rise problem in both lakes.

The Rift Valley floor is dominated by **Lake Abaya and Lake Chamo** (Fig. 2.23) with a basin area of 18,118 km². Relatively large basins of the Bilate (5,900 km²) to the north, and the Gidabo (3,447 km²) and Gelana (3463 km²) to the east drain the western and eastern highlands. Their flow contributes significantly to the water level of Lake Abaya. Rivers flowing from the western escarpment contribute less but they bring a large amount of sediments particularly to Lake Abaya. Abaya and Chamo lakes form a single basin because the two lakes are hydrologically interconnected

to the River Kulfo, transferring water from Lake Abaya into Lake Chamo with a difference in levels between the lakes of 61 m. Outflow from Lake Abaya with River Kulfo and other rivers such as the Sile and Sege and an ephemeral stream to the south contribute to Lake Chamo. Halcrow (2008) mentioned that there is some flow from Lake Chamo to the Segen River, towards Lake Chew Bahir, when lake levels are extremely high.



Fig. 2.23 Lake Chamo, seen from Tosa Sucha (God's Bridge)

Currently, three large-scale irrigation schemes are planned by the MoWR for rivers contributing to Lake Abaya. On the Gelana River there are plans for a net irrigation command area of 5,356 ha. The command area currently being considered for the River Gidabo has a net area of 9,215 ha, and there are plans for a rehabilitation scheme for existing state farms on the Lower Bilate River providing a net area of 7,715 ha.

Bed load to Lake Abaya is assumed to be 8 % of the suspended sediment load, given an average total sediment load of approximately 27,000 tons/year. (Study and Design of Gelana, Gidabo and Bilate Irrigation Project, WWDSE).

The hydrological and hydrogeological conditions of the studied area have recently been comprehensively summarized by Tilahun and Šima (2014).

3. Geological Settings

The Dila sheet (NB 37-6) of the geological map at a scale of 1 : 250,000 is located in the central part of the NNE – SSW to NE – SW trending Main Ethiopian Rift which belongs to the regional East African Rift System (e.g. Hayward and Elbinger 1996; Bonini et al. 2005). The Precambrian or “basement” rocks of the Horn of Africa are divided by Kazmin (1973) into median “Archaen” domains separated by “Upper proterozoic” belts, the whole comprising part of the Mozambique Belt of Eastern Africa. Within the Main Ethiopian Rift, only one young, extensionally faulting (the Wonji fault system) belt affects the rift floor. The belt varies in the intensity of its development and progressively displaces from the western side of the rift floor to the eastern side, proceeding northward along the rift axes. In the Main Ethiopian Rift active and dormant trachyte-pantellerite caldera volcanoes are situated on the Wonji fault at fairly regular intervals of 30 to 40 km, but no such volcanoes are found in the Dila sheet area.

3.1 Previous studies

The Main Ethiopian Rift is shown in generalized form on 1:2,000,000 scale maps by Merla et al. (1973), Kazmin (1973) and Mengesha et al. (1996). Compilation of the geological maps of the Ethiopian Rift at a scale of 1:500,000 and their accompanying reports was carried out in early 1980s by Kazmin et al. (1980). More detailed maps of the central part of the rift at a scale of 1:250,000 were published by Nazret (Seife Michael, 1978), Akaki Beseka (Ephrem, 2009), and Dodola sheets (Gobena et al. 1996). During the course of the exploration of geothermal resources in the Rift Valley performed by the Geological Survey of Ethiopia, the geothermal project exploration teams produced geological maps (unpublished) of the Lake Ziway area at a scale of 1:500,000 (Berhane et al., 1976).

3.2 Stratigraphy

A general stratigraphy scheme of the area with the age and generalized lithological descriptions of the formations is shown in Tab. 3.1. The thickness of the formation is based on data published by various sources. Quaternary sediments and various volcanic rocks of Quaternary to Tertiary age cover the Rift Valley floor, tectonic escarpment and adjacent plateau.

Tab. 3.1 Lithostratigraphy of the mapped area (Part 1)

Era	Age	Formation	Thickness [m]	Lithology
Pleistocene–Holocene		Quaternary sediments	200	Re-sedimented pyroclastics, lacustrine silt, clay and diatomite
		Central volcanic complexes	850	Rhyolite, trachyte and obsidian lavas, pumices, tuffs, ignimbrites
		Basalts of the rift floor	250	Basaltic lavas, scoriae, phreatomagmatic tuffs

Tab. 3.1 Lithostratigraphy of the mapped area (Part 2)

Era	Age	Formation	Thickness [m]	Lithology
Pleistocene	1.5–0.8	Dino Formation	300	Ignimbrites, pumices
Pliocene–Pleistocene	4.5–1.5	Chilalo volcanics	700	Alkaline basalt
			850	Trachyte, trachybasalt and peralkaline rhyolite, ignimbrites
Upper Miocene–Pliocene	9.2	Nazret Group	30	Bofa basalt: mildly alkaline basalt
			800	Alkaline and peralkaline felsic ignimbrites, pumices, tuffs, ash-flow deposits, rhyolite and trachyte
Oligocene–Miocene	30–15	Alaji Group (pre-rift volcanics)	1,200	Sub- and mildly- alkaline transitional basalt and rhyolite

3.3 Lithology

Proterozoic metamorphic rocks

Biotite quartz-oligoclase gneisses and medium-grained amphibolites are exposed on the southeast part of the area covering 963 km², around the towns of Girja, Harsu, Bwanbwa Woha and Meleka. The north-south trending shear zone crosses this lithological association. The dominant rock type is biotite-quartz-oligoclase gneiss, which is leucocratic and mostly fine-grained, with a subordinate coarse-grained variety. Moderately developed thin lenticular banding indicates a certain degree of migmatitization. The second most important rock type is fine to medium-grained amphibolite which occurs mainly as bands. It is homogeneous, with rare, thin interbeds of quartzite, amphibolite and muscovite or biotite bearing schists and gneisses. Gneiss and undistinguished granites are exposed nearby Lake Abaya in the southeast part of the Nech Sar National Park along the Amaro horst.

Mafic and ultramafic rocks are exposed along the north-south trending shear zone located on the southeastern part of the map sheet. The Bonsa-Girja asphalt road crosses this unit. Mafic and ultramafic rocks are frequently weathered and/or altered (Fig. 3.1) to talc, chlorites and epidote. Fresh amphibolites are dominated by greenish amphibole and plagioclase (Fig. 3.2). Within the belt of mafic and ultramafic rocks, a granodiorite intrusion is exposed along the Wondena River. It is a light yellow and coarse-grained rock composed of K-feldspar, mica, quartz and xenocrysts. The rocks are sheared with quartz veins following a northeastern trending foliation. It also contains lineation perpendicular to that of the foliation direction with a NW orientation.

Mica-shist and chlorite-shist are exposed to the southeast of the area on the left side of the Bonsa to Kibre Mengist main road (Fig. 3.3), where these rocks form small hills along the road. The color of these muscovite- and/or chlorite-rich rocks varies from green (chloritization) to light brown (biotite admixture). These rocks are strongly weathered and highly friable.

Rocks traditionally mapped as granites are strongly deformed and locally also metamorphosed. Therefore, they should be preferably classified as metagranites or even orthogneisses. Such rocks of a granitic origin occur mostly in the southeastern part of the map sheet. In horizontal section, the granitic plugs have a circular to elliptical shape. Intrusive contacts with country rocks are sharp and homogeneous. Metagranites (Fig. 3.4) are hard, compact, coarse-grained, generally pink and characteristically coherent in hand specimens.



Fig. 3.1 Outcrop of altered greenschists and amphibolites

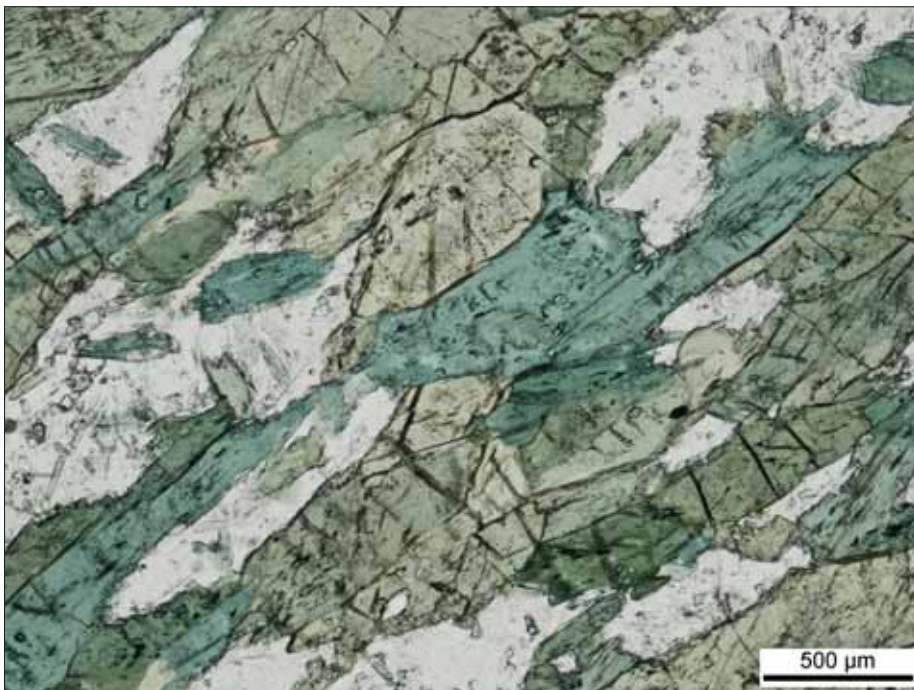


Fig. 3.2 Microphotograph of amphibolite (sample KV122). Plane-polarized light



Fig. 3.3 Outcrop of mica-shist with amphibolite dykes exposed in a road cut near Kibre Mengist



Fig. 3.4 Outcrop of metagranite

Neogene volcanic rocks (Nazret Group)

Lower basalt, rhyolites and trachyte represent the oldest volcanic rocks on the map sheet and occur in the southern and southeastern part of the map sheet covering an area of 774 km². The Lower Basalt is characterized by thick, extensive lava flows that locally show columnar jointing (Fig. 3.5) and intense weathering. There is considerable variation in texture among the flows of the Lower Basalt. This unit also comprises minor bodies of rhyolite, ignimbrite and olivine-plagioclase-phyric basalt.

Transitional mildly alkaline and subalkaline basalt and rhyolite spread from the central to southern part of the map sheet area. The towns of Dilla, Wenago, Chinchu, Bedesa, Teferi Kela, Guangua, and Kebado are constructed on this unit. The transitional mildly alkaline and subalkaline basalts are usually strongly weathered, namely along fractures and joints. Where exposed, basalts tend to create cliffs. Transitional basalts are overlain by rhyolites. Locally, this unit comprises minor ignimbrite and trachyte bodies, generally with too small an aerial extent to be mapped at actual scale.

Aphyric and porphyritic basalt with minor alkali trachyte flows and tuffs cover a large area on the southern part of the map sheet. This unit also usually caps small hills along the Bonsa (Daye) - Kibre Mengist main road on the very eastern edge of the map sheet area. Fresh aphyric basalt has a dark gray color and shows a slight to moderate degree of weathering. The color tends to change to a lighter gray to brownish shades when weathered. The subordinate vesicular basalt is brown colored and medium to highly weathered and forms cliffs. Porphyritic (px, ol-px, ol-px-plg) basalts and aphyric basalts are exposed in the southern part of the area. There are scarcely exposed trachytes in some parts of this unit but the size of trachytic plugs does not allow their presentation on a map of 1:250,000 scale.



Fig. 3.5 Columnary jointed lower basalt



Fig. 3.6 *Fiamme* in rhyolitic ignimbrite of the Dino Formation

In the northwestern and northeastern parts of the map sheet, rocks of the Nazret Formation cannot be distinguished from rocks of the Dino Formation.

Quaternary volcanic rocks (Wonji Group)

Dino Formation: Coarse unwelded pumiceous pyroclastics and ignimbrites, mixed lithology consisting of intercalations of non-welded pyroclastic deposits and non-welded to welded ignimbrites is exposed in the northern part of the map sheet around Midre Genet, Morocho and Yirga Alem. Pyroclastic deposits consist of pumice fragments within a fine ground-mass; they are light, highly friable and light gray to yellowish colored. Welded ignimbrites contain abundant black *fiamme* of compacted pumice fragments (Fig. 3.6).

Quaternary basalts and scoria cones form the Hamasa River (Humbo) Volcanic Field (Fig. 3.7) between Lake Abaya and Dimtu town. The basalt is dark gray in color whereas slightly differentiated trachybasalts are light gray. The Quaternary lavas are faulted by a system of graben parallel to the Bilate River. Numerous scoria cones rise above the basaltic lava plain.

Central Volcanoes: Pumice and unwelded tuff are surrounded by rhyolite lavas and volcano-sedimentary deposits, and are exposed on the northeastern part of the map sheet to the north of Lake Abaya. They cover an area of about 145 km². The non-welded pumice and tuff deposits were produced by voluminous rhyolitic eruptions of the Late Pleistocene to Holocene central volcanoes. Rhyolite lavas are distributed over an area of 265 km² on the northern and north eastern shores of Lake Abaya, comprising also Damota Mountain in the very northwest of the map sheet. On the surface, the rhyolites tend to be moderately to intensively weathered. The cumulated thickness of the rhyolite lavas may reach up to 900 m in the case of the central volcanoes. Intrusions of trachyte can also be found within the edifices of the central Quaternary volcanoes. Trachytic intrusion within Damota Mountain is exposed by quarry operations (Fig. 3.8). Holocene obsidian lavas can be found forming an obsidian dome complex of the Korke Seluwa Volcano near Humbo



Fig. 3.7 Aligned scoria cones within the Hamasa River (Humbo) Volcanic Field

in the northwestern part of the map sheet. The obsidians of the Korke Seluwa Volcano are rich in crystals dominated by plagioclase with less abundant Fe-clinopyroxene and Fayalite.

Quaternary sediments occur in various positions and result from distinct processes on the Dila sheet. Alluvial deposits comprising gravels, sands and silts form alluvial fans where rivers enter Lake Abaya (Fig. 3.9). A large delta of the Bilate River is located on the northern shore of Lake Baya and a large alluvial plain can be found on its western shores to the north of Arba Minch.



Fig. 3.8 Active quarry exploiting trachytic intrusion from a central rhyolitic volcano (Mt. Damota near Wolaita Sodo)

Polygenetic infill forms infill of tectonic depressions and former calderas. These deposits are dominated by resedimented pyroclastic deposits, mostly resedimented pumice and tuffs. On the map sheet, this lithology surrounds the southern margin of Lake Hawasa.

Some of the hot springs within the rift are associated with travertine and/or geysirite mounds. A group of several travertine mounds can be found at Bolocho (Fig. 3.10; Tadiwos 2011).



Fig. 3.9 Gravels of an alluvial fan filling the river channel on the shore of Lake Abaya to the north of Arba Minch

Residual clayey to silty soils of significant thicknesses represent products of in-situ intensive weathering of both volcanic and metamorphic rocks.



Fig. 3.10 Travertine mound on an active hot spring (Bolocho)

3.4 Tectonics

The geological map sheet of Dila at a scale of 1 : 250.000 is situated in the central part of the NNE – SSW to NE – SW trending Main Ethiopian Rift which is part of the East African Rift System (e.g., Hayward and Ebinger 1996; Bonini et al. 2005; Ebinger 2005). This structure recorded a typical evolution of continental rifting, from fault-dominated rift morphology in the early stages of the continental extension (transtension) toward magma-dominated extension during break-up due to extension between the Nubian and Somalian plates (e.g., Agostini et al. 2011; Acocella 2010). The mapped area itself is built by: (a) high-grade metamorphic rocks of the Neoproterozoic to lower-Palaeozoic Arabian-Nubian Shield (e.g., Tsige and Abdelsalam 2005), (b) effusive rocks and volcanoclastic deposits of the Nazret, Chilalo and Dino Formations followed by rift-floor basalts with associated pyroclastics and rhyolites with cognate pyroclastics of the Central Volcanic Complexes and (c) limited Holocene re-sedimented pyroclastic deposits with intercalations of alluvial and lacustrine sediments which fill NNE – SSW trending tectonic depressions. Across the mapped lithologies a different set of high-grade metamorphic structures, volcanic and sedimentary fabrics (magmatic banding, foliation and bedding) and brittle rift-related structures (for example normal to strike-slip faults and extensional joints) were identified.

3.4.1 Primary structures

The Holocene pyroclastic deposits and alluvial sediments include bedding mainly in a subhorizontal orientation (Fig. 3.11, 3.12). Inclined bedding with a dip of up to 30° occurs on the pyroclastic cones (Fig. 3.13). The rhyolites of the Central Volcanic Complexes show flow-banding defined by a planar preferred orientation of rock-forming minerals or domains with variable amounts of micro-vesicles or micro-crysts. Flow-banding is frequently significantly folded, for example near the edges of lava flows.

3.4.2 Ductile structures

Neoproterozoic to lower-Palaeozoic rocks of the Arabian-Nubian Shield are composed of amphibolites, mica-schists, paragneisses and small bodies of orthogneisses (e.g., Tsige and

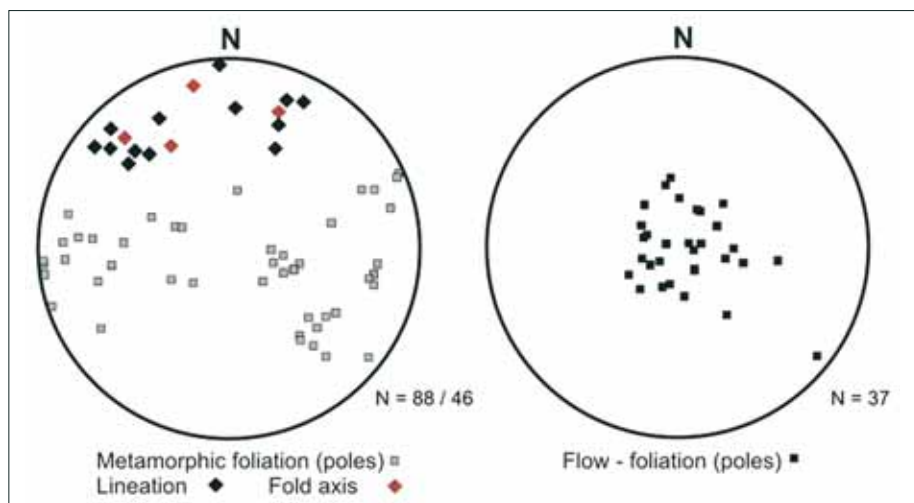


Fig. 3.11 Orientation diagrams of ductile and primary structures: (left) – Metamorphic fabrics in Neoproterozoic to lower-Palaeozoic rocks of the Arabian-Nubian Shield. (right) – Primary fabrics in volcanic sequence of the Central Volcanic Complexes and Nazret, Chilalo and Dino Formations. Equal projection to the lower hemisphere.



Fig. 3.12 Flat-lying depositional fabrics in volcanic sequence (Arbe Gona)

Abdelsalam 2005). The regional metamorphic foliation or compositional banding is mostly parallel to the contacts and lithological boundaries dip steeply to ~ W (WNW) or E ~ (Fig. 3.11, 3.14).



Fig. 3.13 Bedding in pyroclastic deposits of a basaltic scoria cone near Arbe Minch



Fig. 3.14 Stretching lineation and parallel elongation of a mafic microgranular enclave in biotite orthogneiss (Mejo)



Fig. 3.15 Asymmetric folds of leucogranite dike (Meleka)



Fig. 3.16 Asymmetrically stretched quartz-feldspar melt indicating oblique thrusting (NW-side-up) kinematics (Chebe)

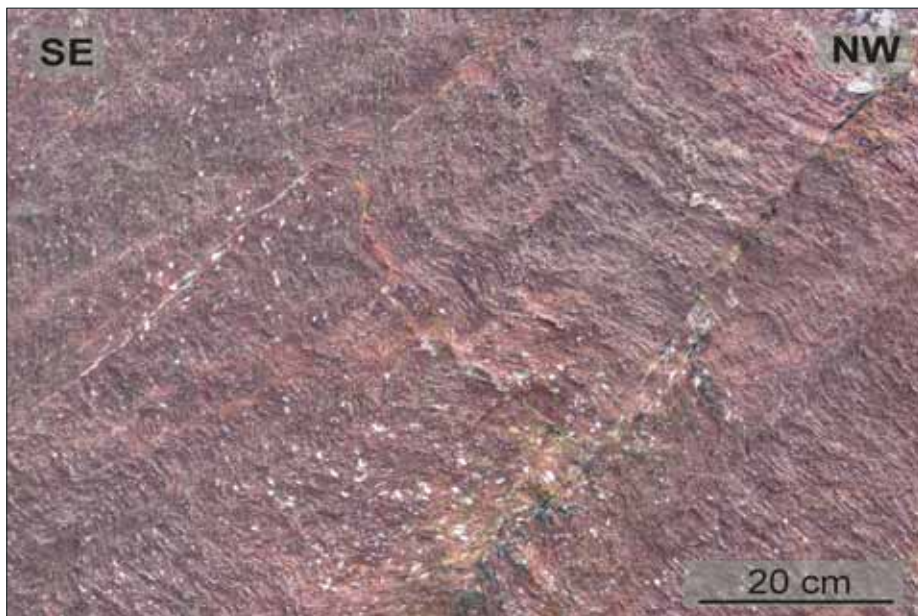


Fig. 3.17 Superposition of \sim S to SW dipping axial cleavage (Meleka)

In some places these fabrics locally contain minor rootless, close to isoclinal folds with variably trending fold axes or symmetric folds of leucogranite dikes (Fig. 3.15). Mesoscopic lineation was not observed. These foliations have been folded into asymmetric folds with fold axes parallel to the lineation or pervasively reworked into foliation dipping shallowly to the ~W or WNW. Distinct mineral or stretching lineation (Fig. 3.14) suggests a plain-strain fabric ellipsoid. The lineation dips gently to the ~NNW or ~ENE (Fig. 3.11). Consistent with the fold asymmetry, an asymmetrically stretched recrystallized quartz–feldspar melt (Fig. 3.16) and σ -type porphyroclasts indicate oblique thrusting (NW-side-up kinematics). In some places superimposition of a steeply to moderately ~S to SW dipping axial cleavage was observed (Fig. 3.17).

3.4.3 Brittle structures

Faults and fault zones

Various different sets of brittle structures were observed across the mapped area (for example regional normal faults to strike-slip faults and fault zones, and extensional joints). Rare caldera-related faults are associated with the evolution of individual volcanic bodies (e.g., Wobitcha Caldera in the northern part of the map sheet) and have a curved asymmetric shape, mostly parallel to the caldera rim, bearing evidence of normal kinematics. Regional faults and fault zones related to the East African Rift System significantly affect the geological framework of the area (e.g. Tesfaye et al. 2003) and are mostly parallel to the main axis of the rift and morphological escarpments. These faults dip steeply to ~E or ~W bearing well developed steeply plunging slickensides (Fig. 3.18, 3.19). The observed slickenside asymmetry reveals normal movement in the direction of the lineation (Fig. 3.19). A subordinate set of normal faults has a ~W (WNW) to E (ESE) trend. Next, minor strike-slip faults with both left- and right-lateral kinematic indicators were identified (Fig. 3.20). At several locations across the mapped area the strike-slip faults appear to be older than the regional normal faults.



Fig. 3.18 Regional NNE – SSW trending fault with a normal component of movement (Chencha)



Fig. 3.19 Subvertical slickensides associated with WNW – ESE trending faults (Dila)

Extensional joints

Extensional joints occur in three distinct sets with similar direction frequencies (Fig. 3.21). Across all of the lithological units on the map sheet extensional joints trending ~ N – S, NNE – SSW and E (WNW) – W (ESE) were measured (Fig. 3.22). Their orientation is largely consistent with the regional faults (compare the rose diagrams in Fig. 3.20 and 3.22).

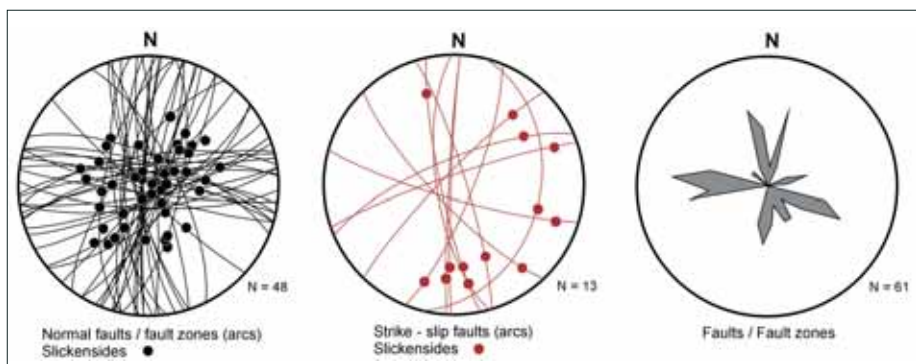


Fig. 3.20 Orientation diagrams of faults and associated slickensides. (left) – Normal faults / fault zones in all units with steeply plunging slickensides; (centre) – Minor strike-slip faults in all units; (right) – Rose diagram showing the dip-direction of faults and fault zones in all units. Equal projection to the lower hemisphere



Fig. 3.21 Regional N - S trending extensional joints (Aleta Wondo)

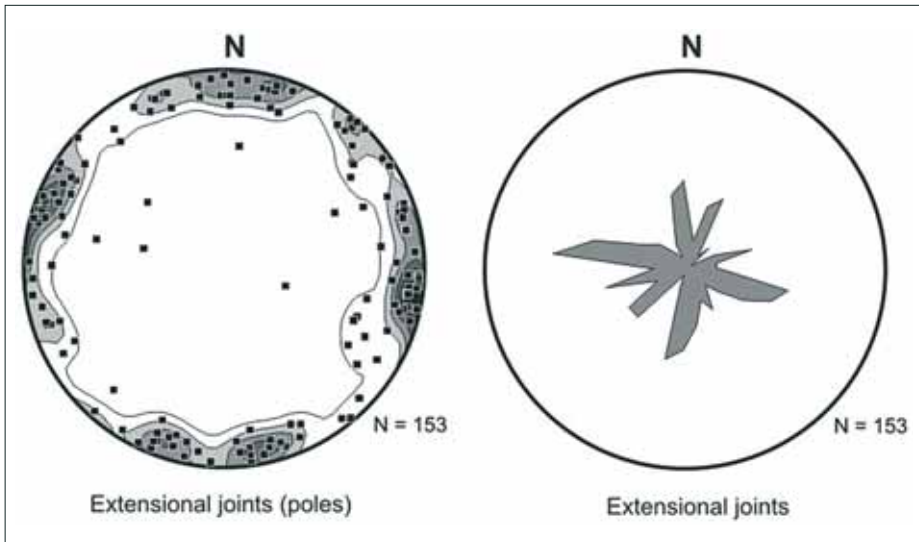


Fig. 3.22 (left) - Orientation diagram of the extensional joints in different units (poles). Equal projection to the lower hemisphere (right) - Rose diagram indicating the dip-direction frequency of extensional joints in all units

3.5 Geochronology

Within the framework of the project, a total of 20 samples of volcanic rocks were dated using the K-Ar method, 3 of which were from the area of the Dila map sheet and an additional 3 from the North Chamo Volcanic Field just to the south of the Dila map sheet. The geochronological

Tab. 3.2 K-Ar data obtained on volcanic rocks from different volcanic fields (2013)

Sample	Rock type	K (%)	$^{40}\text{Ar}_{\text{rad}}$ (ccSTP/g)	$^{40}\text{Ar}_{\text{rad}}$ (%)	K-Ar age (Ma)
DLRVR020 – Kale Korke	scoria	1.176	4.8424×10^{-8}	3.3	1.05 ± 0.46
DLRVR021 – Alakom	trachybasalt	1.853	1.3457×10^{-8}	19.9	1.86 ± 0.13
DLRVR025 – Chamo (Ganjule Is.)	basalt	1.069	2.3197×10^{-8}	2.9	0.55 ± 0.27
DLRVR028 – Arba Minch	trachybasalt	2.134	4.2870×10^{-8}	8.8	0.516 ± 0.078
DLRVR029 – Hamasa River	trachybasalt	1.957	4.2299×10^{-8}	2.7	0.556 ± 0.273
Sd061 – Wendo Genet	trachybasalt	0.813	1.7449×10^{-7}	2.1	5.51 ± 3.8

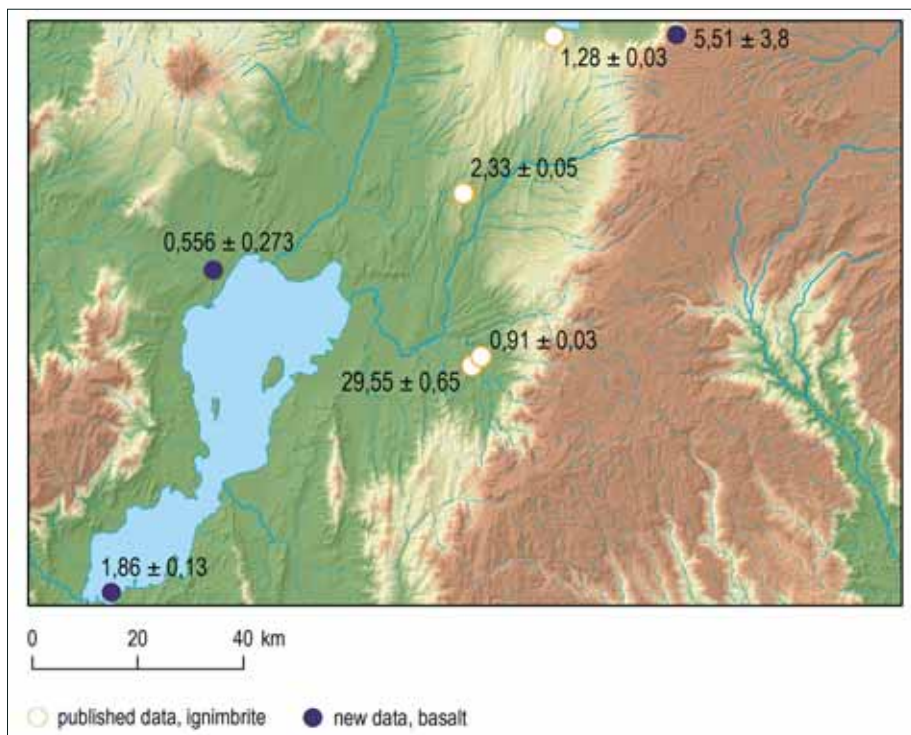


Fig. 3.23 Location of K-Ar geochronological results on the Dila sheet

analyses were carried out in the ATOMKI Laboratories (Debrecen, Hungary) by Dr. Zoltán Pécskay. Potassium concentrations were measured using a CORNING 480 digitized flame photometer machine with a Li internal standard. The analyses were controlled by inter-laboratory standards Asia 1/65, LP-6, HD-B1 and GL-O. Argon was extracted from samples by high frequency induction heating. The A ^{38}Ar -spike was introduced to the system from a gas pipette before the degassing started. The isotopic ratios were measured on a 15 cm radius magnetic sector-type mass spectrometer under a static mode, built in Debrecen, Hungary. Balogh (1985) and Odin (1982) described the methods applied in detail. The calculation of ages was based on atomic constants suggested by Steiger and Jäger (1977). The analytical errors are quoted for a 68 % confidence level (one standard deviation). The results are listed in Table 3.2 and shown in Fig. 3.23.

The obtained data were compared with previously published data, namely those with precise locations (JICA 2012). The oldest obtained age of 5.5 Ma comes from basaltic rock exposed in the lower part of the scarp in Wendo Genet (Žáček et al. 2014). This age corresponds to basaltic members in the upper part of the Nazret Group. The remaining data represent Late Pleistocene basaltic lavas and scoria cones on the rift floor. The results show that no eruption occurred in the area of Tosa Sucha and North Chamo after 500 ka.

3.6 Geological Evolution

Based on field and structural data and taking into consideration previous regional works the geological history of the Dila area can be divided into several episodes. The oldest recorded rocks in the area of interest are Proterozoic metamorphic and deformed intrusive rocks. The Proterozoic rocks were overlain during the Neogene by thick accumulations of volcanic rocks comprising basalts, trachytes, rhyolites and rhyolitic ignimbrites. Uplift, doming and eventual rupture of the Afro-Arabian region resulted in the formation of the East African Rift system oriented in northeast–southwest and north-northwest–south-southwest directions. The initial sagging of the Main Ethiopian Rift began around 15 to 14 Ma. An important event in the rift development took place around 10 Ma (Kazmin et al., 1980; Davidson, 1983, and others). This development caused faulting of the pre-rift volcanic succession. The Miocene-Pliocene to Holocene cover of the floor of the Rift Valley (Kazmin et al., 1980 and others) consists of a thick succession of stratified felsic volcanic rocks such as ignimbrites, non-welded tuffs, ash flow deposits, rhyolite and trachyte lavas. These rocks also outcrop on the rift escarpments and adjacent plateau margins and are referred to as the Nazret group (9.5–4 Ma).

With the formation of the Wonji fault belt (Pleistocene to Holocene), tectonic movements produced step-like structures and associated volcanic activity is represented by ignimbrites, basalts and unwelded pyroclastics. The fault zone is straddled by central volcanoes found along the axial zone of the Wonji fault belt. The main products were obsidian, rhyolite and trachyte lavas, pumice and tuffs. The products of the Wonji fault are referred as the Wonji group (Kazmin et al., 1980 and others). Another type of volcanic activity in the Wonji fault belt was the eruption of basalt lava flows from fissures from the Late Pleistocene to the present. The basalts are controlled by extensional fractures and commonly characterized by fresh aa-surfaces. Chains of scoria- and spatter-cones follow the lines of fractures. These basalts are mostly found on the rift floor; to the north of the Hamasa River and in the northern part of Lake Chamo. Recent flows in many cases follow pre-existing topographic low relief areas. Although the development of the rift was dominated by volcanic activity, deposition of alluvial and lacustrine sediments was also common, for example thick accumulations of alluvial sediments border Lake Abaya. These sediments are mainly represented by coarse gravels and sand.



Fig. 3.24 Phreatomagmatic pyroclastic deposits overlain by basaltic scoria – quarried scoria cone near Arba Minch

4. *4. Rock properties and economic perspectives*

4.1 *Engineering geology*

Engineering geological mapping was carried out by experts from the Geological Survey of Ethiopia (GSE) following their internal standards and methods. Experts from the Czech Geological Survey provided advice in text arrangement and visualization of the results.

In engineering geological mapping, rocks and soil are classified using the principle that the physical or engineering properties of the rocks are a combination of the results of origin, diagenesis, metamorphism, tectonism, alteration, and degree of weathering (IAEG, 1976). Rocks and soils are mapped separately due to the fact that soil has quite different physical and geotechnical properties to rock. Different lithostratigraphic rocks that are homogenous in their geotechnical properties can be grouped into one rock mass unit even though they are mapped as different lithostratigraphic units on geological maps. On the other hand, due to differences in the degree of weathering and alteration, discontinuity, and other properties which affect the geotechnical property of rocks, a single lithological unit may be divided into different engineering rock mass classes. Based on the results of the engineering geological investigation using rock strength, genesis, and laboratory tests as crucial criteria, the rocks within the project area are subdivided into five rock mass strength units:

Engineering geological rock units:

- Rock with very high rock mass strength (VHRMS): Point load index 30–130 MPa
- Rock with high rock mass strength (HRMS): Point load index 10–30 MPa
- Rock with medium rock mass strength (MRMS): Point load index 3–10 MPa
- Rock with low rock mass strength (LRMS): Point load index 1–3 MPa
- Rock with very low rock mass strength (VLRMS): Point load index 0.3–1 MPa

Engineering geological soil units:

- Alluvial soil
- Residual soil
- Lacustrine soil

4.1.1 *Engineering classification of rocks*

Rocks are classified into different rock mass strength units based on various parameters such as intact rock strength values, degree of weathering and joint spacing. Rock mass strength values are obtained from the point load strength index and Schmidt's hammer strength index. Despite the fact that variations in the local engineering attributes are significant, they cannot be displayed on the presented engineering geology map. It must be stated here that the engineering geology

mapping was made at a scale of 1:250,000 with the density of documentation corresponding to this scale. Therefore, this engineering geological map is basically useful for regional planning rather than for specific and detailed site characterization. A detailed study of the selected site is required prior to any larger construction work being performed.

The lithological units mapped in the area of the Dila map sheet were tested to determine their geotechnical characteristics. Rock material strength (UCS) was determined in the field using a point load tester and a Schmidt hammer. In total, 283 rock specimens obtained from various lithological units on the Dila map sheet were tested by the point load tester. All of the specimens were air dried for more than two weeks and were tested perpendicular to the plane of weakness. On each outcrop, representative of the individual rock units, 15 measurements were provided using a Schmidt's hammer tester. Subsequently, the values of the measurements were arranged from the lowest to the highest. The 1st to 5th values and the 11th to 15th values are discarded and the 6th and 10th values are taken as the lowest and highest strength indexes, respectively. The 8th value is then taken as the median rock material strength value.

Weathering is the process of mechanical and chemical disintegration or break down of rocks. The rate of weathering in rocks depends on the climate, the nature of the parent rock, the rock structure and texture, the topography, and the depth of groundwater. Weathering in rocks affects their engineering behavior such as unconfined compressive strength, which in turn has a significant effect on project design and construction operation of the rock-structure interface. The degree of weathering was described based on ISRM terms for weathering description (Tab. 4.1).

Tab. 4.1 ISRM terms for weathering description Rocks with very high rock mass strength (VHRMS)

Terms	Description	Grade
Fresh	No visible sign of rock weathering; perhaps slight discoloration on major discontinuity surfaces	I
Slightly weathered	Discoloration indicates weathering of rock and discontinuity surfaces. Inner part of the rock remains intact.	II
Moderately weathered	Less than half of the rock is decomposed or disintegrated to a soil. Fresh or discolored rock is present either as a continuous framework or as core stones.	III
Highly weathered	More than half of the rock is decomposed or disintegrated to a soil. Fresh or discolored rock is present either as a discontinuous framework or as core stones.	IV
Completely weathered	The entire rock is decomposed and/or disintegrated to soil. The original mass structure is still largely intact.	V
Residual soil	The entire rock is converted to soil. The structure, fabric and primary minerals are destroyed. There is a large change in volume but the soil has not been significantly transported.	VI

According to the above-mentioned parameters, the basalts of the Nazret Group as well as Pleistocene to Holocene basalts are classified as rocks with very high rock mass strength. The Nazret Group basalts are dark grey, fine- to medium-grained, fresh to slightly weathered, and locally moderately weathered. The structure of the basalts is aphyric to porphyritic. They decompose to blocks reaching up to 2 m³. Frequently, the Nazret Group basalts are overlain by up to 6 m of thick reddish/brownish silty residual soil. However, the distribution of the soil is local and not uniform. A representative outcrop is exploited in the Keangnam quarry near Bore, exposing aphyric and

porphyritic basalt with minor vesicular facies. The basalt is dark grey, fine-grained, fresh to slightly weathered, and jointed. The spacing of the joints varies between 2 and 7 m (Fig. 4.1). The joints are slightly curved to straight, and are arranged in two dominant systems. Some joints are filled with clay whereas others remain open. Pleistocene to Holocene basalts are exposed in the Hamasa (syn. Amesa) Volcanic Field to the north of Lake Abaya and form plains between fault scarps concordant with the Wonji fault belt (Halcrow, et al. 2008). These basalts were emitted from fissure eruptions and scoria cones of the Hamasa Volcanic Field. Similarly to the Nazret Group basalts, the Quaternary basalts are dark grey, fresh to slightly weathered, aphyric and sometimes porphyritic. Surface facies are frequently vesicular and blocky (aa-lava). Some of the vesicles are filled with secondary calcite. These basalts are characterized by wide spaced jointing to massive outcrops. Blocky outcrops of Quaternary basalts are rarely observed. The joints originate mostly from cooling of the lava, and are scarcely related to the tectonic activity. The physical properties of the analyzed rocks are listed in Annex 3.



Fig. 4.1 Nazret Group basalt exposed in the Keangnam quarry near Bore town on the eastern plateau

Rocks with high rock mass strength (HRMS)

The unit of rocks with high rock mass strength comprises various ignimbrites and rhyolites of the Nazret Group and the Dino Formation, as well as all of the trachytes, trachybasalts, Proterozoic metagranites, and most of the pre-Quaternary basalts. The ignimbrites as well as coherent rhyolites and trachytes are characterized by a grey to greenish grey (Fig. 4.2) or pinkish color. They are fresh to slightly weathered, locally up to moderately weathered. Calcite locally replaces weathered minerals (namely plagioclase). The ignimbrites are medium- to coarse-grained, mostly massive and columnar jointed (joint spacing 0.25 to 4 m, Fig. 4.3). Disintegration to blocks (up to 1.5 m³) occurs where columnar-jointing is not well-developed. Some joints are filled with clay whereas

others remain open. The coherent rhyolites are pinkish and intensively jointed (Fig. 4.4). On the northeastern corner of the map sheet, the ignimbrites also comprise massive, plain forming, and low strength tuff.



Fig. 4.2 Jointed ignimbrite exposed by an active quarry



Fig. 4.3 Thick-columnary jointed rhyolitic ignimbrite to the north of Dila



Fig. 4.4 Coherent rhyolite exposed in the cut of the road from Birbir to Arba Minch

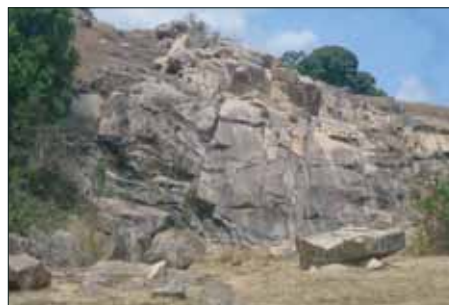


Fig. 4.5 Wide spacing of joints in metagranite

The ignimbrites, rhyolites and trachytes show variable strength characteristics throughout the map sheet. To the north and south of Dila town, these rocks display high strength, whereas in the southwestern part of the map sheet they have a medium strength. The variation in strength properties is due to the difference in the degree of weathering due to variable exposure and joint spacing.

Metagranites have a wide spectrum of colors; they are coarse grained, and are fresh to slightly weathered. The joints penetrating the metagranites are moderately to widely spaced (Fig 4.5). Locally, dikes of coarse grained, highly weathered (and therefore weak) pegmatite penetrate the metagranites. Kaoline placers occur where thick weathering products of the metagranite-weathering are preserved (for example near Bwanbua Woha Village). The physical properties of the analyzed rocks are listed in Annex 3.

Rocks with medium rock mass strength (MRMS)

The unit of rocks with medium rock mass strength comprises transitional mildly alkaline and subalkaline basalts, rhyolites and trachytes. These rocks with medium rock mass strength outcrop in the south central part of the map sheet, whereas similar rocks with low rock mass strength can

be found in the western part of the map sheet. The transitional basalts are dark grey, slightly to moderately weathered and aphyric or sometimes porphyritic. The rhyolites are light to greenish grey and pinkish in color, fresh to slightly weathered, sometimes moderately weathered, thinly banded, medium- to coarse-grained, and porphyritic. Joints in the rhyolites are closely spaced and in addition these rocks are randomly fractured. They form plain rhyolitic lava flows to steep mountains ridges like Damota Mountain rising above the town of Wolayita Sodo.

Rocks with low rock mass strength (LRMS)

This unit comprises weaker facies of the above-mentioned rocks as well as foliated metamorphic rocks and volcanosedimentary sequences. The transitional mildly alkaline and subalkaline basalts and rhyolites with low rock mass strength occur mainly in the southwestern part of the Dila map sheet. The basalts in this area are dark grey, aphyric, moderately to highly weathered (facies of lower degree of weathering can be observed). The weathering tends to spheroidal disintegration. The joints are closely spaced. The foliated high-grade metamorphic rocks comprise amphibolites and various gneisses with prevailing biotite-quartz-microcline gneiss. The foliation is more prominent in fine-grained types and the coarse-grained varieties are generally massive. The biotite-quartz-microcline gneiss is pinkish to brownish in color and moderately to highly weathered. Weathering produces an assemblage of clay minerals, which is responsible for smooth and slippery surface developed upon these rocks (Fig. 4.6 and 4.7). The high-grade metamorphic rocks are overlain by a 10 to 15 m thick layer of residual soil.



Fig. 4.6 Weathered foliated high-grade metamorphic rocks exposed in a road cut



Fig. 4.7 Close up of banded clays resulting from weathering of foliated metamorphic rocks

Foliated low-grade metamorphic rocks comprise mica- and chlorite- schists. Chlorite gives the rocks a greenish color, whereas mica- (muscovite) dominated rocks tend to have brownish shades. The chlorite schist is light grey to greenish grey, medium-grained, slightly to moderately weathered, friable, and flaky to platy. It is strongly sheared, faulted and tilted. The mica schist displays variability in color from yellow to dark gold. It is flaky and platy, weak, friable and moderately weathered. The water absorption capacity and porosity values of samples of metamorphic rocks show low values similar to rocks with high rock mass strength. This is attributed to a high degree of compaction by metamorphism but shows low strength due to the high degree of weathering.

Volcano-sedimentary sequences crop out mainly in the north-central part of the map sheet. These deposits are light to dark grey in color, with variable grain-size and are slightly to moderately weathered. Intense weathering was also locally observed. These sequences comprise pyroclastic, re-sedimented pyroclastic and sedimentary layers, locally intercalated with ignimbrite. Pumices are the most abundant fragments, occasionally forming purely pumiceous deposits. Coarse non-welded clast-supported pumiceous deposits up to 15 m thick occur near Yirga Alem (Fig. 4.18). There are also loose, weak, friable tuffaceous pyroclastic deposits present



Fig. 4.8 Coarse-grained pumiceous deposits near Yirga Alem town



Fig. 4.9 Thick deposits of bedded pumice on the slope of Duguna Fango Volcano

in this unit. Where exposed over large areas, volcano-sedimentary sequences are characterized by badland in which the overlying residual soil is severely eroded and rills and gullies dissect the underlying tuff. Low-grade ignimbrites and non-welded poorly compacted pyroclastics occasionally intercalated with lacustrine beds form plains such as Wara, Gorbato, Danshe, Chuko, etc. Coarse-grained layers frequently alternate with fine tuff. Within such sequences, fresh and strong ignimbrites can be found. Such ignimbrites are exploited for masonry in several places near the towns of Leku and Chuko. The physical properties of the analyzed rocks are listed in Annex 3.

Rock with very low rock mass strength (VLRMS)

The weakest rocks in the Dila map sheet are represented by pumice deposits and non-welded tuffs. Pumice and non-welded tuffs form the dominant part of Duguna Fango Volcano as well as several other central volcanic complexes in the northern part of the Dila map sheet. These deposits usually reach high thicknesses (Fig. 4.9). Pumice deposits are highly permeable and have very low rock mass strength.

4.1.2 Engineering classification of soils

Classification of soils is the arrangement of soils into different groups according to their origin and properties. In engineering geology the term “soil” is defined as unconsolidated material composed of solid particles, produced by the disintegration of rocks. Generally, an area with a soil unit thickness exceeding one meter is mapped as a soil unit. If the soil thickness is less than one meter, it is simply mapped as the underlying bedrock. Of the many different soil classification systems, the unified soil classification system (USC) is used in this work. The USC system uses both particle size analysis and the plasticity characteristics of soils.

The soil type in the study area is classified as alluvial, residual and colluvial. Test pits were dug and representative soil samples were collected for granulometric analysis, atterberg limits and moisture content analysis in the laboratory. The liquid and plastic limits are used for soil classification. If the amount of clay minerals present in a particular soil sample is high then the soil becomes highly plastic and its shrinkage and swelling values become higher. Consequently, such soil properties mean more problems for construction work.

The distribution of variable granulometry of the documented soils is shown in Fig. 4.10.

Alluvial soils

From an engineering geology point of view, alluvial soils represent alluvial sediments deposited by fluvial systems on foothills of highland areas. These sediments are stratified with beds of gravel, sand and clay. It occurs on the map sheet mainly around Lake Abaya. Alluvial soil at Arba Minch silk farm is brown to dark brown in color. It is a medium-grained, firm to stiff, homogenous, slightly plastic and uniformly graded silt-clayey soil. The thickness of the alluvial soil of about 10 m can be documented in several gullies within the area. The unconfined compressive strength measured using a pocket penetrometer ranges from 300 to 400 kg/cm², but on some outcrops these values do not exceed 250 kPa. Alluvial soils in wetlands are dark, fine grained, soft, homogenous, moist, moderately to highly plastic, and uniformly graded. These show slow dilatancy and an unconfined compressive strength of 50 to 150 kPa.

Residual soils

Residual soils derived from decomposition of underlying bedrock are found in various parts of the Dila map sheet. Residual soils are preserved on paleorelief plains unaffected by erosion (Fig. 4.11). Most of the occurrences remain below the recognition limit for the quarter million scale of the map.

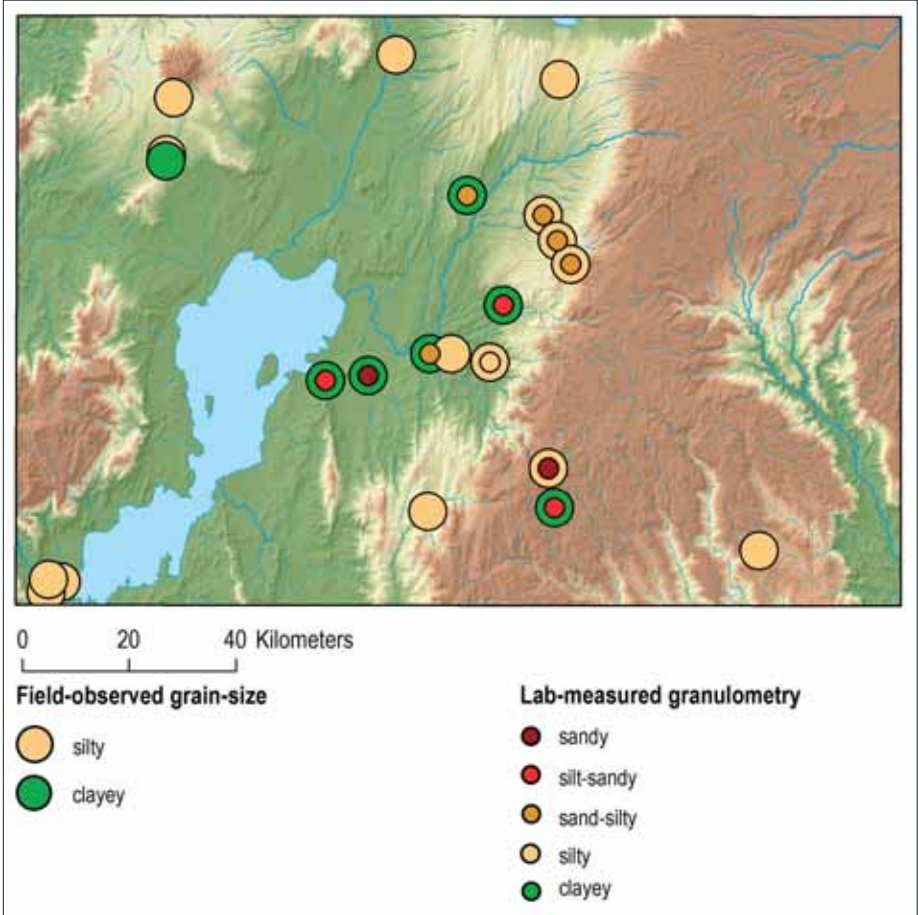


Fig. 4.10 Scheme of soil granulometry variability within the Dila map sheet area

The residual soil exposed along the road from Aleta Wendo to Hagera Selam is derived from the underlying highly weathered Neogene basalts (Fig. 4.12). The soil is brownish silt-clayey, stiff, homogenous, fine- to medium-grained, moderately plastic and gap-graded. It shows slow to medium dilatancy. A manually dug test pit near Wolayita Sodo exposed reddish silt-clayey residual soil. This soil is firm, massive in structure, fine-grained, moderately plastic, and gap-graded. It is derived from highly weathered ignimbrite. The unconfined compressive strength of residual soil in the town of Wolayita Sodo is greater than 200 kPa based on the results of a pocket penetrometer test. The thickness of the residual soil around Wolayita Sodo exceeds 5 m. According to the unified soil classification system (USCS) several samples of residual soils in various areas of the Dila map sheet were classified as being MH and SP meaning inorganic silts, fine sand or silty soils, elastic silts and poorly graded sands, gravely sands with little or no clay. Some of the samples are classified as ML and SM meaning inorganic silts and very fine sands, silty or clayey fine sands, clayey silts and silty sands, sand-silt mixtures, respectively. From the particle size distribution curve the residual soils generally show a gap-grading curve. Badland areas prevalently occurring along

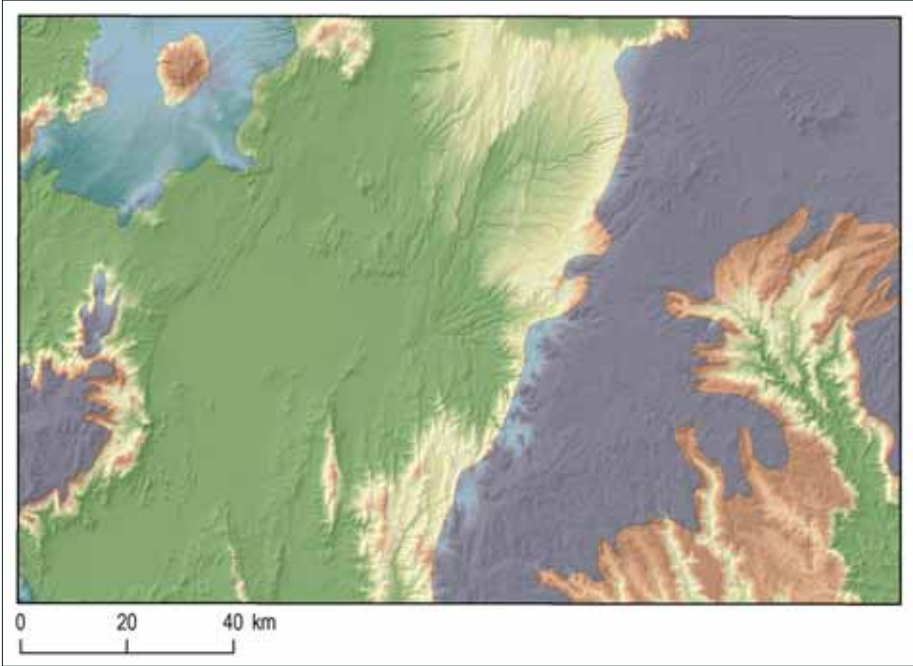


Fig. 4.11 Scheme of distribution of paleorelief plains with thick accumulations of residual soils



Fig. 4.12 Thick residual soil outcropped along the road from Aleta Wendo to Hagere Selam

the River Bilate, and to the north of Lake Abaya mainly resulted from erosion of medium- to coarse-grained, gap-graded, fissured silty residual soils. Residual soils generally show a plasticity index in the range of 12 to 23 meaning they are moderately to highly plastic.

Geophysical survey using vertical electrical sounding (VES) was conducted at two newly planned airports, namely Hawasa in Morocho village and Wolayita Sodo. The aim of the geophysical survey was to identify subsurface vertical distribution of strata and their characteristics as well as to delineate tectonic features. The selected area for the newly planned Hawasa airport in the village of Morocho consists of a flat plain cross cut by small NNE-SSW trending hills. The area is moderately vegetated and densely populated. Schools and health stations with several houses are present within the area. Low electric resistivity suggests the presence of loose, water-saturated sediments. Slightly increased resistivity (over 100 Ω .m) in the thin uppermost layer occurs locally, most likely where the surface (to a maximum depth of 3 m) has dried due to climatic conditions. Similarly, low electric resistivity (under 30 Ω .m to a depth of 100 m) in the area of the planned Wolayita Sodo airport also suggests the presence of thick water-saturated soils and sediments.

Lacustrine soils

From an engineering geology point of view, lacustrine soils are described here as being polygenetic infills of tectonic grabens and calderas on the rift floor. Such deposits are found around Lake Hawasa. These polygenetic deposits are dominated by re-sedimented pyroclastics with intercalations of lacustrine sediments. These soils have a silty-clayey composition, a pale-brown to yellowish color, and are well bedded or laminated.

4.2 Economic geology

4.2.1 Construction materials

The rapid growth of the construction sector demands the supply of raw materials. In this regard, the study area is known for its great potential for construction materials suitable for various purposes e.g. dams, bridges, roads, buildings, cement industry, etc. Several existing and newly proposed quarry sites were documented within the investigated area (Fig. 4.13).

Basalts for concrete and asphalt mixtures

Good quality basalt is available in sufficient amounts in the area of the Dila map sheet. Most of which is concentrated mainly around Hagere Selam and Bore, where the Keangnam Construction Company is mining and crushing good quality, strong basalt (Fig. 4.14). The basalt is fresh or slightly weathered. The quarried basalts have negligible porosity and a water absorption capacity of below 2 %, which allows them to be used as crushed stone for sub base, asphalt and concrete mixtures. Blasting or machinery is used to excavate the basalt in the visited quarries. The basaltic quarries are generally large, usually with very good accessibility. In addition, several proposed moderately weathered basaltic rock quarry sites can be used for road filling as first-rate material.

Basalt for road select material

The moderately to highly weathered, randomly fractured and friable basalts can be used for non-paved roads (Fig. 4.15). These resources are the most widely used material in the map sheet area for pavements beneath the base course layer. Its extent varies from medium to very large with fair to very good accessibility. It can be excavated manually or by machinery. Samples from Ashangi rock quarry sources display water absorption and porosity ranging from 3 to 6.4 % and 5 to 15 %, respectively. Moderately weathered rhyolites and rhyolitic ignimbrites can be used in a similar way.

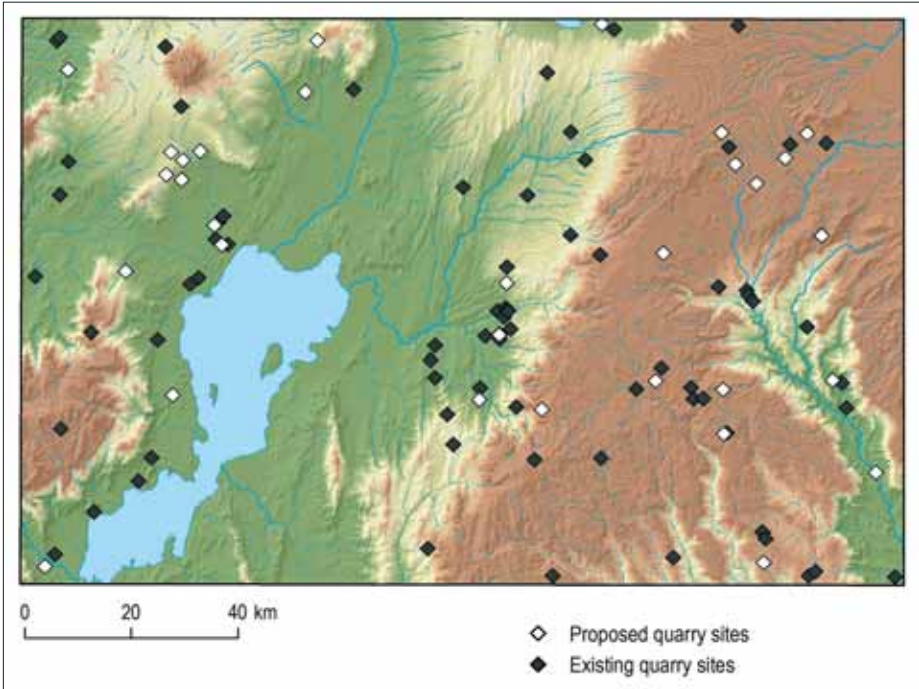


Fig. 4.13 Scheme of existing and proposed quarry sites in the area of the Dila sheet



Fig. 4.14 Keangnam basalt quarry site near Bore town



Fig. 4.15 Quarry for first-rate road and pavement material near Solemo town

Scoriae

On the rift floor cones of scoria are aligned in a NNE-SSW direction along the rift axis and the Wonji fault system. Several quarries of scoria are found to the north of Lake Abaya (Fig. 4.16). The scoriae are exploited for first-rate road and pavement material. In the area of the quarries, the scoria is usually fresh or slightly hydrothermally altered, and friable, allowing for easy excavation by machinery or manpower. The quarries have good accessibility.



Fig. 4.16 Scoria quarry to the north of Lake Abaya

Rhyolite and rhyolitic ignimbrites for masonry

Large volumes of rhyolites and rhyolitic ignimbrites of various stratigraphic units are found in the map sheet area. The rhyolites and rhyolitic ignimbrites are expected mainly for masonry from newly proposed quarry sites. The quarries for rhyolites and ignimbrites are located mainly around Yirga Chefe, Dila, Arba Minch, Wolayita Sodo, etc. (Fig. 4.17). Generally, the ignimbrite quarries serve as a good source of masonry stone for buildings, drainage structures, bridges, and crushed stones. The degree of weathering varies from fresh to slightly weathered. Some moderately to highly weathered rhyolitic ignimbrites are exploited for first-rate road materials.



Fig. 4.17 Quarry in rhyolitic ignimbrite to the north of Dila

Granite and metagranite for dimension stone

Hard and strong outcrops of relatively fresh metagranite with widely spaced joints can be found in the southeastern part of the map sheet near the town of Meleka. This is one of the most popular building materials. It can be used as dimension stone and as flooring tiles in public and commercial buildings and monuments.



Fig. 4.18 Quarry in massive granite for dimension stone near Meleka town

Pumice

The rapidly increasing construction industry requires cement for its activities. Different cement factories use pumice as a raw material for cement production. The eastern part of the study area has a good potential for pumice rock. The use of pumice in concrete is doubtful due to its high fluorine content. Acidic reaction of hydrogen-fluoride attacks the concrete and reduces the lifespan of concrete constructions.

Soil

Sites of good quality clayey soil are inventoried and selected in the map sheet area for soil quarries. Such soils can be used as borrow embankment material and dam cores and should be fine-grained, stiff, and homogenous in structure, slightly plastic, gap-graded and best if residual in origin. The inventoried soil quarries mainly occur near Dila where it has been used for the core of the Gidabo earth dam construction and around Wolayita Sodo for the newly planned Wolayita airport. Soil is found mainly on flat topography. The thickness of the soil varies from 3 to 15 m as observed from test pits and open soil quarries.



Fig. 4.19 Soil borrow quarry for the Gidabo dam core material, 20 km to the west of Dila Town

4.2.2 Absorption materials

Talc

Talc can be pulverized into a white powder that is widely known as “talcum powder”. This powder has the ability to absorb moisture, oils, odor, or to serve as a lubricant and produce an astringent effect on human skin. These properties make talcum powder an important ingredient in many baby powders, foot powders, first aid powders and a variety of cosmetics. This soft rock is easily carved and has been used to make ornamental and practical objects for thousands of years. It has been used to make sculptures, bowls, countertops, sinks, hearths, pipe bowls and many other objects. Talc is a metamorphic mineral resulting from the metamorphosis of magnesium minerals such as serpentine, pyroxene, amphibole, olivine, in the presence of carbon dioxide and water. It is used in many industries such as paper making, plastic, paint and coatings, rubber, food, electric cable, pharmaceuticals, cosmetics, ceramics, etc. Talc resources are available in the southeastern part of the map sheet where low grade metamorphic rocks are exposed. Artisanal mining activity of talc is found in the SNNPRS, Sidama zone, in the locality of Fulantu. It is located at the foothill of a ridge formed by faulted and sheared chlorite schist.



Fig. 4.20 Kaolin quarry near Bwanbua Woha

4.2.3 Ceramics materials

Kaolin

Kaolin is a soft, earthy, usually white mineral, produced by the chemical weathering of aluminum silicates like feldspars. It is an essential ingredient in the manufacturing of porcelain and other ceramics and is widely used in the making of paper, rubber, paints, and many other products. Kaolin is exploited near Bwanbua Woha (Meae boko) by the Ethiopian mineral development Share Company (Fig. 4.20) from highly weathered granite or pegmatite.

4.3 Geothermal energy

Volcanic activity is usually associated with hydrothermal systems with a great potential for geothermal power production. Numerous hot springs are arranged along the fault zone followed by the River Bilate (Fig. 4.21 and 4.22). None of these geothermal resources are actually used in the



Fig. 4.21 Bobicho thermal spring

area. A swimming pool constructed on Bobicha hot springs is difficult to access and is without any amenities. Therefore, it is used solely by local inhabitants and brings no economic benefit. Geothermal energy in the Dila sheet area represents an unexploited and poorly investigated resource.

4.4 Geotourism potential

Most of the tourists coming to the area of the Dila map sheet are attracted by the Nech Sar National Park (Fig. 4.23), which preserves plains with zebra, jungle at Tosa Sucha (God’s Bridge) isthmus, and part of Lake Chamo hosting hippopotamus and crocodile (Fig. 4.24). The private sector as well as public budgets both benefit from the existence of this national park.



Fig. 4.22 Northwest Abaya fault-zone hot-springs



Fig. 4.23 Herd of zebra in the Nech Sar National Park

In addition, tourists may be attracted by the thermal springs along River Bilate if the necessary facilities are constructed. The area of the Dila sheet also comprises several geological sites, which could contribute to the local (and federal) economy with proper visitor management. With its high peaks attracting climbers, Mount Damota also has a potential for tourism.



Fig. 4.24 Crocodile at Lake Chamo

5. Geological hazards

5.1 Endogenous geological hazards

5.1.1 Seismic hazards

Seismic hazards in the studied segment of the Main Ethiopian Rift ($6^{\circ} - 7^{\circ}\text{N}$) are conditioned by the extensional tectonics in the rift region. From a global point of view, the seismicity connected with rifts (both oceanic and continental) represents about 6% of the seismic energy release. Continental rifts are characterized by a special type of seismicity, including seismic swarms and volcanic earthquakes. The presence of geothermal phenomena is another typical feature of rift regions. Core fluids (magma, CO_2 , water, vapor) can decrease mechanical friction in tectonic faults and trigger seismic events. Big earthquakes in rift regions are observed less frequently than at convergent margins of lithospheric plates; however, catastrophic earthquakes are not excluded. The controlling earthquakes have long repeating periods and hence the computation of seismic hazards represents a complex problem, which is an important issue for industrial development.

The East African Rift System (and the Main Ethiopian Rift as its segment in Southern Ethiopia) is not adequately explored. Only a very rough estimation of seismic hazards is available. The rapid growth of the urban population, extensive house building, and infrastructure development call for seismological investigation, which is the basis for a more detailed estimation of seismic hazards. A probabilistic approach to seismic hazard estimation is recommended as a standard used in western countries over the last decade. The probabilistic seismic hazard assessment (PSHA) is also suitable for the Rift Valley in Southern Ethiopia. The most important input data include a catalogue of historical earthquakes, seismograms of (small) recent local earthquakes which were instrumentally measured, paleoseismological studies, seismotectonic data and a model of geological media including seismic velocities and attenuation of seismic waves. The computation is performed in four basic steps:

1. Definition of all relevant source zones based on seismological and geological databases and on a seismotectonic model. This step has not been done properly in Southern Ethiopia. Seismological databases are extremely incomplete. This is the main reason for the list of active tectonic faults, which can generate catastrophic earthquakes, being deficient.
2. Definition of magnitude-frequency distribution (Gutenberg-Richter law - GR law) for all source zones. This task has not been performed in Southern Ethiopia yet. Only average parameters of GR-law have been derived for the whole region, while the specific parameters for individual zones are needed. A very important parameter is the maximum regional magnitude. It is unknown but it is clear that it exceeds 7.
3. Definition of the ground motion prediction equation (GMPE). Site-specific GMPEs do not exist for Southern Ethiopia. However, this holds true for many other regions. The average

parameters of GMPE could be adopted from global databases. The situation in the Rift Valley is complicated by the fact that it is filled with thick sedimentary layers, which amplify amplitudes of seismic waves. The shape of the valley significantly affects the propagation of seismic waves. The GMPE has to reflect these facts.

4. Computation of Probabilistic Seismic Hazard Curves (PSHC) The computation involves many scenarios, which can occur in the future. The importance of individual source zones for seismic hazard is also evaluated. The results are presented in the form of curves, which describe the probability that the earthquake exceeds the defined value of Peak Ground Acceleration (PGA).

Historical seismicity

In Southern Ethiopia reliable descriptions of historical earthquakes are sparse. Available data were compiled by Gouin, 1979. In his paper, the territory of Ethiopia is divided to five seismic zones. The region under study belongs to zone C – “Ethiopian Main Rift, Afar, and the Southern Red Sea”. Most earthquakes in this zone are connected to volcanic eruptions. Earthquakes of large magnitudes are located mainly in the northern part of the rift and the Red Sea. However, this is due to the fact that written testimonials were better preserved in the northern part of Ethiopia. Certainly, it does not exclude the possibility of large earthquakes in the southern part of the rift. Gouin (1979) states that, “No documents never equates to no earthquakes”. This statement is supported by local Galia legends about former locations presumably destroyed by seismic tremors and now covered by lakes. The legends are heard in the Rift Valley from Lake Ziway to Abaya, and on its western escarpment in Gemu-Gofa.

The oldest documented earthquake within the investigated area was recorded on the 4th of October 1928 on the scarp of the rift, to the west of Lake Abaya, and had a magnitude of 6. The most probable location is (N 7.0°, E 38.0°). The reports of a magnitude 6 earthquake on the 6th of September 1944 are disputable due to war. The location of the epicenter is inaccurate as the error reaches 200 km. The most probable location is (N 7.0°, E 38.5°). It cannot be proven that the epicenter is situated inside the rift. Several smaller earthquakes with a magnitude below 5 were detected on the 11th January 1972 (N 6.8°, E 38.4°), 13th April 1972 (N 6.0°, E 37.7°) and 30th June 1974 (N 6.3°, E 37.7°). A seismic swarm was observed in March 1974 (N 6.2°, E 37.7°). A global catalogue of earthquakes has been available from United States Geological Survey (USGS) since 1973. However, there are no earthquakes from Southern Ethiopia reported in the catalogue prior to 1983. The events reported in the catalogue are included in Table 5.1. Five earthquakes with a magnitude of more or equal to 4.4 are reported from the mapped area from 1983 to 2013. The epicenters are shown on the map.

Tab. 5.1 Earthquakes of magnitude $M > 4.3$ between 1983 and 2013 in the map sheet area (USGS catalog)

Date	Time	North (°)	East (°)	Depth (km)	Magnitude
1987-10-07	22:29:24.58	6.223	37.814	10.0	5.3
1989-06-08	06:24:09.61	6.837	37.878	18.6	4.9
1999-01-05	18:27:40.44	6.018	37.513	10.0	4.7
2005-07-07	16:57:57.40	6.289	37.697	10.0	4.7
2011-03-19	20:08:10.36	6.659	38.521	10.0	5.0

Conclusions and recommendations: A seismic hazard assessment for the Horn of Africa using the probabilistic method was published by Kebede and van Eck (1997). This paper identifies eight

source zones. Zone 2 comprises the southernmost rifts of Ethiopia and the Main Ethiopian Rift and also includes the region under this study. The upper magnitude for this zone was estimated to be 7.0 with an error of 0.2. Probabilistic hazard curves were constructed for seven sites in the Horn of Africa but none for Southern Ethiopia. The nearest studied site is Addis Ababa (Central Ethiopia), where a PGA of 150 cm/s^2 was determined for an annual probability of exceedance of 10^{-3} . According to the distribution of historical earthquakes, the seismic hazard in Southern Ethiopia can be expected to be even higher than in Addis Ababa. Better seismic hazard estimation can only be performed after collecting more reliable input data.

Intensive urban development has taken place around the lakes inside the rift, which is very worrying considering the seismic hazard. The subsoil in the most populated localities is composed of sediments and loose pyroclastic deposits with extremely low S-wave velocities, which can amplify the amplitude of seismic waves by several times compared to bedrock sites. As previously discussed, the last strong earthquake occurred in 1906, when the population in the region was much sparser and the distribution of urban housing was sporadic. Anti-seismic measures are not satisfactorily applied during house construction and the public is not prepared for a strong earthquake. For these reasons, Southern Ethiopia has to be considered as a region with a high seismic risk.

5.1.2 Ground cracks (fissures)

Ground cracks (fissures) have been documented in various locations in the Ethiopian Rift Valley (Asfaw 1998) and represent a dangerous geological hazard. The occurrence of fissures on the Dila sheet is mainly in the northern part of sheet, in the southern margin of the Muleti sub-basin located to the west of Hawasa Lake.

Fissure formations are likely to be related to the tectonic opening of cracks within solid rocks in the basement of the rift floor. When sediment coverage is present above the solid basement, soft sediments plastically accommodate the extension in the first phase, the ground cracks may remain unobserved until a devastating collapse of their thin roof. Subsequent subsurface erosion of loose material overlying the bedrock, rapid and unexpected subsidence of the surface, and a collapse of the sidewalls of the fissure occur in these cases.

In the case of the Muleti sub-basin fissures are developed in highly populated areas. Development of these structures and the accompanying processes represent a very dangerous geological hazard resulting in the loss of buildings, infrastructure and agricultural land. The destruction of houses and infrastructure as well as loss of human lives and animals has been documented in connection with ground fissure development.

Isolated fissures were also documented near Belala and Derara, where the solid basement is not covered by sediments, thus the crack openings are not accompanied by rapid and unexpected subsidence.

Recommendations:

Geophysical investigation is recommended for detecting and verifying faults and other discontinuities of rocks where fissures could be developed. The most dangerous of these are fractures with an intact sedimentary roof; their detection by electrical resistivity profiling is the crucial point of any subsequent survey. The rate of opening of these cracks also remains unclear. To obtain such data, a system of measuring points was located at selected sites. The distance between the points in solid rocks should be repeatedly measured every 6 months to observe the rate of dilatation. In the future, this simple method should be replaced by automatic extensometers.

5.1.3 Volcanic hazards

Continental rifting is associated with intense volcanic activity. As a result, several active or dormant volcanoes and volcanic fields can be found within the rift on the Dila map sheet.

Rhyolitic composite (central) volcanoes

Large rhyolitic composite volcanoes are not as frequent in the area of the Dila sheet as in the area of the Hosaina sheet (Nida, Bizuye, Rapprich eds. 2014). Chernet (2011) supposed the existence of nine Quaternary rhyolitic volcanoes to the north of Lake Abaya, but our observations suggest most of them are extinct and represent only tectonic remnants of volcanic edifices or mafic volcanic centers. Although we did our best to visit all of the known Quaternary volcanoes to investigate them in terms of the character and distribution of volcanic products, freshness of the deposits as well as the volcanic edifice suggesting the status of the volcano (dormant/extinct), our results represent only a brief basic description. More detailed conclusions would require a more in-depth study as the current research published as a map at the scale of 1:250,000 is only of an inventory nature.

Duguna Fango

The northernmost rhyolitic volcano in the investigated area is Duguna Fango Volcano (Fig. 5.1). The complex rhyolitic volcano has experienced several explosive eruptions and numerous effusions of obsidian lavas. All of the deposits that have erupted from this volcano, including obsidian lavas, are now covered by soil and vegetation. Although Chernet (2011) supposes recent obsidian flows from Duguna Fango Volcano, we observed no signs of recent activity. Several road cuts expose pyroclastic deposits of Duguna Fango Volcano (Fig. 5.2). Most of the observed deposits are bedded, ill-sorted and clast-supported. Effective fragmentation combined with ill-sorting near the source vent suggests a phreatomagmatic (Vulcanian) style of eruptions. A layer of whitish tuff about ten centimeters thick is embedded within brownish soil over a large area to the north, east and southeast of Duguna Fango Volcano (Fig. 5.3). The exact source vent of this tuff remains unclear but its distribution points to Duguna Fango being the most likely candidate. Intense sheet soil erosion disables estimations of how deep below the recent soil this tuff is buried and hence not even a rough estimate of the age of the eruption can be made. Numerous hot springs and



Fig. 5.1 Duguna Fango Volcano



Fig. 5.2 Pyroclastic deposits of Duguna Fango Volcano exposed in a road cut on the eastern slope of the volcano



Fig. 5.3 White tuff embedded within brown soil to the east of Dimtu

fumarolic fields (Fig. 5.4) surrounding Duguna Fango are most likely associated with the Bilate River Fault Zone.

Chericha Volcano

We were not able to access Chericha Volcano (Fig. 5.5) during the geological hazard mapping project. Therefore, no data were collected from this volcanic edifice. From remote observations,



Fig. 5.4 Obsidians altered by fumaroles (Bilbo fumaroles) on the southern foothill of Duguna Fango Volcano

Chericha Volcano appears as a rhyolitic complex. On the other hand, Gegesa Volcano about 5 km to the north of Chericha has an appearance of a basaltic crater. It is larger than the surrounding scoria cones but similar in color and morphology. The other hills on the northern banks of Lake Abaya are only tectonic remnants and blocks of Pleistocene volcanic relief.



Fig. 5.5 Chericha Volcano seen over the Bilate River from the Bolocho hot springs

Korke Seluwa Volcano

The widespread Hamasa Volcanic Field with numerous basaltic scoria cones comprises also the rhyolitic Korke Seluwa Volcano (Fig. 5.6). Activity of this volcano was represented by emissions of crystal-rich obsidian lavas associated with minor pumice emissions. The obsidian lavas are rich in phenocrysts, namely feldspars, but the youngest lava (sample DLRVR014) contains also abundant fayalite (Fe-olivine) and Fe- pyroxene. In addition, this youngest lava has no soil cover and only scarce vegetation suggesting very recent volcanic activity.

Presence of crystals motivated us to determine the age of the two youngest lava flows by U-Th series disequilibria. The Th and U isotopic ratios were analysed at the University of Bristol with an aim to obtain ages of two youngest lavas (Tab. 5.2). Plagioclase and pure-glass fractions were separated from both samples. The samples were analyzed for U-Th disequilibria following the methods described in Zellmer et al. (2013). The reproducibility of obtained results was controlled by measurement of standards BCR-2, IRMM036 and Harwell Uraninite. The data plotted in the equiline diagram (Fig. 5.7) do not produce any isochron for either of the samples. Sample DLRVR014 has a slope parallel to the equiline and in sample DLRVR015 the glass and plagioclase almost overlap within error, leading to a high uncertainty of the slope. Obtained results hence do not allow any age estimation and suggest inheriting of pre-existing crystals from older, non-comagmatic rocks. Therefore, complex magmatic processes including assimilation of country rocks of volcanic origin and magma mixing are expected within the magmatic reservoir and feeding system of the Korke Seluwa Volcano.

Conclusions and recommendations: Korke Seluwa is the only rhyolitic volcano with recent activity. This volcano is characterized by predominantly effusive eruptions (obsidian lavas)

Tab. 5.2 Measured U and Th isotopic ratios

Sample		U (ppb)	Th (ppb)	$^{234}\text{U}/^{238}\text{U}$	$\pm 2\sigma$	$^{230}\text{Th}/^{232}\text{Th}$	$\pm 2\sigma$	$^{230}\text{Th}/^{232}\text{Th}$	$\pm 2\sigma$	$^{238}\text{U}/^{232}\text{Th}$	$\pm 2\sigma$	$^{230}\text{Th}/^{238}\text{U}$	$\pm 2\sigma$
DLRVR014 plg		202.9	880.9	0.9976	0.0008	4.573E ⁻⁰⁶	1.5E ⁻⁰⁸	0.8464	0.0028	0.6988	0.0012	1.211	0.004
DLRVR014 glass		5123.7	22605.3	1.0001	0.0010	4.510E ⁻⁰⁶	8.2E ⁻⁰⁹	0.8347	0.0015	0.6878	0.0008	1.214	0.003
DLRVR015 plg		1225.8	5065.4	0.9998	0.0009	4.371E ⁻⁰⁶	1.0E ⁻⁰⁸	0.8091	0.0019	0.7343	0.0015	1.102	0.003
DLRVR015 glass		7878.5	32395.3	1.0004	0.0023	4.365E ⁻⁰⁶	9.9E ⁻⁰⁹	0.8080	0.0018	0.7379	0.0014	1.095	0.003
standards	BCR-2	1701.1	5932.6	0.9998	0.0012	4.742E ⁻⁰⁶	1.2E ⁻⁰⁸	0.8777	0.0021	0.8701	0.0011	1.009	0.003
	IRMM036					3.059E ⁻⁰⁶	6.2E ⁻⁰⁹						
	Uraninite			1.0004	0.0009								



Fig. 5.6 Korke Seluwa Volcano and its recent obsidian lava

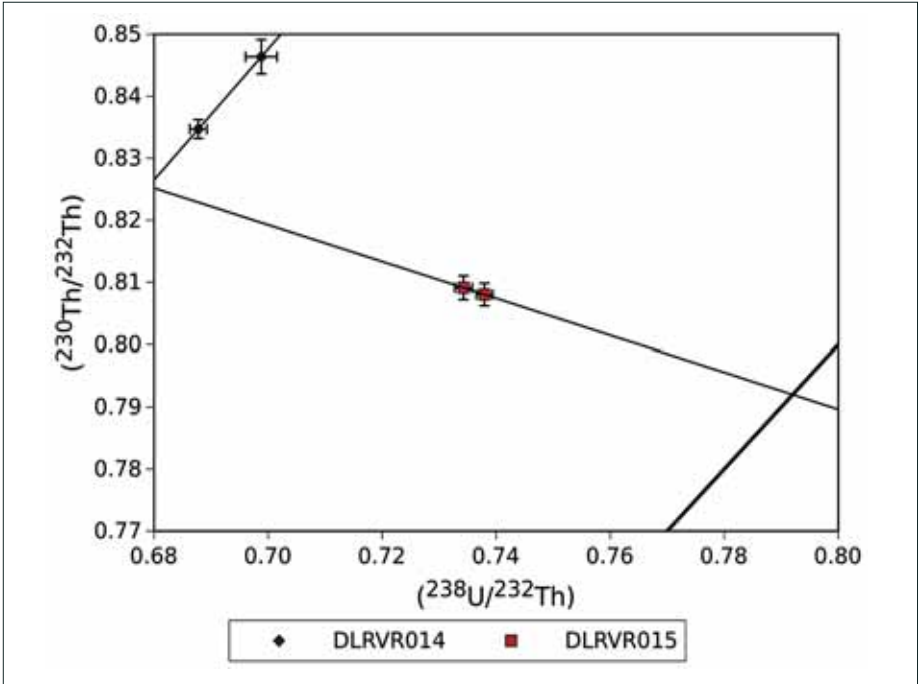


Fig. 5.7 Equiline diagram of $^{230}\text{Th}/^{232}\text{Th}$ and $^{238}\text{U}/^{232}\text{Th}$ isotopic ratios

associated with minor explosive events (pumice emissions). The lava extent is limited to the edifice of the volcano and the pumice also has a small extent. In such a scarcely populated area this volcano represents relatively little risk. Distal fall of a small amount of fine pumice might affect the larger town of Humbo about 12 km to the west if an eruption occurs during November-March, when winds frequently blow from the east.

Basaltic monogenetic volcanic fields

Basaltic volcanism in the studied area forms fields of small monogenetic volcanoes represented by scoria-, spatter- and tuff-cones. These small volcanoes are present in two areas i.e. Hamasa Volcanic Field and North Chamo Volcanic Field.

Hamasa Volcanic Field

Numerous basaltic scoria cones (Fig. 5.8) are scattered in a north-south elongated zone to the north of Lake Abaya. Most of these cones are located on the western (right) bank of the River Bilate but several cones also occur on the eastern (left) side. The volcanic cones consist of clast-supported scoria suggesting Stromolian styles of eruptions. No signs of phreatomagmatic events were observed. There are neither analytical data nor eye-witnessed reports on recent volcanic activity; however, the fresh shape of most of the scoria cones as well as scoria unaffected by weathering suggests a very young age of these volcanic cones. Moreover, numerous hot springs and fumaroles are present within this area. Therefore, we suppose this volcanic field is still active.

This area is only scarcely inhabited and therefore despite the high probability of repeated volcanic activity it does not represent a high risk area.



Fig. 5.8 Scoria cones of the Hamasa Volcanic Field on the faulted tectonic landscape

North Chamo Volcanic Field

Several scoria cones are scattered around the northern part of Lake Chamo and the adjacent part of the Nech Sar plain (Fig. 5.9). Although most of these cones are located to the south of the studied map sheet, we have included this volcanic system due to its presence near the town of Arba Minch. The scoria cones are dispersed to the south and east of the extinct Tosa Sucha Volcano, which they post-date in activity. According to George and Rogers (1999), activity of Tosa Sucha Volcano (God's Bridge) ceased approximately 0.7 Ma. Our data show activity of North Chamo Volcanic Field in the time span 1-0.5 Ma. Some of these cones form islands on Lake Chamo (Fig. 5.10). All of the volcanoes on the lake or in its near vicinity became active with phreatomagmatic events as documented from



Fig. 5.9 Kale Korke scoria cone on Nech Sar plain

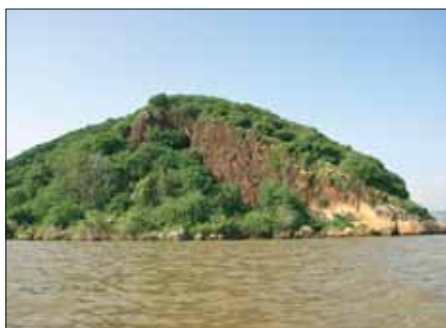


Fig. 5.10 Ganjule Island – scoria cone on Lake Chamo

a bedded and intensively fragmented unit in the lower part of succession overlain by clast-supported massive scoria (Strombolian phase; Fig. 5.11). Despite a small number of cones, the North Chamo Volcanic Field is unique due to a wide range of chemical compositions of erupted scoria. The magmatic system of the North Chamo Volcanic Field evolved from basalt to trachyte (Fig. 5.12).



Fig. 5.11 Pyroclastic deposits of a scoria cone exposed by a quarry on the shore of Lake Chamo. Deposits of the phreatomagmatic phase at the base and scoria of the Strombolian phase at the top.

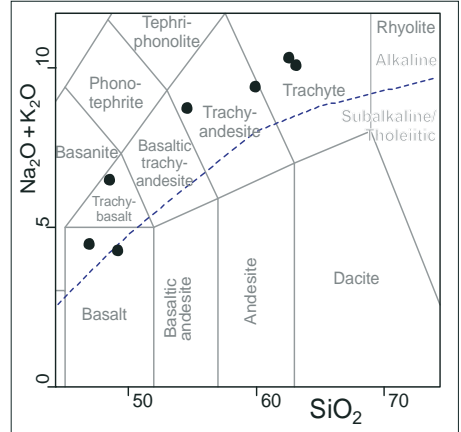


Fig. 5.12 TAS diagram (Le Bas et al. 1986) with chemical analyses of volcanic rocks erupted in the North Chamo Volcanic Field

Recommendations: Currently no monitoring apparatus is installed on any of the volcanic systems in Southern Ethiopia. We also lack historical and geochronological data on the potentially hazardous volcanic systems in order to understand the evolution of these volcanoes, the frequency of eruptions and the time since the last eruption. Repeated low-energy eruptions can be expected in the Hamasa Volcanic Field. Stronger eruptions may be experienced in the area of North Chamo due to the presence of water. On the other hand, none of the systems were determined under the age of 0.5 million years old, even though geochronological research in the area of Tosa Sucha and Chamo was intense and all of the major cones were investigated.

5.2 Exogenous geological hazards

5.2.1 Erosion hazards

Alluvial erosion is one of the most important exodynamic processes in the area of the Dila sheet and represents a major cause of land devastation. Erosion processes are the most intensive in landforms formed by fault scarps, erosional and structure slopes. As a natural exogenous process of the landscape, erosion is frequently accelerated by human activities in the form of intense agriculture associated with deforestation. In addition, climatic characteristics with stormy rains producing rapid runoff (Fig. 5.13) promote favorable conditions for erosion. Areas with weakly compacted alluvial and lacustrine deposits, re-sedimented volcanoclastics and weathered ignimbrites producing light sandy residual soils are the most prone to erosion. Rapid surface flow and channeling of runoff water are the most common mechanisms of the creation of erosional rills and gullies. Piping as a result of subsurface erosion can also result in gully growth (e.g. Morgan 1996, Bryan and Jones 1997). The creation of erosional structures is accompanied by subsequent processes, gravitational collapse of the sidewalls of gullies, and mass flow movement.

Intensive erosional processes lead to deeply dissected erosional landscapes with a high drainage density of rills and gullies – badlands. The development of badlands usually supports sparse vegetation, erodible rocks and stormy precipitations. Badlands can also be formed as a result of human activities like deforestation and intensive agriculture.

The areas most affected by erosion are in the **Bilate river catchment** (mainly on the eastern bank between Dimtu and the Bilate River Delta, Bisare and the Bedesa river sub-catchment on the western bank), and the south-western part of the **Gibado river catchment** (e.g. Tiliku Mancha sub-catchment located to the northwest of Dila and northeast of Lake Abaya). This area is mainly formed by highly weathered ignimbrites and tuffs producing silty and sandy residual soils, locally pumice and unconsolidated sediments, sands and gravels (Fig. 5.14). When the residual soils and weathered horizons are only a few meters thick and sheet erosion is predominant then rills and gullies (Fig. 5.15) can be centimeters to meters deep and wide. However, some ephemeral streams create canyons and gully systems tens of meters deep (e.g. Tiliku Mancha sub-catchment, Fig. 5.16). Badlands with very deep gullies are developed to the south of Belela village. This area is formed by thick accumulations of sands, gravels and unconsolidated volcanoclastics with several layers of clayey palaeosoils. Due to retrograde erosion, the sedimentary succession is cut by up to 40-meter deep gullies (Fig. 5.17). Incising of gullies is accompanied by lateral erosion, which leads to slope collapse, landsliding and lateral spreading (Fig. 5.18), which represents a very dangerous complex of exodynamic processes. Erosion with gully formation also takes place in inactive parts of alluvial fans formed by sediments (Fig. 5.19).

Recommendations: Reforestation is necessary to decrease the rates of erosion and planting of trees in the margin of badlands can help slow down badland extension. To decelerate the runoff of surface water it is recommended to plant rows of trees and construct small dams in the gullies (the sediment trapped in the dams could be later used as a fertilizer for arable land). Trees and



Fig. 5.13 Surface run-off during stormy rains in badlands situated to the northwest of Dila town



Fig. 5.14 Residual silty soils and pumice prone to erosion, to the east of Dimtu, Bilate river catchment



Fig. 5.15 Rill erosion in highly weathered tuffs, to the west of Belela



Fig. 5.16 Badlands along a deep canyon of the Tiliku Mancha River, to the north-east of Lake Abaya

deep-rooted bushes should also be planted on the boundaries of land plots to prevent soil erosion. Fortunately, the presence of paleosols and the climatic conditions can aid the possible recovery of soils if the erosion is stopped.



Fig. 5.17 System of deep gullies, to the south of Belela



Fig. 5.18 Landslide of gully slope triggered by lateral erosion, to the south of Belela

5.2.2 Inundations and accumulation of sedimentary material

Inundations and flood-related hazards are present in flood basins of fluvial systems and in active alluvial fans. However, ephemeral streams must also be regarded as an inundation risk due to flooding during rainy seasons. Inundations are usually accompanied by other exodynamic processes.

Lateral Erosion of river banks is related to flood events and high discharge. Banks of silty, sandy or gravel material along unstable braider streams with high variability of discharges make particularly favorable conditions for lateral erosion.

Avulsion is a very dangerous process. It is the relatively rapid change of the path of a river or stream into a new channel in the lower part of a floodplain or alluvial fan. The principal trigger factor is a decrease in channel gradient. The height difference between the channel and floodplain increases due to the aggradation of sediment within an active channel and the capacity of the channel for transporting water is reduced. Avulsion may lead to abandoned channels becoming reoccupied, levees belong active channels breaking and new channels being created. This process is accompanied by crevasse splay formations (fluvial deposits in a flood basin).

Accumulation is usually connected with floods as well as with earth flow processes. The greatest risk of high accumulation occurs in areas with an abrupt decrease in slope gradient. The loss of transporting medium power and carrying capacity result in rapid sedimentation of material eroded and transported from upper parts of the scarps and catchments and the creation of alluvial fans in the foothill of slopes, mouths of gullies as well as erosional and stream valleys.

Bilate River Catchment with an area of 5,418 km² represents an axial drainage system in the southern part of the MER terminating in Lake Abaya, and it is one of the principal fluvial systems of the Dila Sheet. Most of the Bilate River system has the character of a bedrock river with straight channels or low sinuosity braided channels with the limited occurrence of a flood basin, where deep and lateral erosion of banks are the principal hazards connected with high discharge (Fig. 5.19). The lower most part of catchment and the **Bilate River Delta** are characterized by a decrease in gradient and alternation of the fluvial character from a bedrock or braided river into an anastomosing system with multiple channels and an large inundation zone. There the river channels are very sensitive to avulsion with the creation of crevasse splays. The inundation related hazards affect a large area of the delta including agriculture zones and villages. For example



Fig. 5.19 Lateral erosion of banks of the Bilate River, Dimtu village

in 2013 a large area of the delta was inundated including farms (Fig. 5.20). The floods were accompanied by reoccupation of abandoned channels, the creation of crevasse splays (Fig. 5.21) and accumulation of sediments (Fig. 5.22 and Fig. 5.23).

The **Gibado** and **Gelana** rivers draining the eastern highlands into Lake Abaya also have a character of erosional streams in the upper part of catchment. In the lower part the rivers enter tectonically predisposed depressions located to the east of Lake Abaya and terminate in delta systems on the eastern margin of Lake Abaya. The flat surface of these sparsely populated areas



Fig. 5.20 Inundated farm located in surface crevasse splay, Bilate River Delta, July 2013. Image from Google Earth View



Fig. 5.21 Crevasse splay formed during floods in 2013, Bilate River. Image from Google Earth View



Fig. 5.22 Sandy accumulation of crevasse splay after floods in 2013, Bilate river flood basin



Fig. 5.23 Lateral sandy bar accumulated during floods in 2013, Bilate River

forms a wetland landform with meandering and anastomosing channels, and it is periodically also inundated with temporal lake formations (Fig. 5.24).

The flood basin of the Kulfa River between Lake Abaya and Lake Chamo is also frequently inundated (Fig. 5. 25). This causes the frequent inaccessibility of Nechi Sar National Park and negatively affects tourism in the Arba Minch area.



Fig. 5.24 Wetland with temporal lake in tectonic graben situated in the lowermost part of the Gibado River catchment. Image from Google Earth View



Fig. 5.25 Temporarily active overflow channel in the flood basin of the Kullfa River between Arba Minch and Nechi Sar National Park



Fig. 5.26 Active part of alluvial fan situated on the western shore of Lake Abaya near Dante village



Fig. 5.27 In-channel bars of the Kulfa River on the northern margin of Arba Minch



Fig. 5.28 Abandoned river channel, filled with gravel, to the north of Arba Minch



Fig. 5.29 Abandoned channel in an alluvial fan near Lante



Fig. 5.30 Avulsion points in the Kulfa River, northern margin of Arba Minch



Fig. 5.31 Lateral erosion along braided channels, alluvial fan near Lante



Fig 5.32 Bridge construction over the Sodo-Arba Minch road, high lateral erosion risk, to the north of Arba Minch

to Schütt et al. (2002) the shallow depth of Lake Abaya (maximum of 26 m), the lake level is very sensitive to high sediment input. The key role of high sediment input in the increase in lake levels is also documented by the progradation and extension of the Bilate River Delta.

Recommendations: Eliminate human activity in inundation areas, i.e. settlements due to the potential loss of life during floods and industry as a source of contamination, these places are more convenient for agriculture. To reduce loss of agricultural soil, infrastructure, settlements, environment etc. during floods in alluvial fans it is recommended to remove the accumulated material from active channels. Construction of houses and roads should be completely restricted



Fig 5.33 Floods in the Amaro River causing inaccessibility to Arba Minch, November 2012 (photo V. Žáček)

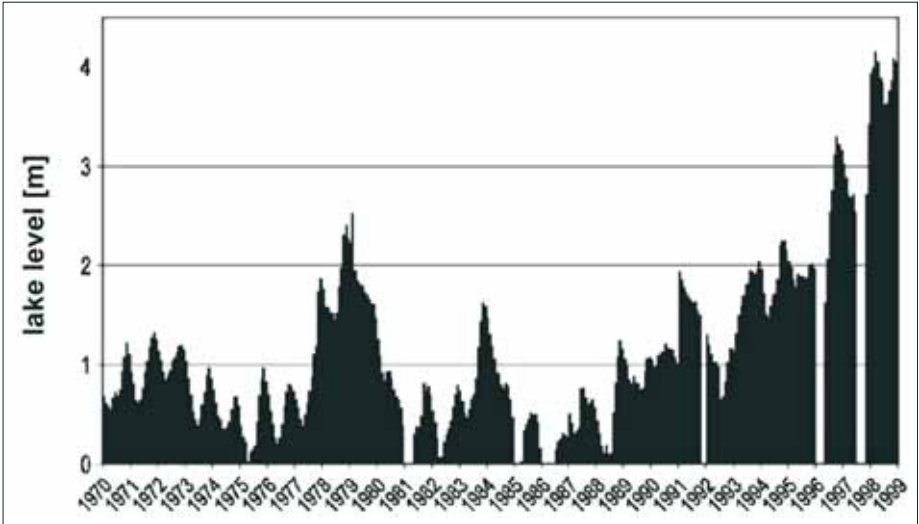


Fig 5.34 Monthly lake water levels of Lake Abaya at the Arba Minch gauging station (Seleshi 2001)

near the mouth of erosional valleys, in abandoned channels and crevasse splays. Also, construction of roads and bridges should respect geological, geomorphological and hydrological conditions. Frequent floods, lateral erosion and instability of streams in the alluvial fan on the western shore of Lake Abaya cause inaccessibility from Sodo to Arba Minch. In the future plans for alternative roads avoiding the alluvial fan system should be developed.

These geological hazards significantly increase poverty and morbidity in the region. More detailed geomorphological and geological analysis (based on high resolution DEM and detailed topographic data) is necessary in order to predict natural hazards and eliminate their impacts. These studies and geological hazard maps represent a basic dataset for effective mitigation projects, spatial planning and development in the region.

5.2.3 Slope deformation hazards

Slope deformations do not occur as frequently on the Dila map sheet as in the area of the Hosaina sheet. Only in a few limited areas several types of slope deformation – landslides, lateral spread and earth-/debris-flows – were documented. In general, the investigated area has a low susceptibility to slope movement. Most of the areas prone to slope movement are concentrated in the eastern part of the Genale River gorges. Very impressive but not risky lateral spreading was observed near Belela village. Slope deformations were mapped and evaluated based on a combination of remote sensing and fieldwork.

Landslides

Gorges of the Genale River

The eastern to southeastern parts of the Dila map sheet are dominated by large erosion valleys of the Logita, Bonora and Gambelto rivers, being segments of a larger area known as the Genale Gorges (Fig. 5.35). The Bonora River flows into the local main stream of the Logita River at 6.355°N 38.840°E. Further to the south at 6.296°N 38.898°E the Logita River flows into the Gambelto

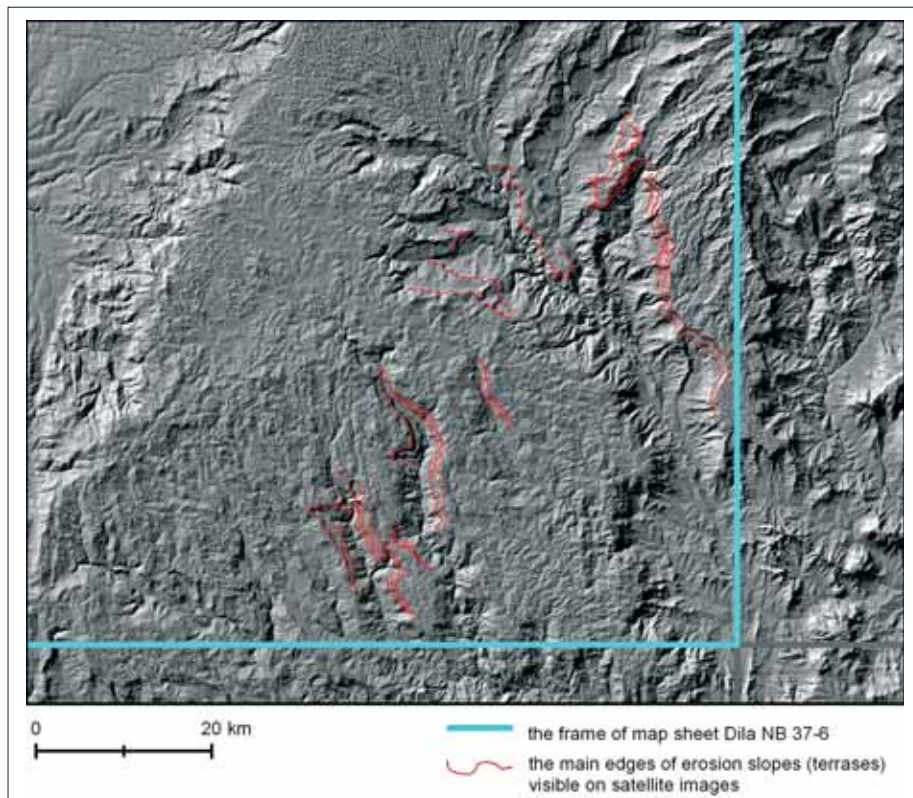


Fig. 5.35 The hillshade of the south-eastern quadrant of the Dila map sheet with highlighted slope edges as the result of retrograde erosion and slope movement

River creating one great Gambelto Valley running further to the south. These three rivers are local erosion bases and they form their own separate valleys.

While the erosion of the aforesaid rivers deepens, their tributaries cause retrograde erosion on the edges of slopes. This leads to extension of valleys and formation of erosion slopes with a terraced shape, or stair-step terrain. These slopes are susceptible to soil or rock slope movement, especially near the edges of terraces. In addition to these relatively shallow slope deformations the slopes can also be susceptible deep-seated deformations (Fig. 5.39). The most distinct amphitheatre-shaped valley edges (or edge terraces) are developed on left-bank tributaries of the Gambelto River as the result of retrograde erosion and slope movement. These occur in the upper part of this river between Hebeleshe and Gonjobe (Mejo sub-sheet 0638-D2), on the left-bank tributaries of the Logita River, and on Odiboko Ridge. This valley slope shape is also developed on other rivers (Bekeka–Lebetu River; Koke–Boye–Hawata River; Shela–Boda River and Gejaba River) and their tributaries.

Genale River slope movement

Slope movement mainly occurs on escarpment terraces covered with colluvial and alluvial sediments consisting of boulders, debris, and silt. Anthropogenic interventions such as road



Fig. 5.36 Shallow debris slide on the toe of a rock rotational slide (Fig. 3) on an escarpment terrace

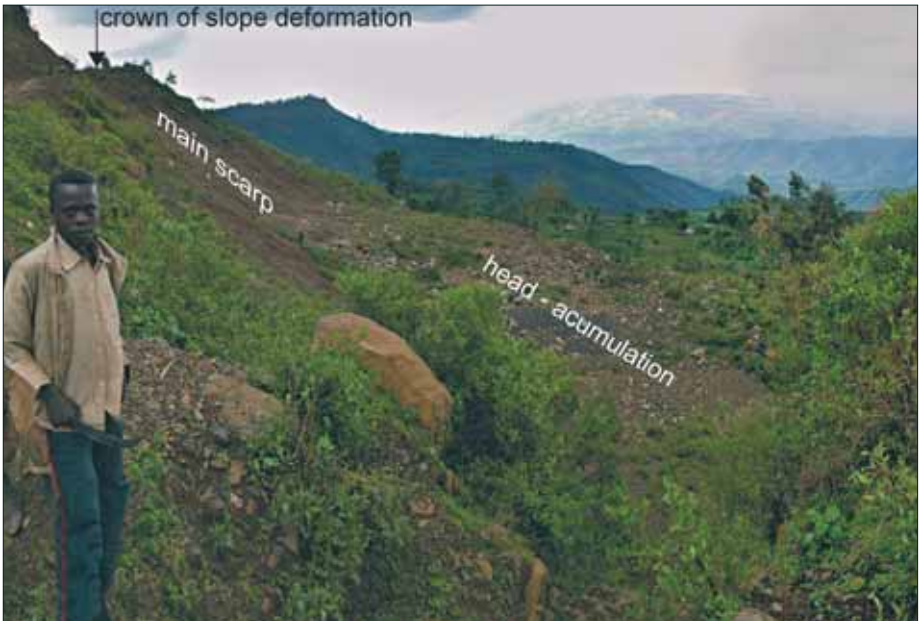


Fig. 5.37 Slope deformation of Rock rotational slide on escarpment terrace, occur below the road leading from Gambelo river valley to Mejo town

constructions, changing the slope geometry and drainage settings, disrupt the slope stability. The slope deformation on the upper edge of the Gambelo River valley, below the road from the valley to Mejo town is given as an example. The recent debris flows originate on older rock rotational landslides. These older landslides have a combined (rotational and lateral) shear zone with an approximate depth of 5–10 m, approximate width of 120 m and approximate length of 150 m (Fig. 5.36, 5.37). After the main slide, shallow and small movements occur in the accumulation of



Fig. 5.38 Boulders and debris fall to debris slide in the Gambelo – Mejo road cut

the main slope deformation, namely on its toe (usually in the form of debris slide; Fig. 5.37). The shallow slope deformations, like boulder and debris fall or debris slide, may also occur in road (Fig. 5.38) or river cuts.



Fig. 5.39 Position of a deep-seated slope deformation in the Gonjobe river valley (Google Earth)

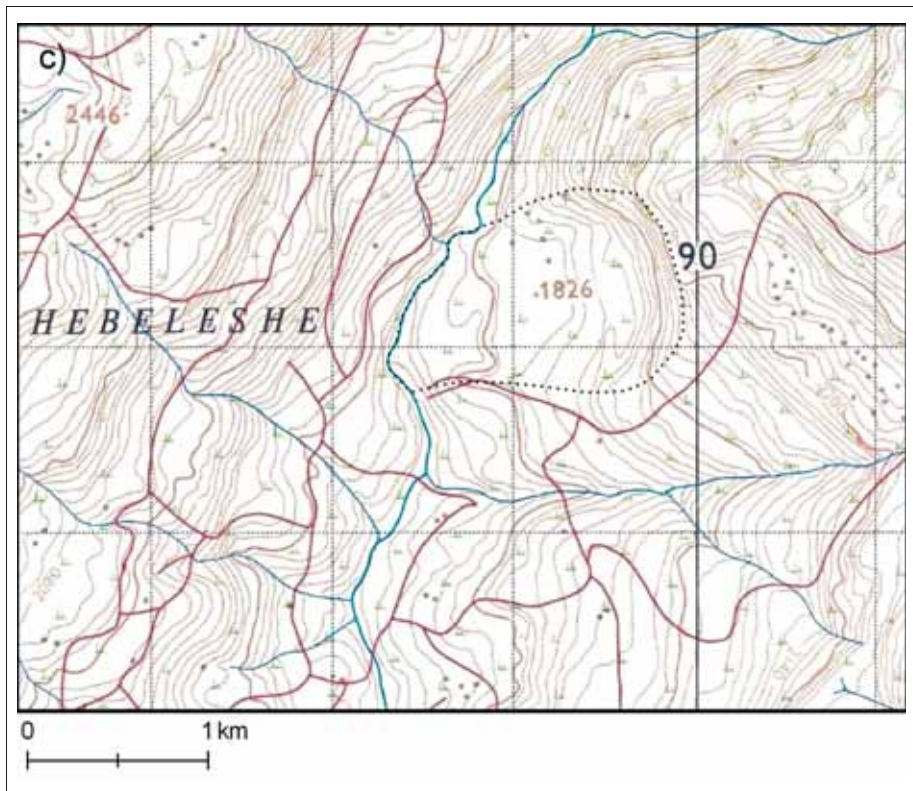


Fig. 5.40 Detail of the topographic map Mejo 0638-D2

Gonjobe deep-seated slope deformation

The deep-seated nature of the deformation of the Gonjobe river valley is concluded from its extremely high main scarp (around 200 m at its highest point; 6.646°N 38.909°E; Fig. 5.39, 5.40, 5.41). The accumulation body has a relatively flat surface. Landslide accumulation in the valley has changed the river channel geometry (Fig. 5.41 and 5.45). This is an old slope deformation as the original bedding has been heightened by selective erosion and the main scarp is affected by rill erosion (Fig. 5.40) of the streams that flow over the crown.

Dorze rock slides

Two small rock slide areas (rock collapse *sensu* Hunger et al. 2012) were documented around Dorze. Deposits of collapsed blocks are spread in two areas with dimensions of approximately 1×1 km (Fig. 5.42) and 0.5×0.5 km, respectively. The thickness of the deposits is unclear but most likely it does not exceed 10 m. We suppose that the sliding of the rock mass on this slope was on an irregular rupture surface. As observed on the main scarp, the exposed ignimbrites are jointed by numerous randomly oriented joints, which separate segments of intact rock. Such conditions increase the susceptibility for sliding. These movements may include events of toppling in the initial stages. Movements in the final stage are very sudden and rapid.

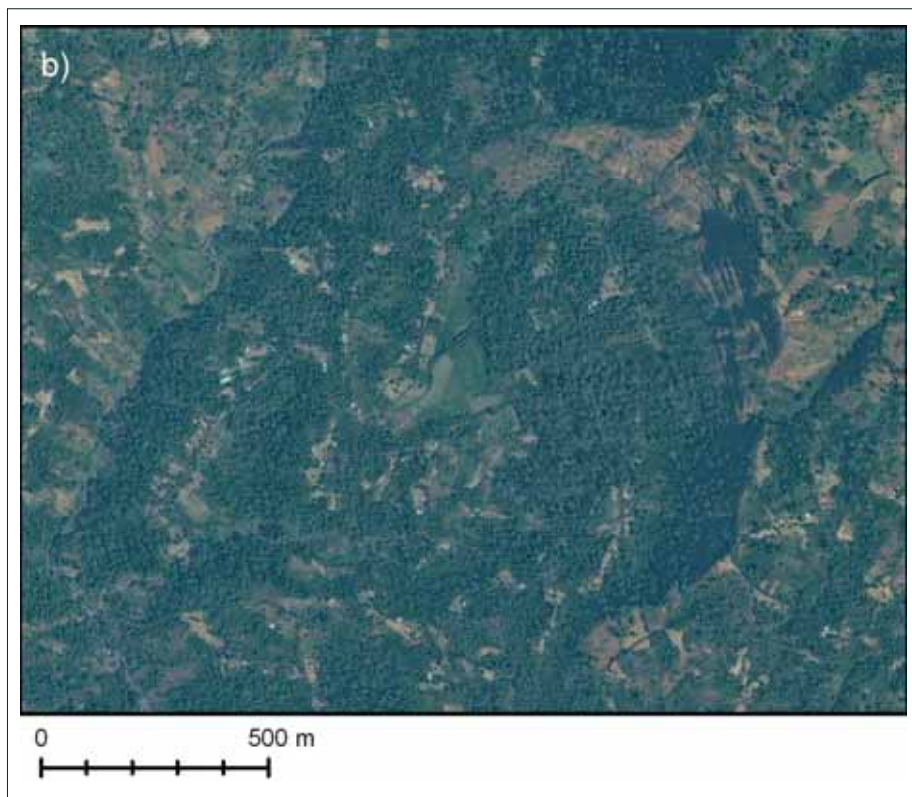


Fig. 5.41 The main scarp is affected by selective rock and linear erosion (Bing maps)



Fig. 5.42 View on deposits of blocky ignimbrites representing of slide accumulation

Lateral spread

Belela village

A very impressive slope movement which can be described as a “lateral spread” (Fig. 5.43, Varnes 1978) is located about 2 km to the south of Belela village, 40 km southwest of Hawasa city. Hunger et al. (2012) classify this type of movement as a “compound slide”, with typical horst and graben features at the head (Fig. 5.43) and many secondary shear surfaces (Fig. 5.44). The basal segment of the shear zone in this case follows a weak horizon of paleosoil (Fig. 5.45). This is an active and developing phenomenon but represents no risk to infrastructure. The main scarp of the lateral spread is over 10 m high and exposes non-welded ignimbrites and loose pyroclastic deposits, with mechanical characteristics corresponding to soils from an engineering geology point of view. The slid masses shifted the stream channel in the bottom of erosional gully (Fig. 5.46). We documented open cracks (Fig. 5.47) on the surface in the foreground of movements in November 2013. The frequency of movements increased in April 2014.



Fig. 5.43 Horst and graben features in the upper part of the deformation.

Conditions: Heavy rain and the 1 m thick layer of paleosoil below the soft volcanic rock are the main conditions for sliding and lateral erosion of streams.

Debris flows (earth flow)

Baso River debris flow

The landscape is most vulnerable to the formation of debris flows on the tectonic scarps of the Main Ethiopian Rift (MER), for example on the slopes of Degena Ridge. The geological settings of



Fig. 5.44 Detail of the shear zone



Fig. 5.45 Basal segment of the shear zone in this case follows a weak horizon of paleosols



Fig. 5.46 Masses of the rock body have shifted the stream channel



Fig. 5.47 Open cracks mapped in November 2013

the slopes in the source area consist of highly weathered ignimbrites (Fig. 5.48). Debris flow can occur on steep slopes with highly weathered rocks and represents a high risk phenomenon. This debris flow was triggered by heavy rains and represent important source of sedimentary material subsequently resedimented by alluvial processes and accumulated along the Baso River channel (Fig. 5.49 and 5.50) as lateral and in-channel gravels bars or sheet floods deposits.. These processes are closely related to the development of alluvial fans.



Fig. 5.48 The source area of debris flow is shaped by landslides



Fig. 5.49 Alluvial gravels representing resedimented debris-flow deposits along the Baso River



Fig. 5.50 View of the Baso River channel from Dorze Giyorgis church

Recommendations: The whole area of the MER scarps is potentially susceptible to debris/earth flows. Therefore, tectonic scarps and alluvial fans below should be indicated as a high risk zone (Fig. 5.49). Debris/earth flows are a very rapid and dangerous phenomenon. For the future, construction of houses and roads should be restricted, especially near erosion gullies and on the scarp foothills. This area is used mainly for agriculture but in the lower part the river channels cross the main asphalt road connecting Arba Minch with Soddo. Construction of bridges on this main asphalt road should respect the geological conditions and requires detailed engineering geology studies.

Rock falls and toppling

Vertical slopes, especially on tectonic scarps, are prone to rock falls and toppling. These processes do not occur over large areas. The risk of rock falls is documented in tectonic scarps situated between Leku and the Bilate River or tectonic scarps above the western bank of Lake Abaya. The main rock fall triggering factors are heavy rains and seismic events.

Recommendations: The foothills below the affected scarps are at permanent risk of rock falls. Therefore, we do not recommend construction of houses. In populated areas or in cases of road constructions, mining etc. detailed geological investigation is recommended.

5.3 Hydrological and hydrogeological hazards

5.3.1 Fluoride

The problem with the high fluoride content in the water of the Hawasa and Shashemene area is very well known and is described in many studies. The fluoride concentration frequently exceeds 3 mg/l which can cause mild fluorosis (mottling of teeth). Higher fluoride concentrations in drinking water cause both dental and skeletal fluorosis resulting in serious public health problems. The treatment of fluoride in groundwater, if viable, could resolve a number of pressing water supply problems in the area.

Fluoride concentrations are particularly high in areas with an occurrence of thermal waters or near areas of recent volcanism within the MER (Fig. 5.51). There is a direct correlation between silicic volcanic rocks such as obsidian and pumice and high concentrations of fluoride in groundwater. It is considered that leaching of water soluble Na-fluorides coating pyroclasts is the most likely source of fluoride. The rhyolitic rocks are extremely poor in phosphorus which would lead to fixing of the fluorine in apatite and they lack calcium which would react with fluorine producing non-leachable calcium fluoride. The interaction of the rhyolitic pyroclastic rocks with a large effective surface and percolating groundwater and carbon dioxide at high pH causes the release of fluoride into the groundwater. It is suggested (Rango et al. 2009) that the fluoride concentration in groundwater is inversely related to the concentration of Ca. This permits free mobility of the fluoride ion into groundwater at a lower Ca content. This effect (Ca deficiency) is magnified where

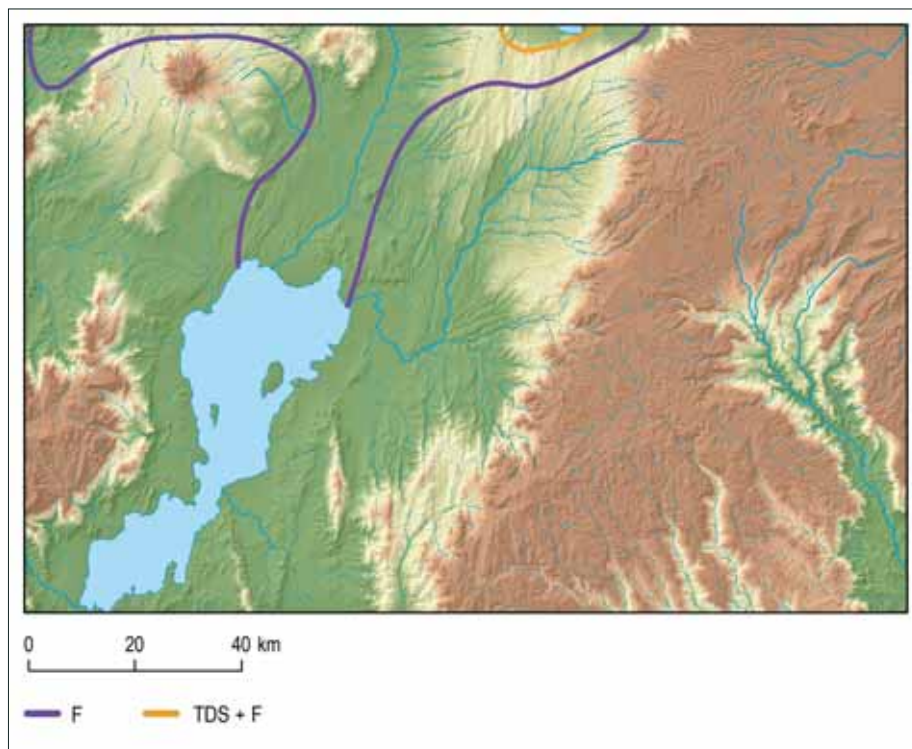


Fig. 5.51 Scheme of the area affected by high fluorine concentrations in the Dila map sheet area

cation exchange takes place within the sediments (fluvio-lacustrine, volcano-lacustrine) causing the removal of ions from the solution (mainly Ca^{2+}) and replacement with Na^+ ions from the clay. Such hydrogeochemical processes are responsible for the evolution of Ca (Mg)- HCO_3 types of water of the highlands and the escarpment area to Na- HCO_3 types of groundwater (including the thermal water of the rift floor).

Thermal water tends to have a higher fluoride content than cold water as the water temperatures allow greater dissolution of fluoride. This probably explains the preponderance of high fluoride in waters around Hawasa town. Closed terminal lakes attain high fluoride, salinity and alkalinity as a result of evaporation and the groundwater flux that comes through the acidic rocks. High concentrations can also be observed in the northeastern area of the Bilate River, the surroundings of Lake Hawasa as well as in the lake itself.

Tadesse and Zenaw (2003) and by JICA (2012) showed that the fluoride content decreases with increasing depth of the water source (testing wells). This confirms that the main source of fluoride is related to infiltration of rain water through young deposits of silicic volcanic activity. The concentration of fluoride can be enhanced in geothermal systems. The same is also valid for the concentration of chlorides as well as nitrates. Tadesse and Zenaw (2003) noted that the decrease of fluoride with depth in the area indicates that the shallower lacustrine aquifer has a high concentration of fluoride (Fig. 5.52).

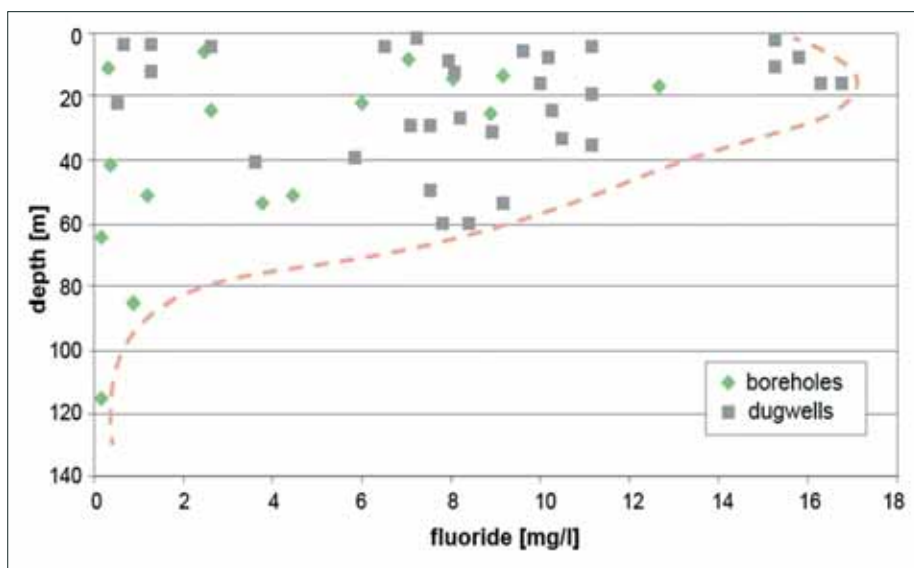


Fig. 5.52 High content of fluoride is caused by its leaching from silicic pyroclastic deposits. A decrease in fluoride content in groundwater with increasing depth is most likely the effect of depletion of older pyroclastic deposits and lacustrine sediments due to greater age and longer leaching of fluoride in the past. After Tadesse and Zenaw (2003).

A number of fluoride removal methods are practiced in basic water treatment plant design. The method of adding gypsum to the artificial sand-pack filter of a borehole and mixing of hot water with cold water was successfully tested in fluoride rich groundwater in Mexico (Carrillo-Rivera, 2002).

5.3.2 Unexpected discharge of thermal water

Active volcanic zones are associated with hydrothermal systems. The thermal waters can be used for power production or balneological purposes. On the other hand, an unexpected discharge of hot water also represents a serious hazard in the studied area. Drilling of a well not equipped for an unexpected hot water discharge occurred in Dimtu on the bank of the Bilate River. The river flows from north to south following the Main Ethiopian Rift Valley and represents an important geothermal structure in this part of the rift. There are numerous hot springs along the river and hot water was found in several wells. The river is one of the main surface water sources of the Lake Abaya and flows in a system of grabens and young volcanic centers of the Lake Abaya Geothermal Field for 10 km prior to reaching the lake. The well in Dimtu was drilled about 1 km to the south of the group of thermal springs to a depth of 250 m b.g.l.

Lithologically, formations encountered up to 42 m b.g.l. were described as weathered to fresh basalt with some basaltic breccia around 13 to 24 m b.g.l. Massive fresh basalt alternates with reddish basaltic breccia up to 90 m b.g.l. The formation changes to acidic members such as rhyolitic tuff and welded tuff of a white to pale green color below 90 m up to around 160 m b.g.l. These acidic volcanic sediments are moderately to highly weathered. The remaining section is dark gray to green tuff and welded tuff nearly to the bottom. This section is highly weathered/ altered and the samples are in a clay form in most cases and the drilling rate is very low.

Water was struck at around 26 to 31 m b.g.l. and another large amount of water was observed at around 54 to 58 m b.g.l. The well suddenly started to overflow during the well development due to air lifting. The water was hot with a temperature of about 54 °C, without any sign of high concentrations of dissolved components when sniffed and tasted. The flow rate of the overflowing water measured in the draining channel indicated that it was nearly 100 l/sec. The thermal water



Fig. 5.53 Overflow of the hot water from well at Dimtu

in the well is under high pressure and it was not possible to prevent the well from overflowing (Fig. 5.53).



Fig. 5.54 Documentation of slope deformations at the edge of erosional gully near Bedele

References

- Acocella V.** (2010): Coupling volcanism and tectonics along divergent plate boundaries: Collapsed rifts from central Afar, Ethiopia. *Geological Society of America Bulletin* 9-10: 1717–1728.
- Agezew, T., Regassa, T., Šíma, J.** (2014): Hydrogeological and hydrochemical maps of Dila NB 37-6. Explanatory notes. Aquatest a.s., Praha, Czech Republic.
- Agostini, A., Bonini, M., Corti, G., Sani, F., Manetti, P.** (2011): Distribution of Quaternary deformation in the central Main Ethiopian Rift, East Africa. *Tectonics* 30.
- Asfaw, L. M.** (1998): Environmental hazard from fissure in the Main Ethiopian Rift. *Journal of African Earth Sciences*. 27, 481-490.
- Ayenew, T.** (2009): *Natural Lakes of Ethiopia*, Addis Ababa University press, ISBN 978-99944-52-21-7, pp. 197
- Balogh, K.** (1985): K/Ar Dating of Neogene Volcanic Activity in Hungary: Experimental Technique, Experiences and Methods of Chronologic Studies. *ATOMKI Rep., D/1: 277–288*.
- Berhane et al.** (1976): Geological map of Lake Ziway area, 1:500,000 scale. Unpublished report.
- Bonini, M.; Corti, G.; Innocenti, F.; Manetti, P.; Mazzarini, F.; Abebe, T.; Pécskay, Z.** (2005): Evolution of the Main Ethiopian Rift in the frame of Afar and Kenya rifts propagation. *Tectonics* 24.
- Bryan, R.B.; Jones, J.A.A.** (1997): The significance of soil piping processes: Inventory and prospect. *Geomorphology* 20, 209–218.
- Carrillo-Rivera, J.J.** (ed. 2002): Use of abstraction regime and knowledge of hydrogeological condition to control high-flouride concentration in abstracted groundwater: San Luis Potosí basin, Mexico, *Journal of Hydrogeology* 261, 24–47.
- Davidson** (1983): The Omo River Project, Reconnaissance Geology and Geochemistry of Parts of Ilubabor, Kefa, Gemu Kefa and Sidams, Ethiopia.
- Ebinger, C.** (2005): Continental breakup: The East African perspective: *Astronomy and Geophysics*, 46: 216–221.
- Ephrem** (2009): Geology of the Akaki-Beseka area. Basic Geoscience Mapping Core process, Geological Survey of Ethiopia, Addis Ababa.
- FAO-UNESCO** (2000): Soil map of the World, 1:5,000,000 (download for ArcGis) - <http://www.lib.berkeley.edu/EART/fao.html>
- Gamatchu D.** (1977): *Aspects and Water budget in Ethiopia*, AA University Press, Addis Ababa.
- Gebreegzeibher, Y.** (2004): Assessment of water balance of Lake Hawasa Catchment, Ethiopia. PhD. Thesis. International Institute for Geo-Information Science And Earth Observation. Enschede, The Netherlands.
- George, R., Rogers, N.** (1999): The Petrogenesis of Plio-Pleistocene alkaline volcanic rocks from the Tosa Sucha Region, Arba Minch, southern Main Ethiopian Rift. *Acta Vulcanologica*, 11: 121–130.
- Gobena, H.; Belayneh, M.; Kebede, T.; Tesfaye, S.; Abraham, A.** (1996): Geology of the Dodola area. Geological Survey of Ethiopia, Addis Ababa.
- Gouin, P.** (1979): Earthquake history of Ethiopia and the Horn of Africa. Ottawa, Ont., IDRC, 259 p.

- Gozalbez, J.; Cebrian, D.** (2006): Touching Ethiopia 2nd English edition, 2006, Shama Publisher.
- Halcrow** (2008): Rift Valley Lakes Basin Integrated Resources Development Master Plan Study Project, Draft Phase 2 Report Part II Prefeasibility Studies, Halcrow Group Limited and Generation Integrated Rural Development (GIRD) consultants. Unpublished report. Addis Ababa.
- Hayward, N.J., Ebinger, C.J.** (1996): Variations in the along-axis segmentation of the Afar Rift system. *Tectonics* 15: 244-257.
- Hunger, O., Leroueil, S., Picarelli, L.** (2012): Varnes classification of landslide type, an update. *Landslide and Engineered Slopes*, Eberhardt et al. (eds) pp.47-58, Taylor and Francis Group, London.
- IAEG** (1976): Engineering geological map: a guide to their preparation. UNESCO Press, Paris, 79 pp.
- JICA** (2012): The Study on Groundwater Resources Assessment in the Rift Valley Lakes Basin in the Federal Democratic Republic of Ethiopia, Japan International Cooperation Agency (JICA), Kokusai Kogyo Co., Ltd., Ministry of Water and Energy (MoWE), The Federal Democratic Republic of Ethiopia. Final Report (Main Report).
- Kazmin, V.** (1973): Geological Map of Ethiopia. Geological Survey of Ethiopia: Addis Ababa, Ethiopia.
- Kazmin, V.; Seife, M.B.; Nicoletti, M.; Petrucciani, C.** (1980): Evolution of the northern part of the Ethiopian Rift. *Accad. Naz. Lincei, Rome* 47, 275-291. Italy.
- Kazmin, V.; Berhe, S.M.; Wondm-Agennehu, B.** (1981): Geological Map of the Ethiopian Rift. The Ethiopian Government – Ministry of Mines, Energy and Water Resources, Addis Ababa.
- Kebede, F.; Van Eck, T.** (1997): Probabilistic seismic hazard assessment for the Horn of Africa based on seismotectonic regionalisation. *Tectonophysics*, 270, 221-237.
- Koepen in NMSA** (1989): Climatic and Agroclimatic Resources of Ethiopia, NMSA, AA, August 1989.
- Le Bas, M.J., Le Maitre, R.W., Streckeisen, A., Zanettin, B.** (1986): A chemical Classification of volcanic rocks based on the total alkali-silica diagram. *J. Petrol.* 27: 745-750.
- Mengesha, T.; Tadiwos, C.; Workneh, H.** (1996): The geological map of Ethiopia, 1:2,000,000 scale, (2nd editon), EIGS, Addis Ababa.
- Merla, G.; Abbate, E.; Canuti, P.; Sagri, M.; Tacconi, P.** (1973): Geological map of Ethiopia and Somalia, 1:2,000,000. Consiglio Nazionale delle Ricerche Italy, Stabilimento Poligrafico Fiorentino, Firenze.
- Morgan, R.P.C.** (1996): Soil erosion and conservation, 2nd edition. Longman: Harlow.
- Nida, D., Bizuye, Y., Rapprich, V.** (2014): Engineering geology and geohazard maps of Hosaina NB 37-2. Explanatory notes. Aquatest a.s., Praha, Czech Republic.
- NMSA** (1996): Assessment of Drought in Ethiopia, Meteorological Research Reports Series No. 2, Addis Ababa, Ethiopia.
- Odin, G.S.** (1982): Numerical Dating in Stratigraphy. John Wiley and Sons, New York, pp 1-1040.
- Rango, T.; Bianchini, G.; Beccaluva, L.; Ayenew, T.; Colombani, N.** (2009): Hydro-geochemical study in the Main Ethiopian Rift: new insights to the source and enrichment mechanism of fluoride. *Environmental Geol.* 58: 109-118.
- Schütt, B., Förch, G., Bekele, S., Thiemann, S.** (2002): Modern water level and Sediment accumulation changes of Lake Abaya, southern Ethiopia-A case study from the northern lake area. *Water Resources and Environment Research*, 2: 418-422.
- Seife Michael, B.** (1978): Geological map (1:250,000) of the Nazret area. Ethiopian Inst. Geol. Surv., Addis Ababa, sheet NC37-15.
- Bekele, S.** (2001): Investigation of water resources aimed at multi-objective development with respect to limited data situation: The case of Abaya-Chamo basin, Ethiopia. Institut für Wasserbau und Technische Hydromechanik, Wasserbauliche Mitteilungen, 19.
- Setegn, S.G.** (2010): Modeling Hydrological and Hydrodynamic Processes in Lake Tana Basin, Ethiopia, KTH. TRITA-LWR PhD Thesis 1057.
- Steiger, R.H.; Jäger, E.** (1977): Subcommittee on Geochronology: convention on the use of decay constants in geo- and cosmochronology. *Earth and Planetary Science Letters*, 36: 359-362.
- Tadesse, D.; Zenaw, T.** (2003): Hydrology and Engineering Geology of Awasa Lake Catchment, Geological survey of Ethiopia, 1-67 + 2 maps.

- Tadiwos , C.** (2011): Geology and hydrothermal resources in the northern Lake Abaya area (Ethiopia). *Journal of African Earth Sciences*, 61: 129–141.
- Tesfay, T.** (2001): Nile question: Hydropolitics, Legal Wrangling, Modus Vivendi and Perspectives.
- Tesfaye, Ch.** (1993): Hydrogeology of Ethiopia and Water Resources Development – MS EIGS, Ministry of Mines and energy, Addis Ababa.
- Tesfaye, S., Harding D.J., Kusky, T.M.** (2003): Early continental breakup boundary and migration of the Afar triple junction, Ethiopia Geological Society of America Bulletin 115/9: 1053–1067.
- Tilahun, K.; Šíma, J.** (2013): Hydrogeological and hydrochemical maps of Hosaina NB 37-2. Explanatory notes. Aquatest a.s., Praha, Czech Republic.
- Tsigie L., Abdelsalam M.G.** (2005): Neoproterozoic–Early Paleozoic gravitational tectonic collapse in the southern part of the Arabian-Nubian Shield: The Bulbul Belt of southern Ethiopia. *Precambrian Res.* 138 (3), 297-318.
- Varnes, J.D.** (1978): Slope Movement Types and Processes. In: Landslides, Analysis and Control, Special Report 176, editors: R. L. Schuster, R.J. Krizek, National Academy of Sciences, Washington, D.C., pp. 11–33.
- WHO** (2006): World Health Statistics, <http://www.who.int/countries/eth/eth/en/>
- WWDSE** (2001) The study of Lake Awassa level rise (Main Report, Vol II). Unpublished report of the Water Works Design and Supervision Enterprise, Addis Ababa, Ethiopia, pp 291.
- Žáček, V.; Rapprich, V.; Aman, Y.; Berhanu, B.; Čížek, D.; Dereje, K.; Erban, V.; Ezra, T.; Firdawok, L.; Habtamu, M.; Hroch, T.; Kopačková, V.; Kycl, P.; Málek, J.; Mišurec, J.; Orgoň, A.; Pécskay, Z.; Šíma, J.; Tarekegu, D.; Verner, K.** (2014): Explanation Booklet to the Set of Geoscience maps of Ethiopia at scale 1 : 50,000, subsheet 0738-C4 Hawasa. Czech Geological Survey/Aquatest/Geological Survey of Ethiopia, Praha/Addis Ababa, Czech Republic/Ethiopia.



Annex No. 1
Annex No. 1

Sample	locality	rock	Coordinates (UTM)		LAB	SiO ₂	TiO ₂	Al ₂ O ₃	Fe ₂ O ₃	FeO	MgO	MnO	CaO
			X	Y									
DLRVR011	Apala	scoria	374340	732866	CGS	47,59	3,43	14,66	10,99	2,32	4,69	0,223	8,68
DLRVR012	Apala	basalt	372116	735303	CGS	45,10	3,74	14,44	4,48	9,92	5,70	0,220	9,95
DLRVR013	Bula	trachyte	377048	743062	CGS	65,57	0,46	15,41	3,50	1,27	0,23	0,223	1,21
DLRVR014	Korke	obsidian	378121	742020	CGS	70,43	0,33	12,05	1,72	2,86	0,05	0,216	0,52
DLRVR015	Korke	obsidian	378547	740549	CGS	74,69	0,20	10,32	1,76	2,03	0,02	0,104	0,22
DLRVR019	Abela Malaga	basalt	371697	729389	CGS	46,51	4,05	14,29	4,40	9,85	5,10	0,229	8,13
DLRVR020	Kale Korke	scoria	352028	661706	CGS	48,01	1,61	15,19	5,70	3,83	8,66	0,158	9,95
DLRVR021	Alakom	basalt	351437	663734	CGS	47,42	2,24	16,52	4,02	5,22	7,19	0,133	7,91
DLRVR025	Chamo	basalt	342684	655936	CGS	46,23	1,46	15,38	4,06	5,50	10,48	0,169	10,56
DLRVR026A	Chamo	pumice	337627	656719	CGS	62,19	0,56	16,75	4,23	1,74	0,56	0,174	2,28
DLRVR026C	Chamo	scoria	337627	656719	CGS	58,33	0,83	16,85	5,60	1,83	1,02	0,195	3,28
DLRVR026D	Chamo	phonolite	337627	656719	CGS	62,14	0,62	16,66	3,59	2,48	0,65	0,182	2,59
DLRVR028	Arba Minch	basalt	338062	660575	CGS	54,00	1,27	18,67	4,57	3,15	2,14	0,135	5,75
DLRVR029	Hamasa river	basalt	369935	726486	CGS	51,44	2,77	13,58	3,90	7,19	3,44	0,224	6,97
Sd061	Shashemane	basalt	456389	771511	CGS	48,63	2,17	16,87	3,13	7,66	5,50	0,174	9,21
KV122	Dila	amphibolite	483635	705564	CGS	48,62	0,19	15,51	2,40	5,85	10,65	0,186	12,73

Sample	Li ₂ O	Na ₂ O	K ₂ O	P ₂ O ₅	F	CO ₂	C	S(tot.)	H ₂ O(+)	H ₂ O(-)	F(ekv)	S(ekv)	Total	Cu_XRF	Cr
DLRVR011	0,001	3,68	1,43	1,190	0,076	< 0,01	0,038	< 0,010	0,59	< 0,05	-0,032	-0,002	99,63	19	5,9
DLRVR012	0,001	3,30	1,12	0,846	0,116	< 0,01	0,055	< 0,010	0,52	0,22	-0,049	-0,002	99,75	24	16,5
DLRVR013	nest.	5,85	5,00	0,037	0,083	< 0,01	0,025	0,017	0,81	0,12	-0,035	-0,004	99,81	4	3,2
DLRVR014	0,005	5,68	4,96	0,030	0,181	< 0,01	0,021	< 0,010	0,46	0,08	-0,076	-0,002	99,61		3,0
DLRVR015	0,006	5,23	4,31	0,013	0,293	0,01	0,011	< 0,010	0,74	< 0,05	-0,123	0,000	99,98	4	8,7
DLRVR019	0,002	3,56	1,42	1,128	0,146	< 0,01	0,022	< 0,010	0,31	0,08	-0,061	-0,001	99,23	16	5,1
DLRVR020	< 0,001	2,79	1,38	0,347	0,096	0,21	0,027	< 0,010	1,13	0,35	-0,040	-0,001	99,44	54	362,2
DLRVR021	0,001	4,16	2,17	0,693	0,101	0,05	0,007	< 0,010	1,51	0,21	-0,043	-0,001	99,54	58	124,8
DLRVR025	0,002	3,05	1,36	0,295	0,106	0,11		< 0,010	0,53	0,22	-0,045	0,000	99,52	54	343,5
DLRVR026A	0,003	5,96	3,96	0,137	0,046	0,02	0,010	< 0,010	0,43	0,08	-0,019	-0,001	99,12	10	3,5
DLRVR026C	0,003	5,62	3,52	0,253	0,104	< 0,01	0,049	0,011	1,52	0,14	-0,044	-0,003	99,16	13	4,72
DLRVR026D	0,002	6,08	4,13	0,147	0,032	0,01	0,008	< 0,010	0,21	< 0,05	-0,013	0,000	99,57	9	2,2
DLRVR028	0,002	5,42	3,20	0,614	0,071	0,01	0,007	< 0,010	0,60	0,09	-0,030	-0,001	99,70	39	9,5
DLRVR029	0,001	3,75	2,28	1,577	0,163	0,26	0,022	< 0,010	1,24	0,37	-0,069	-0,001	99,18	7	4,3
Sd061	0,001	3,47	1,00	0,395	0,073	0,16		< 0,010	0,69	0,19	-0,031	-0,002	99,33		34,1
KV122	< 0,001	1,07	0,14	0,023	0,021	0,05		0,044	1,82	0,11	-0,009	-0,011	99,41	101	

Sample	Cr_XRF	Ga	Hf	Mo_XRF	Nb	Nb_XRF	Ni	Ni_XRF	Pb	Pb_XRF	Rb	Rb_XRF	Ta	Th	U
DLRVR011	7	20,9	4,7	< 1	68,8	56	13,9	5	21,8	< 2	20,6	25	13,5	12,0	1,7
DLRVR012	15	21,6	2,7	< 1	45,9	50	24,2	9	44,9	2	9,9	18	23,5	5,8	0,7
DLRVR013	< 2	29,7	7,0	4	83,8	123	12,7	4	12,3	8	56,4	84	11,7	10,4	2,6
DLRVR014		33,6	29,5		142,7		5,5		29,9		98,0		13,6	22,6	5,0
DLRVR015	5	31,9	17,7	4	145,0	276	29,9	14	33,4	33	93,7	186	24,0	23,5	8,7
DLRVR019	5	21,9	3,4	< 1	70,7	59	12,2	4	14,0	< 2	19,3	26	41,8	6,7	1,0
DLRVR020	297	16,8	2,5	< 1	55,2	60	126,4	140	39,0	3	24,5	36	10,9	7,1	1,4
DLRVR021	94	18,1	2,9	1	58,6	70	99,8	91	10,7	2	39,6	50	9,3	6,4	2,0
DLRVR025	187	14,6	3,3	< 1	35,0	54	123,9	77	0,9	3	34,3	35	< 5,0	8,7	0,7
DLRVR026A	4	19,6	4,0	2	68,5	120	11,6	4	13,6	4	53,2	125	9,4	14,0	4,8
DLRVR026C	< 2	23,60	3,72	3	88,30	125	12,60	5	10,10	4	73,00	101	18,40	11,19	3,15
DLRVR026D	< 2	21,2	4,5	2	81,3	123	8,2	6	13,8	7	74,3	116	11,1	15,1	4,2
DLRVR028	6	21,6	3,9	3	98,7	115	14,9	7	23,4	4	91,0	103	34,8	16,1	4,4
DLRVR029	2	24,1	4,5	< 1	43,0	45	14,9	2	42,4	3	24,1	33	22,3	5,6	1,2
Sd061		18,8	4,0		24,0		20,3		2,2		11,2			4,3	0,4
KV122	87			< 1		< 1		82		< 2		2			

Sample	U_XRF	V	Zn_XRF	Zr	Zr_XRF	Sn_XRF	Sr	Sr_XRF	Sc	Ba	Y	Y_XRF	La	Ce	Pr
DLRVR011	< 2	232,8	114	187,3	193	3	725,5	684	38,2	749,5	29,00	43	45,3	84,9	10,63
DLRVR012	< 2	352,6	95	132,1	136	2	677,0	641	44,2	606,5	24,31	35	36,1	64,0	8,14
DLRVR013	3	5,0	128	458,1	524	4	44,3	37	22,8	1116,0	38,67	55	82,6	149,2	16,27
DLRVR014		1,3		1005,2			8,0		10,4	83,4	117,81		181,8	253,4	27,73
DLRVR015	7	2,5	304	1128,5	1370	7	7,0	1	13,0	32,4	102,15	148	109,5	207,9	24,18
DLRVR019	< 2	278,5	87	181,1	175	< 2	706,5	680	41,7	726,5	25,44	42	38,4	70,6	9,03
DLRVR020	< 2	234,6	74	126,6	124	5	558,5	524	33,9	560,0	16,96	29	36,2	58,0	6,27
DLRVR021	< 2	183,1	63	183,1	197	3	939,5	882	26,9	753,0	16,90	32	40,3	65,7	7,10
DLRVR025	< 2	206,4	53	118,1	110	3	774,0	477	< 1,0	507,5	19,26	28	41,4	75,1	7,56
DLRVR026A	< 2	7,8	102	284,5	347	< 2	311,5	304	15,9	1333,0	28,26	37	87,0	133,7	13,60
DLRVR026C	< 2	8,53	94	277,20	303	< 2	462,1	427	14,4	1239,0	28,55	37	88,1	136,7	14,00
DLRVR026D	2	5,2	69	300,8	331	8	331,6	311	16,8	1391,0	31,22	34	94,1	145,5	14,24
DLRVR028	< 2	92,4	68	269,7	283	6	792,5	729	16,2	1132,5	24,02	28	99,8	146,7	14,03
DLRVR029	< 2	119,7	119	293,5	316	< 2	659,5	596	32,0	2521,5	63,35	68	69,3	132,7	18,31
Sd061		249,1		150,0			950,0		< 1,0	370,9	19,66		20,3	43,1	5,70
KV122	< 2		62		< 1	< 2		91				12			

Sample	Nd	Sm	Eu	Gd	Tb	Dy	Ho	Er	Tm	Yb	Lu
DLRVR011	47.6	9.03	3.69	7.30	1.17	6.66	1.19	2.92	0.37	2.42	0.38
DLRVR012	36.1	7.29	2.93	5.86	0.93	5.32	1.00	2.43	0.33	1.93	0.30
DLRVR013	60.8	10.45	2.80	8.36	1.36	8.24	1.63	4.50	0.65	4.38	0.71
DLRVR014	103.7	20.11	2.44	14.58	2.73	16.21	3.28	9.22	1.42	8.48	1.28
DLRVR015	95.5	19.50	2.46	16.79	3.09	20.29	4.14	10.95	1.66	10.57	1.66
DLRVR019	40.4	7.65	3.21	6.42	0.99	5.53	1.07	2.57	0.36	2.01	0.34
DLRVR020	23.9	4.26	1.58	3.57	0.57	3.52	0.68	1.79	0.25	1.72	0.26
DLRVR021	27.9	4.92	1.77	4.02	0.63	3.65	0.70	1.72	0.23	1.51	0.25
DLRVR025	27.8	4.68	1.42	4.55	0.63	3.66	0.73	2.13	0.28	2.01	0.29
DLRVR026A	45.5	7.05	2.24	6.92	0.96	5.72	1.14	3.24	0.50	3.51	0.60
DLRVR026C	49.0	7.56	2.65	6.93	1.00	5.92	1.16	3.27	0.49	3.41	0.56
DLRVR026D	49.6	7.50	2.37	6.76	1.01	6.32	1.23	3.57	0.52	3.83	0.64
DLRVR028	48.0	6.90	2.47	6.52	0.85	4.96	0.98	2.64	0.39	2.61	0.44
DLRVR029	85.3	17.87	7.16	14.78	2.35	13.67	2.62	6.36	0.87	5.12	0.81
Sd061	23.8	4.63	1.70	4.88	0.75	4.01	0.78	2.09	0.28	1.83	0.28
KV122											



Annex No. 2
Annex No. 2

Locality	Coordinates (Adindan)		Elevation	Land-use	Protection	Morphology	Persistence	Origin
	X	Y						
Ada Gurati	444772	693473	2825	Grass land	None	Plain surrounded by small hills	Moderate	Alluvial
Tibiru	436891	691506	2841	Grass land	None	Plain surrounded by small hills	Moderate to high	Alluvial
Alayo	462319	699703		Grass land	None	Gentle slope	Moderate	Alluvial
Kao	487353	749981		Grass land	None	Plain	Moderate	Alluvial
Dodola	482972	749929		Grass land	None	Plain	Moderate	Alluvial
Kofele goyo	435029	681532	2585	Grass land	None	Plain surrounded by medium ridges	Moderate to high	Alluvial
Haro welabu	428788	686266		Grass land	None	Plain surrounded by small hills	Moderate	Alluvial
Kao kebele	487353	749981		Grass land	None	Plain	Moderate	Alluvial
Dodola	482972	749929		Grass land	None	Plain	Moderate	Alluvial
Eriba	473672	667620	2193	Grass land	None	Slightly undulating	Moderate	Alluvial
Gujji	473177	675045		Grass land	None	Slightly undulating	Moderate	Alluvial
Adola	482151	664921	2154	Grass land	None	T-Shaped wetland	Moderate	Alluvial
Abaya Choke	379786	733810		Grass land	None	Plain surrounded by fault escarpment	High	Lacustrine



Annex No. 3
Annex No. 3

sample ID	Coordinates (Adindan)		elevation	lithology	Point Load test		Schmidt hammer compressive strength			weathering	water absorption (%)	porosity (%)	bulk density (gm/cm ³)
	X	Y			IS 50 (MPa)	UCS (MPa)	Schmidt median (MPa)	Schmidt min. (MPa)	Schmidt max. (MPa)				
R-GNS-MLK-12B	491768	673058	1422	Gneiss	0.59	13.64	45.90	39.5	54.6	SW	1.53	4.12	2.69
R-GNT-MLK-01	475238	671046	2290	Gneiss	0.10	2.41	<10.3	<10.3	<10.3	MW to HW	45.94	53.33	1.16
R-GNS-MLK-13	495800	683094	1375	Gneiss	2.32	53.38	59.40	54.6	61.5	SW to F	2.08	5.23	2.51
R-GNS-MLK-11	493619	669324	1528	Gneiss	0.16	3.70	<10.3	<10.3	<10.3	SW to MW	9.49	20.89	2.20
R-GNT-MLK-05	482151	664921	2154	Granite	4.19	96.36	61.00	52.5	65	SW to F	3.97	9.37	2.36
R-GMT-MLK-03B	473672	667620	2184	Granite	0.25	5.65	43.90	39.9	52.5	SW to F	4.31	9.91	2.28
R-GNS-MLK-14A	494788	685205	1383	Granite	2.46	56.52	36.10	32.5	45.9	SW to F	2.43	6.08	2.51
R-GNT-MLK-09	498908	663180	1444	Granite	4.42	101.55	48.70	43.9	54.6	SW to F	1.48	3.77	2.55
R-GNT-MLK-03A	473672	667620	2184	Granite	0.26	5.89	43.90	39.9	52.5	SW to F	3.43	8.17	2.38
R-GNT-MLK-05A	482151	664921	2154	Granite	4.19	96.36	61.00	52.5	65	SW to F	0.57	1.48	2.60
R-CSCH-MLK-08	499058	663285	1467	Chlorite schist	0.79	18.06	36.10	34.4	42	SW to F	1.70	4.80	2.87
R-GNT-MLK-14B	494788	685205	1383	Granite	1.65	37.95	36.10	32.5	45.9	SW to F	2.33	5.77	2.48
R-CSCH-MLK-08A	499058	663285	1467	Chlorite schist	0.79	18.06	36.10	34.4	42	SW	1.70	4.80	2.84
R-CSCH-MEJ-14	488732	703304	1665	Chlorite schist	0.87	19.97	24.30	17.5	24.9	SW to MW	6.51	14.66	2.26
R-CSCH-MLK-10	493394	669209	1493	Chlorite schist	1.04	23.97	<10.3	<10.3	<10.3	SW to MW	0.46	1.33	2.93
R-MSCH-MEJ-04	489746	696988	1449	Mica schist	0.71	16.40	32.50	24.3	32.5	F	1.78	4.59	2.58
R-MSCH-MEJ-06	487665	699553	1544	Mica schist	1.01	23.15	22.80	20.3	31.6	SW to F	2.56	6.40	2.50
R-MSCH-MEJ-01	491948	691934	1390	Mica schist	2.74	63.00	<10.3	<10.3	<10.3	SW	0.81	2.45	3.03
R-MSCH-MEJ-09	484954	704521	1603	Mica schist	3.72	85.57	30.70	28.2	31.6	SW to MW	0.44	1.36	3.14
R-MSCH-MEJ-10	485889	703562	1650	Mica schist						SW to F	2.30	6.07	2.64
R-AMP-MEJ-16	483484	705877		Amphibolite	8.83	203.05	43.90	36.1	52.5	SW to F	0.15	0.46	3.01
R-RHY-YLM-09	420584	741273	1664	Rhyolite	2.98	68.43	41.60	41.6	48.1	SW	5.59	12.16	2.17
R-RHY-YLM-10	417901	740402	1700	Rhyolite	6.33	145.58	69.80	64	69.8	SW	1.50	3.51	2.35
R-TUFF-KOT-06	413378	710416	1296	Ignimbrite	0.31	7.18	27.60	25.9	29.1	SW	34.74	45.34	1.31
TUFF-KOT-05	408213	710714	1246	Ignimbrite	0.67	15.40	67.60	64	69.8	SW	14.62	27.06	1.85
R-IGM-KOT-06	413378	710416	1296	Ignimbrite	0.31	7.18	27.60	25.9	29.1	SW	21.19	32.73	1.54

sample ID	Coordinates (Adindan)		elevation	lithology	Point Load test		Schmidt hammer compressive strength			weathering	water absorption (%)	porosity (%)	bulk density (gm/cm ³)
	X	Y			IS 50 (MPa)	UCS (MPa)	Schmidt median (MPa)	Schmidt min. (MPa)	Schmidt max. (MPa)				
R-RHY-WRA-11	445516	771689	1714	Pumecious rhyolitic flow	2.52	57.97	46.50	41.6	48.7	SW to F	5.88	13.19	2.24
R-RHY-KIL-02	393329	732278	1410	Rhyolite	0.93	21.39	32.50	24.3	32.5	SW	8.96	19.35	2.16
R-IGM-KIL-04	403852	730765	1490	Ignimbrite	1.19	27.26	21.50	17.5	22.8	SW	14.52	27.56	1.90
R-IGM-KIL-01	389038	731739	1246	Ignimbrite	1.38	31.83	32.50	24.3	32.5	SW to F	4.98	10.61	2.13
R-RHY-SOD-02	367679	763849	2452	Rhyolite	0.15	3.45	25.90	22.8	26.5	SW to F	9.65	20.25	2.09
R-BAS-KIL-03	397530	730516	1317	Basalt	4.44	102.07	21.50	17.5	22.8	SW	29.43	40.18	1.37
R-BAS-KIL-03	397530	730516	1317	Basalt	4.44	102.07	21.50	17.5	22.8	SW	6.01	15.21	2.53
R-BAS-ABM-08	338597	668661	1362	Basalt	3.86	88.73	48.10	45.9	55	SW to F	2.01	5.35	2.66
R-BAS-WRA-10	447971	769172	1818	Basalt	2.59	59.62	23.30	21.4	26.5	SW to MW	2.99	7.98	2.67
R-IGM-HSM-05	451387	719124	2555	Ignimbrite	2.73	62.86	33.60	29.1	39.6	SW	2.33	5.22	2.24
R-IGM-ARB-04	469578	735473	2464	Ignimbrite	1.75	40.21	63.00	63	66.4	SW to F	14.67	27.23	1.86
R-IGM-ARB-06	470495	720651	1960	Ignimbrite	4.32	99.28	64.00	57.5	68.3	F	2.98	6.69	2.25
R-IGM-ARB-10	471668	718491	1919	Ignimbrite	3.77	86.60	52.70	43.9	61	SW to F	8.01	17.08	2.13
R-IGM-ARB-01	468292	745378	2650	Ignimbrite	0.75	17.14	30.70	29.1	37.5	SW	24.75	38.48	1.55
R-IGM-GSB-06	341688	732114	1222	Ignimbrite	0.67	15.37	33.60	27.4	36.1	SW to F	12.81	23.51	1.83
R-IGM-TEB-02	361359	743167	1881	Ignimbrite	1.37	31.50	35.50	29.1	43.9	SW to MW	12.52	24.40	1.95
R-IGM-SOD-07	367803	747834	1740	Ignimbrite	0.69	15.77	28.20	27.4	32.5	SW to F	6.93	15.42	2.23
R-IGM-GSB-02	353776	724377	1688	Ignimbrite	3.21	73.79	65.00	64	69.8	SW to F	6.63	14.31	2.15
R-RHY-BEL-10	341445	770183	1289	Rhyolite	1.83	42.18	39.90	37.5	45.9	SW to F	7.49	16.22	2.16
R-IGM-BEL-01	361226	768350	2054	Ignimbrite	1.89	43.52	38.20	36.1	45.9	SW to F	2.59	6.37	2.46
R-IGM-YRG-02	414240	696588	1850	Ignimbrite	3.78	86.84	36.10	29.1	37.9	SW to F	7.53	15.61	2.07
R-RHY-YRG-01	410531	670343	2140	Rhyolite	1.29	29.60	25.90	20	25.9	SW to MW	5.67	13.51	2.39
R-IGM-KOT-03	411116	707160	1342	Rhyolitic ignimbrite	3.05	70.18	58.80	56	61.5	SW to F	5.32	12.30	2.31
R-IGM-KOT-04	407793	711233	1195	Ignimbrite	2.54	58.48	67.60	64	69.8	SW	8.08	17.13	2.12

sample ID	Coordinates (Adindan)		elevation	lithology	Point Load test		Schmidt hammer compressive strength			weathering	water absorption (%)	porosity (%)	bulk density (gm/cm ³)
	X	Y			IS 50 (MPa)	UCS (MPa)	Schmidt median (MPa)	Schmidt min. (MPa)	Schmidt max. (MPa)				
R-RHY-DLA-07	424964	703563	1739	Rhyolite	2.03	46.62	22.80	18.6	32.5	SW to MW	2.27	5.54	2.43
R-IGM-DLA-15A	425654	716699	1623	Rhyolitic ignimbrite	2.22	51.04	20.30	18.8	22.8	SW to F	12.09	22.71	1.88
R-RHY-KOT-02	408961	704093	1486	Rhyolite	2.75	63.22	30.00	24.5	33.6	SW to MW	3.56	8.49	2.38
R-IGM-DLA-17	421386	711695	1439	Trachytic ignimbrite	2.42	55.69	45.90	41.6	57	SW to F	3.71	8.30	2.24
R-RHY-DLA-12	424155	711140	1656	Rhyolite	3.13	71.92	30.70	26.5	37.9	SW to MW	4.81	10.98	2.28
R-RHY-DLA-8	432881	718244	1845	Rhyolitic ignimbrite	0.29	6.68	26.60	20	28	Sw to MW	23.39	37.69	1.61
R-IGM-DLA-01	420195	699437	1665	Ignimbrite	35.43	814.78	48.10	39.9	50.4	SW	7.45	16.25	2.18
R-IGM-DLA-16	425197	717190	1616	Rhyolitic ignimbrite	0.81	18.71	26.50	23.3	26.5	SW	20.02	33.69	1.68
R-RHY-DLA-5	431976	697577	2570	Rhyolite	4.18	96.23	54.60	41.6	60.2	SW	4.69	10.82	2.31
R-IGM-DLA-02	420375	701738	1558	Ignimbrite	1.74	40.13	33.60	18.6	35.5	SW to MW	10.34	20.50	1.98
R-RHY-DLA-09	424893	715426	1700	Rhyolite	3.61	83.03	38.20	33.8	43.9	SW	2.30	5.70	2.48
R-OBS-DLA-15B	425654	716699	1623	Rhyolitic ignimbrite	3.07	70.71	32.50	32.5	37.9	SW to F	1.06	2.42	2.30
R-IGM-ABM-03	358674	688069	1290	Ignimbrite	2.39	55.00	38.20	37.9	50.2	SW to F	5.58	11.70	2.09
R-RHY-ABM-04	358106	686966	1331	Rhyolite	4.15	95.56	52.50	37.5	52.7	SW to F	3.21	7.72	2.40
R-THR-MEJ-07	492015	702773	2370	Trachyte	1.29	29.75	36.10	26.5	39.9	SW to MW	6.12	1.16	1.99
R-BAS-DAY-01	489852	719294	2419	Basalt	1.49	34.33	45.90	43.9	55	SW	0.67	1.71	2.57
R-IGM-DAY-06	484592	731424	2463	Ignimbrite	2.44	56.21	46.10	39.9	48.1	SW	3.12	7.03	2.26
R-BAS-DAY-05	475758	719664	2141	Basalt	6.84	157.38	50.20	42	57	SW	0.66	1.86	2.83
R-BAS-DAY-02	489365	725344	2391	Basalt	0.98	22.65	36.10	36.1	39.9	SW	5.68	12.66	2.24
R-BAS-SOL-03	456000	673047	2190	Basalt	4.01	92.20	50.20	42	57	SW	1.04	2.83	2.74
R-BAS-REP-02	426226	666456	2610	Basalt	10.45	240.44	41.60	37.5	45.9	SW	0.98	2.79	2.87

sample ID	Coordinates (Adindan)		elevation	lithology	Point Load test		Schmidt hammer compressive strength			weathering	water absorption (%)	porosity (%)	bulk density (gm/cm ³)
	X	Y			IS 50 (MPa)	UCS (MPa)	Schmidt median (MPa)	Schmidt min. (MPa)	Schmidt max. (MPa)				
R-BAS-REP-4	422344	688442	2364	Basalt	6.13	140.94	59.10	57	61	F to SW	0.27	0.75	2.89
R-IGM-BIR-01	384266	703484	1187	Ignimbrite	0.71	16.26	36.10	29.1	37.9	SW	12.73	26.47	2.08
R-TRH-HSM-01	450427	701470	2624	Trachyte	2.50	57.58	57.00	48.1	59.1	SW	6.09	13.54	2.22
R-BAS-HSM-10	460486	699588	2670	Basalt	5.71	131.40	57.00	50.2	59.2	MW to CW	0.49	1.38	2.83
R-BAS-REP-06	429401	686695	2975	Basalt	5.63	129.57	24.90	18.9	27.4	SW to MW	0.38	1.05	2.78
R-BAS-HSM-13	454445	705648	2679	Basalt	3.92	90.18	61.00	60	68.3	SW	0.56	1.56	2.78
R-BAS-HSM-11	459984	701803	2669	Basalt	4.45	102.45	64.00	60	69.8	SW	0.59	1.67	2.79
R-BAS-HSM-03	447702	697953	2786	Basalt	9.81	225.65	45.90	31.8	50.4	SW	0.95	2.52	2.66
R-BAS-HSM-02	449749	701487	2660	Basalt	3.61	83.03	35.50	27.4	36.1	SW	0.76	2.17	2.83
R-BAS-DLA-13	423929	711953	1571	Basalt	3.99	91.79	20.30	18.2	25.9	SW to MW	1.71	4.63	2.72
R-BAS-REP-7B	430614	687719	2938	Basalt	4.64	106.82	52.50	36.1	61	SW to MW	0.79	2.12	2.72
R-BAS-REP-7A	430614	687719	2938	Basalt	5.85	134.56	52.50	36.1	61	SW to MW	0.61	1.65	2.73
R-BAS-HSM-6	466229	692732	2681	Basalt	3.54	81.39	55.00	39.9	57	SW to F	0.68	1.91	2.84
R-BAS-REP-05	430574	684698	2865	Basalt	3.34	76.91	45.90	43.9	55	SW to MW	0.90	2.44	2.73
R-BAS-DLA-6	427132	697967	2174	Basalt	5.26	121.03	33.60	18.6	35.5	SW to MW	0.67	1.93	2.89
R-BAS-MLK-06	483434	665873	2206	Basalt	6.17	141.96	45.90	41.6	55	SW to F	0.43	1.25	2.95
R-BAS-MLK-06	483434	665873	2206	Basalt	6.17	141.96	45.90	41.6	55	SW to F	0.43	1.25	2.95



Annex No. 4
Annex No. 4

ID	Coordinates (Adindan)		Lithology	Weathering*	Purpose	Operated by	Large	Accessibility
	X	Y						
1	336784	723422	Rhyolite	SW to F	Road select material/pavement	Manual / Machinery	Large	Fair
2	340475	669160	Basalt	SW to MW	Road select material/pavement	Machinery	Large	Good
3	340856	769509	Igimbrite	SW to F	Masonry	Manual	Large	Fair
4	341443	739307	Rhyolite	SW to MW	Road select material/pavement	Machinery	Large	Good
5	341445	770183	Igimbrite	SW to F	Masonry	Manual	Large	Fair
6	341527	693762	Basalt	SW to MW	Road select material/pavement	Manual	Large	Good
7	343022	745795	Igimbrite	SW	Masonry	Manual	Large	Good
8	347276	712409	Basalt	MW to HW	Road select material/pavement	Manual	Large	Good
9	347827	677517	Rhyolite	SW to F	Masonry	Manual	Large	Good
10	356236	683492	Rhyolite	SW to F	Masonry (cobble stone)	Manual	Large	Good
11	358670	688073	Igimbrite	MW to HW	Masonry	Manual	Large	Good
12	359769	710938	Basalt	MW to HW	Road select material/pavement	Manual / Machinery	Large	Fair
13	361226	768350	Igimbrite	SW to F	Masonry + cobblestone	Manual / Machinery	Large	Fair
14	364239	756594	Igimbrite	SW to F	Masonry	Manual	Large	Fair
15	365855	721842	Basalt	SW to MW	Road select material/pavement	Manual	Large	Fair
16	367447	723093	Basalt	MW to HW	Road select material/pavement	Manual	Large	Fair
17	370658	730658	Basalt	SW to F	Concrete mixtures	Manual	Large	Fair
18	371190	734023	Scoria	SW to F	Road select material/pavement	Manual / Machinery	Large	Good
19	372108	735232	Scoria	SW to F	Road select material/pavement	Manual / Machinery	Large	Good
20	372980	729641	Scoria	SW to F	Road select material/pavement	Manual	Large	Good
21	396625	759867	Rhyolite	SW to F	Masonry	Manual	Large	Fair
22	410531	670343	Rhyolite	SW to MW	Road select material/pavement	Machinery	Medium	Good
23	411119	707166	Igimbrite	SW to F	Masonry	Manual / Machinery	Large	Fair
24	411905	703754	Basalt	SW to MW	Road select material/pavement	Machinery	Large	Good
25	411922	709915	Silt-clayey soil	SW	Earth fill material	Machinery	Large	Good
26	414243	696571	Igimbrite	SW to F	Masonry	Manual	Medium	Fair

ID	Coordinates (Adindan)		Lithology	Weathering*	Purpose	Operated by	Large	Accessibility
	X	Y						
27	415387	690716	Rhyolite	SW to MW	Road select material/pavement	Machinery	Medium	Fair
28	417158	740818	Ignimbrite	SW to F	Masonry	Manual	Medium	Good
29	420375	701742	Ignimbrite	SW	Masonry	Manual	Large	Good
30	421387	711695	Ignimbrite	SW	Masonry	Machinery	Large	Fair
31	423679	716637	Ignimbrite	SW	Masonry	Manual	Large	Fair
32	424054	712133	Basalt	MW to HW	Road select material/pavement	Machinery	Large	Good
33	424155	711140	Rhyolite	SW to MW	Masonry	Machinery	Large	Good
34	424911	715457	Ignimbrite	SW to MW	Masonry	Machinery	Medium	Good
35	425198	717190	Ignimbrite	SW	Masonry	Manual	Large	Fair
36	425396	725248	Ignimbrite	SW	Masonry	Manual	Large	Fair
37	425599	716736	Basalt	SW to MW	Road select material/pavement	Machinery	Medium	Fair
38	425679	716637	Ignimbrite	SW	Masonry	Manual	Large	Fair
39	426137	713087	Rhyolite	SW	Masonry	manual	Medium	Fair
40	427150	697972	Basalt	SW to MW	Masonry	Machinery	Large	Good
41	429329	739276	Ignimbrite	SW to MW	Masonry	Manual / Machinery	Large	Good
42	430614	687719	Basalt	SW to MW	Road select material/pavement	Manual / Machinery	Medium	Fair
43	432972	763282	Rhyolite / Ignimbrite	SW to F	Masonry	Manual / Machinery	Large	Good
44	434059	664994	Rhyolite	HW	Road select material/pavement	Manual / Machinery	Medium	Very good
45	437397	731467	Ignimbrite	SW	Masonry	Manual	Medium	Good
46	437418	751707	Ignimbrite	SW to F	Masonry	Manual	Large	Fair
47	440118	746173	Ignimbrite	F	Masonry	Manual	Medium	Poor
48	442939	727558	Ignimbrite	SW to MW	Road select material/pavement	Machinery	Large	Good
49	443066	688035	Basalt	SW to MW	Road select material/pavement	Machinery	Large	Fair
50	445516	771689	Unidentified	SW to F	Road select material and Masonry	Manual	Large	Good
51	449752	701480	Basalt	SW to MW	Road select material and Masonry	Machinery	Medium	Good
52	454445	705648	Basalt	SW to F	Base course	Blasting and Machinery	Large	Very good
53	456694	668559	Basalt	SW	Road select material/pavement	Machinery	Large	Very good

ID	Coordinates (Adindan)		Lithology	Weathering*	Purpose	Operated by	Large	Accessibility
	X	Y						
54	459984	701803	Basalt	SW	Asphalt mixtures	Blasting and Machinery	Large	Good
55	460486	699588	Basalt	MW to HW	Road select material/pavement	Machinery	Medium	Fair
56	462297	699698	Basalt	SW to F	Masonry	Manual	Large	Poor
57	465229	721370	Basalt	MW	Road select material/pavement	Machinery	Large	Very good
58	466691	692942	Basalt	MW to HW	Road select material/pavement	Machinery	Medium	Fair
59	467081	748682	Igimbrite	SW to F	Masonry	Manual	Large	Fair
60	468851	772875	Igimbrite	SW to F	Masonry	Manual	Large	Fair
61	470495	720651	Igimbrite	SW to F	Masonry	Manual	Large	Fair
62	470758	719642	Igimbrite	SW to F	Masonry	Manual	Large	Fair
63	471668	718488	Igimbrite	SW to F	Masonry	Manual	Large	Very good
64	473450	673507	Reddish silty soil	SW	Road select material/pavement	Machinery	Large	Very good
65	473507	673507	Basalt	MW to HW	Road select material/pavement	Machinery	Large	Good
66	474018	672226	Kaoline	HW	Kaoline production	Benching and berming	Large	Good
67	478586	749197	Igimbrite	SW	Masonry	Machinery	Medium	Good
68	481859	713446	Rhyolite	SW	Masonry	Manual	Medium	Good
69	482150	665034	Granite	SW to F	Dimension stone	Blasing or jack hammer Excavation	Large	Fair
70	483446	665872	Basalt	F	Asphalt mixtures, Masonry	Blasting and Machinery	Large	Very good
71	485401	749481	Igimbrite	MW to HW	Road select material/pavement	Machinery	Medium	Fair
72	488402	702738	Talc	F	Soapstone	Manual	Medium	Fair
73	489201	697848	Igimbrite	F	Masonry	Machinery	Large	Fair
74	498908	663180	Granite	SW to F	Masonry	Manual	Large	Fair

* F - fresh; SW - slightly weathered; MW - moderately weathered; HW - highly weathered



Annex No. 5
Annex No. 5

ID	Coordinates (Adindan)		Region / Zone / Woreda / Locality	Lithology	Weathering*	Purpose	Operated by	Size	Accessibility
	X	Y							
2	338597	666861	South/Gamo Gofa/Arba Minch Zuria	Basalt	SW to F	Masonry	Manual	Large	Poor
3	342966	763765	South/Wolayta Sodo/Kindo Koysha	Rhyolite	SW to F	Masonry	Blasting	Large	Good
4	353776	724377	South/Gamo Gofa/Boreda	Ignimbrite	F	Masonry	Machinery	Large	Fair
5	361368	743316	South/Wolayta Sodo/Humbo Tabela	Rhyolite	SW to MW	Masonry	Manual / Machinery	Medium	Fair
6	362275	747697	South/Wolayta Sodo/Sodo Zuria	Silty soil	SW to F	Embankment	Manual	Medium	Good
7	362616	700399	South/Gamo Gofa/West Abaya	Basalt	SW to F	Masonry	Manual	Large	Very good
8	364243	742326	South/Wolayta Sodo/Humbo Tabela	Ignimbrite	SW to F	Masonry	Manual	Large	Very good
9	364499	746143	South/Wolayta Sodo/Humbo Tabela	Ignimbrite	SW to F	Masonry	Manual	Large	Very good
10	367799	747837	South/Wolayta Sodo/Humbo Tabela	Ignimbrite	SW to F	Masonry	Manual / Machinery	Large	Good
11	370480	733388	South/Wolayta Sodo/Humbo Tabela	Basalt	SW to F	Masonry, asphalt mixtures	Manual	Large	Very good
12	371792	729582	South/Wolayta Sodo/Humbo Tabela	Basalt	SW to F	Masonry, con- crete mixtures	Manual	Large	Very good
13	387517	759432	South/Wolayta Sodo/Damot Weyde	Rhyolite	SW to F	Masonry	Manual / Machinery	Large	Fair
14	389737	769557	South/Wolayta Sodo/Diguna Fango	Rhyolite	SW to F	Masonry	Manual	Large	Good

ID	Coordinates (Adindan)		Region / Zone / Woreda / Locality	Lithology	Weathering*	Purpose	Operated by	Size	Accessibility
	X	Y							
15	420195	699437	South/Gedeo/Wanago/Betel	Ignimbrite	SW	Masonry	Manual / Machinery	Large	Fair
16	423929	711955	South/Sidama/Dara/Mechiso	Basalt	SW	Embankment	Machinery	Large	Fair
17	425347	722102	South/Sidama/Dara/Tesso	Ignimbrite	SW to F	Masonry	Manual	Large	Fair
18	431946	697513	South/Gedeo/Bule/Songo Nejo	Rhyolite	SW to MW	Masonry	Manual / Machinery	V.large	Fair
19	443247	773051	South/Sidama/Hawela tula/Hawela tula	Rhyolite	SW to F	Masonry	Manual / Machinery	V.large	Fair
20	453367	703144	Oromia/Guji/Borite/Borite	Ignimbrite	SW	Masonry	Manually	Large	Good
21	454851	727895	South/Sidama/-/Bursa	Ignimbrite	SW to F	Masonry	Manual	Large	Fair
22	465751	751548	Oromia/West Arsi/Kokosa	Ignimbrite	SW to F	Masonry	Manual / Machinery	Large	Fair
23	466067	701417	Oromia/Guji/Bore/Goda	Basalt	SW	Concrete mixtures	Machinery	Large	Fair
24	466229	692731	Oromia/Guji/Ana sora/kotowotye	Basalt	SW	Masonry, concrete mixtures	Machinery	Large	Fair
25	468292	745376	Oromia/West Arsi/Kokosa/Shelo bele	Ignimbrite	SW to F	Masonry	Manual	Large	Fair
26	472313	741562	Oromia/West Arsi/Kokosa/Bochesa	Ignimbrite	SW to F	Masonry	Manual	Large	Fair
27	473671	667620	Oromia/Guji/Eriba/Wache sololo	Granite	F	Dimension stone	Blasting and machinery	Large	Poor
28	477710	746577	Oromia/West Arsi/Kokosa/Hurufa	Ignimbrite	SW	Masonry	Manual / Machinery	Large	Good

ID	Coordinates (Adindan)		Region / Zone / Woreda / Locality	Lithology	Weathering*	Purpose	Operated by	Size	Accessibility
	X	Y							
29	481799	751389	Oromiya/West Arsi/Kokosa/ Kawo tulu	Rhyolite	SW	Masonry	Machinery	Large	Poor
30	484591	731424	South/Sidama/Bensa/Da- lacha	Ignimbrite	SW to F	Masonry	Manual / Machinery	Large	Fair
31	486639	703233	South/Sidama/Aroresa	Ignimbrite	SW to F	Masonry	Manual	Medium	Good
32	494788	685205	South/Sidama/Aroresa/ Sadeka	Granite	F	Dimension stone	Manual / Machinery	Large	Fair

* F - fresh; SW - slightly weathered; MW - moderately weathered